

Electronic Thesis and Dissertation Repository

4-24-2014 12:00 AM

Modeling and Control of Steerable Ablation Catheters

Mahta Khoshnam Tehrani
The University of Western Ontario

Supervisor
Dr. Rajni V. Patel
The University of Western Ontario

Graduate Program in Electrical and Computer Engineering
A thesis submitted in partial fulfillment of the requirements for the degree in Doctor of
Philosophy
© Mahta Khoshnam Tehrani 2014

Follow this and additional works at: <https://ir.lib.uwo.ca/etd>



Part of the [Biomedical Commons](#), and the [Controls and Control Theory Commons](#)

Recommended Citation

Khoshnam Tehrani, Mahta, "Modeling and Control of Steerable Ablation Catheters" (2014). *Electronic Thesis and Dissertation Repository*. 2004.
<https://ir.lib.uwo.ca/etd/2004>

This Dissertation/Thesis is brought to you for free and open access by Scholarship@Western. It has been accepted for inclusion in Electronic Thesis and Dissertation Repository by an authorized administrator of Scholarship@Western. For more information, please contact wlsadmin@uwo.ca.

Modeling and Control of Steerable Ablation Catheters

(Thesis format: Integrated-Article)

by

Mahta Khoshnam Tehrani

Graduate Program in Engineering Science
Department of Electrical and Computer Engineering

A thesis submitted in partial fulfillment
of the requirements for the degree of
Doctor of Philosophy

The School of Graduate and Postdoctoral Studies
The University of Western Ontario
London, Ontario, Canada

© Mahta Khoshnam Tehrani 2014

Abstract

Catheters are long, flexible tubes that are extensively used in vascular and cardiac interventions, *e.g.*, cardiac ablation, coronary angiography and mitral valve annuloplasty. Catheter-based cardiac ablation is a well-accepted treatment for atrial fibrillation, a common type of cardiac arrhythmia. During this procedure, a steerable ablation catheter is guided through the vasculature to the left atrium to correct the signal pathways inside the heart and restore normal heart rhythm. The outcome of the ablation procedure depends mainly on the correct positioning of the catheter tip at the target location inside the heart and also on maintaining a consistent contact between the catheter tip and cardiac tissue. In the presence of cardiac and respiratory motions, achieving these goals during the ablation procedure is very challenging without proper 3D visualization, dexterous control of the flexible catheter and an estimate of the catheter tip/tissue contact force.

This research project provides the required basis for developing a robotics-assisted catheter manipulation system with contact force control for use in cardiac ablation procedures. The behavior of the catheter is studied in free space as well in contact with the environment to develop mathematical models of the catheter tip that are well suited for developing control systems. The validity of the proposed modeling approaches and the performance of the suggested control techniques are evaluated experimentally.

As the first step, the static force-deflection relationship for ablation catheters is described with a large-deflection beam model and an optimized pseudo-rigid-body 3R model. The proposed static model is then used in developing a control system for controlling the contact force when the catheter tip is interacting with a static environment. Our studies also showed that it is possible to estimate the tip/tissue contact force by analyzing the shape of the catheter without installing a force sensor on the catheter.

During cardiac ablation, the catheter tip is in contact with a relatively fast-moving environment (cardiac tissue). Robotic manipulation of the catheter has the

potential to improve the quality of contact between the catheter tip and cardiac tissue. To this end, the frequency response of the catheter is investigated and a control technique is proposed to compensate for the cardiac motion and to maintain a constant tip/tissue contact force.

Our study on developing a motion compensated robotics-assisted catheter manipulation system suggests that redesigning the actuation mechanism of current ablation catheters would provide a major improvement in using these catheters in robotics-assisted cardiac ablation procedures.

Keywords: Cardiac Ablation, Steerable Ablation Catheter, Robotics-Assisted Catheter Manipulation, Large-Deflection Beam Model, Pseudo-Rigid-Body 3R Model, Force Control, Shape Analysis, Motion Compensation.

Statement of Co-Authorship

The thesis presented here has been written by Mahta Khoshnam Tehrani under supervision of Dr. Rajni V. Patel. Parts of the content of this thesis has been published in refereed conference proceedings, or is under review for publication. The research published in each paper has been mainly conducted and written by the principal author. The presented research is guided and supported by Dr. Patel as the research supervisor.

A version of the material presented in Chapter 2 has been published in

- Mahta Khoshnam, Mahdi Azizian, and Rajni V. Patel, “Modeling of a Steerable Catheter Based on Beam Theory,” in *Proceedings of IEEE International Conference on Robotics and Automation (ICRA)*, 2012, pp. 4681-4686.
 - M. Khoshnam - developed the model, collected experimental data, analyzed the results, evaluated the model and wrote the manuscript.
 - Dr. M. Azizian - designed the experimental setup and discussed the results.

A version of the material presented in Chapter 3 has been published in

- Mahta Khoshnam and Rajni V. Patel, “A Pseudo-Rigid-Body 3R Model for a Steerable Ablation Catheter,” in *Proceedings of IEEE International Conference on Robotics and Automation (ICRA)*, 2013, pp. 4412-4417.

The material presented in Chapter 4 has been partially published in

- Mahta Khoshnam, Aaron Yurkewich, and Rajni V. Patel, “Model-Based Force Control of a Steerable Ablation Catheter with a Custom-Designed Strain Sensor,” in *Proceedings of IEEE International Conference on Robotics and Automation (ICRA)*, 2013, pp. 4464-4469.
 - M. Khoshnam - designed the experiments and the control system, collected data and analyzed the results, wrote the major part of manuscript and revised the rest.
 - A. Yurkewich - designed the strain sensor, helped with preparing the experimental set-up and calibrating the strain sensor for use with the catheter, and

wrote the first draft of the sections in the manuscript regarding the specifications of the experimental setup and the designed strain sensor.

The material presented in Chapter 5 is currently under peer review for publication in

- Mahta Khoshnam and Rajni V. Patel, “Modeling and Estimation of Tip Contact Force for Steerable Ablation Catheters,” submitted to *IEEE Transactions on Biomedical Engineering*, 2013.

Part of this chapter is currently under peer review in

- Mahta Khoshnam and Rajni V. Patel, “Estimating Contact Force for Steerable Ablation Catheters based on Shape Analysis,” submitted to *IEEE/RSJ International Conference on Intelligent Robots and Systems (IROS)*, 2014.

Part of the material presented in Chapter 7 is currently under peer review in

- Mahta Khoshnam and Rajni V. Patel, “Robotics-Assisted Catheter Manipulation for Improving Cardiac Ablation Efficiency,” submitted to *IEEE International Conference on Biomedical Robotics and Biomechatronics (BioRob)*, 2014.

To my dearest parents;

Mohammad

who taught me to pursue my dreams,

and

Zahra

who taught me to be patient and persistent along the way.

Acknowledgements

This thesis would not have been possible without the help of many people who in one way or another contributed to the completion of this study.

First and foremost, I wish to express my deepest gratitude to my supervisor, Dr. Rajni Patel, for his insightful supervision, consistent support and constructive advices during the entire project. I would like to express my appreciation and respect for him. Not only for his guidance and encouragement, but also for his human qualities.

I am grateful to the team in the Electrophysiology Laboratory at the London Health Sciences Centre, University Hospital, for all of their help. In particular, I would like to thank Dr. Allan Skanes, for helping me to get a better understanding of the medical procedure and for enduring endless questions. My gratitude also goes to Marilyn Braney, for always being ready to help with a bright smile.

I would also like to thank my examiners: Dr. Ken McIsaac, Dr. Ilia Polushin, Dr. Samuel Asokanthan and Dr. Peter X. Liu for taking the time to review and examine my thesis, and also for their valuable comments.

Special thanks goes to Dr. Mahdi Azizian who dedicated a considerable amount of his time to discuss ideas at the beginning of this project. My sincere thanks to Aaron Yurkewich, Christopher Ward, Abelardo Escoto, Mostafa Hadavand and Dr. Amir Takhmar for their technical support during this project.

My sincere thanks goes to my dear friends at CSTAR, Dr. Ali Talasaz and Dr. Ali Asadian, for their continuous support and encouragement. I am also grateful to Iman Khalaji, Mahya Shahbazi, Farokh Atashzar, Dr. Ana Luisa Trejos and Karen Siroen for their support and friendship. I would like to extend my gratitude to all past and present members of CSTAR for creating such a wonderful environment to work in.

I would like to appreciate the support from the staff in the Department of Electrical and Computer Engineering, in particular, Sandra Vilovski, Chris Marriott and Stephanie Tigert, who helped me along the way on numerous occasions.

I am grateful for being surrounded by amazing friends: Ghodsieh, Mohammad, Fatemeh, Mahdiyeh, Mahdi and little Ehsan. Thank you all for encouraging me and raising my spirits when I needed it most.

My gratitude to my kind and loving family, my parents, my sister, and my wonderful aunt and uncle is beyond words. Their unconditional love, support and encouragement over the years are the greatest gift that make me who I am today.

Finally, I would like to express my most sincere gratitude towards my husband for his constant love during these years. Thank you, Maysam, for all your support and patience, and also for the generous amount of time that you dedicated to long hours of discussion on topics that may have not been your field of interest. Thank you for being my best friend and colleague, and a true blessing in my life.

Table of Contents

Abstract	ii
Statement of Co-Authorship	iv
Dedication	vi
Acknowledgements	viii
Table of Contents	ix
List of Tables	xii
List of Figures	xiii
Nomenclature	xvi
1 Introduction	1
1.1 Cardiac Arrhythmia	1
1.2 Catheter-Based Cardiac Ablation	2
1.3 Literature Review	4
1.3.1 Commercial Products	4
1.3.2 Robotics-Assisted Catheter Manipulation	10
1.3.3 Modeling of Catheters	13
1.3.4 Catheter Prototypes	15
1.4 Research Statement	17
1.5 Thesis Structure and Contributions	20
2 Static Modeling Based on Beam Theory	35
2.1 Introduction	35
2.2 Experimental Setup	38
2.2.1 Camera Registration	39
2.3 2D Static Model for the Catheter tip	40
2.3.1 Large Deflection Beam Model	41
2.3.2 Modeling the Initial Bending of the Catheter Tip	44
2.3.3 Analysing the Effect of Beam Rigidity on the Load-Displacement Relation	45

2.3.4	Finite Element Analysis of the Catheter Tip	45
2.4	Experimental Results	48
2.4.1	Rigidity of the Catheter Tip	48
2.4.2	Evaluating Model Performance	49
2.5	Discussion	52
2.6	Conclusions	53
3	Static Pseudo-Rigid-Body 3R Model	58
3.1	Introduction	58
3.2	Pseudo-Rigid-Body 3R Model of a Cantilever Beam	60
3.3	Experimental Evaluation of the Beam PRB 3R Model for the Catheter Tip	63
3.3.1	Evaluating Model Performance	63
3.4	Pseudo-Rigid-Body 3R Model of a Catheter Tip	65
3.5	Performance Evaluation of the Catheter PRB 3R Model in a More Realistic Environment	68
3.5.1	Experimental Setup	69
3.5.2	Evaluating Model Performance	69
3.5.3	Estimating Contact Force from Catheter Shape and Handle Displacement	71
3.6	Conclusions	73
4	Force Control in Contact with a Static Environment	79
4.1	Introduction	79
4.2	Experimental Setup	81
4.3	Optical Strain Sensor	82
4.3.1	Mapping Analog Voltage to Tip Angle	84
4.3.2	Mapping Handle Displacement to Analog Voltage	86
4.4	Modeling Catheter Behavior	86
4.4.1	Mapping Handle Displacement to Tip Angle	86
4.4.2	Mapping Tip Angle to Applied Loads	87
4.5	Experimental Results	88
4.5.1	Detecting Tip/Environment Contact	90
4.5.2	Regulation Performance	91
4.5.3	Estimating Contact Force from the Tip Shape	91
4.6	Discussion	92
4.7	Conclusions	96
5	Analysis of the Tip Shape in Free Space and in Contact with the Environment	101
5.1	Introduction	101
5.2	Methodology	105
5.2.1	Experimental Setup	105

5.2.2	Extracting the Tip Shape from Images	108
5.3	Analysis of the Tip Curvature in Free Space	110
5.3.1	Kinematic Model	113
5.3.2	Model Performance	119
5.4	Effect of Contact Force on the Tip Shape	121
5.4.1	Force Index	123
5.5	Experimental Validation	126
5.5.1	Experiments Using the Same Catheter	126
5.5.2	Experiments Using a Different Catheter	127
5.5.3	Obtaining the Force Index from Sensor Outputs	128
5.6	Conclusions	130
6	Robotics-Assisted Catheter Manipulation	135
6.1	Introduction	135
6.2	Experimental Setup	138
6.3	System Characteristics	141
6.3.1	Static Response in Free Space	142
6.3.2	Frequency Response in Free Space	143
6.3.3	Achieving a Desired Tip Angle	146
6.4	Tip/Tissue Motion Synchronization	149
6.4.1	Static Environment	149
6.4.2	Moving Environment	150
6.4.3	Online Estimation of Motion Frequency	152
6.4.4	Evaluating Force-Time Integral	153
6.4.5	Evaluating the Static Force-Deflection Model	154
6.5	Discussion	156
6.5.1	Performance Limitations	156
6.5.2	Relevance to Clinical Application	158
6.6	Conclusions	159
7	Concluding Remarks and Future Work	164
7.1	Concluding Remarks	164
7.2	Future Research	168
	Curriculum Vitae	172

List of Tables

2.1	Statistical measures showing model performance evaluated for the large deflection beam model.	52
3.1	Statistical measures showing model performance evaluated for the large deflection beam model and the PRB 3R model.	65
3.2	Statistical measures showing the model performance evaluated for the PRB 3R model of the catheter tip.	67
3.3	Statistical measures showing the performance of the catheter PRB 3R model and the large deflection beam model when the tip end is not fixed.	70
5.1	Link parameters of the proposed kinematic model for the catheter tip.	115
5.2	Statistical measures showing the performance of the kinematic models.	118
5.3	Conditional probability of estimating force ranges for test data with the first catheter.	126
5.4	Conditional probability of estimating force ranges for test data with the second catheter.	128
6.1	Effect of actuation frequency F_a on different features of the response.	145
6.2	FTI calculated for the cases shown in Figures 6.14 and 6.16.	154

List of Figures

1.1	Schematic of the master-slave robotic system for catheter-based cardiac ablation.	19
2.1	Experimental setup.	38
2.2	Deflection of an initially curved cantilever beam caused by external loads concentrated at the free end	41
2.3	Relation between the beam tip deflection Φ and the end force P for different values of $E * I$	46
2.4	A beam element	46
2.5	Pseudo-rigid-body model for an initially curved cantilever beam	48
2.6	Relation between the catheter tip deflection Φ and the value of EI for the catheter tip	49
2.7	Estimation of the tip parameters with the large deflection beam model for dataset \mathcal{A}	50
2.8	Estimation of the tip parameters with the large deflection beam model for dataset \mathcal{B}	51
2.9	Estimation of the tip parameters with the large deflection beam model for dataset \mathcal{C}	51
3.1	Deflection of a loaded cantilever beam and its pseudo-rigid-body model equivalent.	61
3.2	Performance of the large deflection beam model and the PRB 3R model in estimating the shape of the catheter tip under applied loads.	64
3.3	Normalized spring stiffness values vs. load ratio.	67
3.4	Performance of the catheter PRB 3R model in estimating the shape of the catheter tip under applied loads.	68
3.5	A view of catheter tip in the second experimental setup.	69
3.6	Performance of the catheter PRB 3R model and the large deflection beam model when the tip end is not fixed.	70
3.7	Relation between handle displacement and tip angle in different runs.	72
3.8	Estimation of contact force based on the tip angle.	73
4.1	Schematic of the experimental setup.	82
4.2	A view of the catheter tip, camera and strain sensor in the experimental setup.	83
4.3	Relation between analog voltage and tip angle.	84

4.4	Relation between handle displacement and analog voltage.	85
4.5	Relation between the catheter tip angle and the handle displacement.	87
4.6	Deflection of an initially curved cantilever beam under applied loads.	88
4.7	Estimating catheter tip angle from applied loads.	89
4.8	A schematic of the control system.	89
4.9	Performance of the system in detecting catheter tip/environment contact	90
4.10	Regulation performance of the system with measured force feedback for different distances and desired contact force values.	92
4.11	Regulation performance of the system with estimated force feedback for different distances and desired contact force values.	92
4.12	Performance of the system with measured force feedback in maintain- ing the desired contact force value.	93
4.13	Performance of the system with estimated force feedback in maintain- ing the desired contact force value	93
4.14	Performance of the system with measured force feedback in tracking the desired contact force values.	94
4.15	Performance of the system with estimated force feedback in tracking the desired contact force values.	94
4.16	Performance of the system with estimated force feedback (using image data) in tracking the desired contact force values.	95
4.17	Catheter tip angle estimated from sensor output for different contact forces.	95
5.1	Schematic of the experimental setup.	105
5.2	A view of the catheter tip, camera and force sensor in the experimental setup.	106
5.3	A close view of the proximal handle and the bending tip of a steerable ablation catheter	107
5.4	Different configurations of the catheter sheath to determine its effect on the results of the study.	107
5.5	Catheter shape estimation. Step-by-step.	109
5.6	Tip curvature when the proximal handle is actuated.	112
5.7	Tip curvature when handle displacement is 10 mm.	113
5.8	Kinematic model for the catheter tip and the assigned D-H coordinate frames.	114
5.9	Catheter tip workspace in 3D with respect to frame $\{b\}$	116
5.10	(a) Model end-effector and the catheter tip. (b) Section of the tip with constant curvature.	118
5.11	Configuration of links in the kinematic models	120
5.12	Tip curvature when forces are applied at the tip.	121
5.13	Tip curvature versus force magnitude for different handle displace- ments at a number of points along the catheter.	122

5.14	The effect of contact forces can be best seen by studying the section marked in red color on the catheter.	123
5.15	Defined force index for different contact force values.	124
5.16	CDF of fitted Gaussian distribution to the force index corresponding to each force range.	125
5.17	Mean curvature vs. force magnitude for different force range estimations.	127
5.18	Probability of correctly estimating the force ranges.	129
6.1	Different patterns of the contact force between the catheter tip and cardiac tissue.	137
6.2	Schematic of the experimental setup.	138
6.3	A close view of the proximal handle and the bending tip of a steerable ablation catheter.	139
6.4	A view of the catheter tip, camera and force sensor in the experimental setup.	139
6.5	A sample frame. The tip angle is calculated using the centroid points of the red markers.	140
6.6	Static relationship between the handle displacement (d) and deflection of the tip.	142
6.7	The path that the tip follows when the proximal handle is actuated at $F_a = 0.27$ Hz.	143
6.8	Variations in the tip angle when the proximal handle is actuated at $F_a = 0.27$ Hz	144
6.9	Bode diagram for the catheter in free space.	146
6.10	The control system for achieving a desired angle at the catheter tip.	147
6.11	Performance of the control system in following a desired tip angle.	147
6.12	Bode diagram for the system with the desired tip angle as input and the actual tip angle as output.	148
6.13	Catheter interacting with a static environment: (top) commanded handle displacement, (bottom) resulting tip/tissue contact force.	150
6.14	Catheter tip/tissue contact force when the tissue has a sinusoidal motion.	151
6.15	Schematic of the control system with online frequency estimation.	152
6.16	Catheter tip/tissue contact force when the frequency of the tissue motion changes.	153
6.17	Performance of the PRB 3R model in estimating the contact force when the frequency of tissue motion is 0.37 Hz.	155
6.18	Performance of the PRB 3R model in estimating the contact force when the frequency of tissue motion is changing.	155
6.19	The effect of wear of the catheter on the experimental results.	157

Nomenclature

2D	<i>Two Dimensional</i>
3D	<i>Three Dimensional</i>
ABS	<i><u>A</u>crylonitrile <u>B</u>utadiene <u>S</u>tyrene</i>
AF	<i><u>A</u>trial <u>F</u>ibrillation</i>
CDF	<i><u>C</u>umulative <u>D</u>istribution <u>F</u>unction</i>
CGCI	<i><u>C</u>atheter <u>G</u>uidance, <u>C</u>ontrol and <u>I</u>maging</i>
CP	<i><u>C</u>onductive <u>P</u>olymer</i>
CT	<i><u>C</u>omputed <u>T</u>omography</i>
CVD	<i><u>C</u>ardiovascular <u>D</u>isease</i>
D-H	<i><u>D</u>enavit-<u>H</u>artenberg (Convention)</i>
DOF	<i><u>D</u>egree of <u>F</u>reedom</i>
EP	<i><u>E</u>lectrophysiology</i>
EP Lab	<i><u>E</u>lectrophysiology <u>L</u>aboratory</i>
FBG	<i><u>F</u>iber <u>B</u>ragg <u>G</u>rating</i>
FDA	<i><u>U</u>.<u>S</u>. <u>F</u>ood and <u>D</u>rug <u>A</u>dministration</i>
FEM	<i><u>F</u>inite <u>E</u>lement <u>M</u>ethod</i>
FPS	<i><u>F</u>rames <u>P</u>er <u>S</u>econd</i>
Fr	<i><u>F</u>rench Catheter Scale</i>
FTI	<i><u>F</u>orce-<u>T</u>ime <u>I</u>ntegral</i>
gf	<i><u>G</u>ram-<u>F</u>orce</i>
GMM	<i><u>G</u>aussian <u>M</u>ixture <u>M</u>odel</i>
MAE	<i><u>M</u>ean <u>A</u>bsolute <u>E</u>rror</i>
MATLAB	<i><u>M</u>atrix <u>L</u>aboratory</i>
MIS	<i><u>M</u>inimally <u>I</u>nvasive <u>S</u>urgery</i>
MNS	<i><u>M</u>agnetic <u>N</u>avigation <u>S</u>ystem</i>
MRI	<i><u>M</u>agnetic <u>R</u>esonance <u>I</u>maging</i>

PCI	<i><u>P</u>ercutaneous <u>C</u>oronary <u>I</u>nterventions</i>
PDF	<i><u>P</u>robability <u>D</u>istribution <u>F</u>unction</i>
PID	<i><u>P</u>roportional-<u>I</u>ntegral-<u>D</u>erivative</i>
PRB	<i><u>P</u>seudo-<u>R</u>igid-<u>B</u>ody (Model)</i>
PRB 3R	<i><u>P</u>seudo-<u>R</u>igid-<u>B</u>ody (with) Three <u>R</u>evolutes (Joints)</i>
RF	<i><u>R</u>adio <u>F</u>requency</i>
RMSE	<i><u>R</u>oot <u>M</u>ean <u>S</u>quare <u>E</u>rror</i>
RNS	<i><u>R</u>obotic <u>N</u>avigation <u>S</u>ystem</i>
ROI	<i><u>R</u>egion of <u>I</u>nterest</i>
SA	<i><u>S</u>inoatrial (Node)</i>
SMA	<i><u>S</u>hape <u>M</u>emory <u>A</u>lloy</i>
STD	<i><u>S</u>tandard <u>D</u>eviation</i>
TTE	<i><u>T</u>ransthoracic <u>E</u>chocardiography</i>
US	<i><u>U</u>ltrasound</i>
WHO	<i><u>W</u>orld <u>H</u>ealth <u>O</u>rganization</i>

Chapter 1

Introduction

1.1 Cardiac Arrhythmia

Cardiovascular diseases (CVDs) are caused by disorders of the heart and blood vessels. According to the World Health Organization (WHO), CVDs result in the highest number of deaths from disease around the world [1]. In Canada, major CVDs were responsible for 29% of all deaths in 2009, being the second cause of death after cancer [2]. Cardiac arrhythmia is one of the common CVDs and refers to abnormal heart rhythm, *i.e.*, the heart may beat faster, slower or with an irregular rhythm. Arrhythmia is caused by disorders in the heart's electrical system. In a normal heart, the sinoatrial (SA) node emits electrical signals to trigger a heartbeat. The generated signals spread through the atria and cause them to contract and pump blood into the ventricles. After the ventricles are filled with blood, the signals make them contract and send the blood into the body. This process is repeated in every heartbeat and arrhythmia occurs if there is a problem with any of its parts.

Atrial Fibrillation (AF) is the most common serious type of cardiac arrhythmia, during which false electrical signals are generated from different parts in the atria and cause abnormal contractions. As a result, blood clots might form inside the upper chambers and if these clots enter the circulatory system, they can cause a stroke. The Heart and StrokeTM Foundation reports that after the age of 60, one third of all strokes are the result of AF [3]. Thus, effective treatment of AF is of great importance.

Depending on the type and severity of arrhythmia, different methods of treatment are suggested. While several drugs are available for this purpose, in some cases the medications prove insufficient and non-drug treatments should be applied. In this case, catheter-based cardiac ablation is the most commonly suggested method [4].

1.2 Catheter-Based Cardiac Ablation

In order to treat AF, the parts of cardiac tissue that generate erratic electrical impulses should be destroyed. Catheter-based cardiac ablation is a minimally invasive intervention to achieve this goal [4]. Rather than opening the chest to gain access to the heart, in this procedure, small incisions are made in the groin, neck or arm area and catheters are inserted in the blood vessels and steered through the vasculature to reach the heart. Since the source of AF is usually near the pulmonary veins [5], the catheter is passed through a small incision in the septum to provide access to the left atrium. Electroanatomic mapping systems (*e.g.*, [6] and [7]) and preoperative CT or MRI scans, help the electrophysiologists to identify the source of abnormal pulses [8]. Using visual feedback from a medical imaging modality, the catheter tip is then positioned at the target points to perform the ablation. Destroying the sources of false signals can be achieved by either freezing (cryoablation) or heating the tissue. In the latter, usually radio-frequency (RF) energy [9] is transmitted through the catheter to burn the tissue and create lesions to block the pathways of false electrical impulses that cause arrhythmia.

Catheters are long flexible tubes that are used in different medical applications. One of the main uses of catheters is for cardiovascular interventions, since the shape of catheters is well suited for insertion in blood vessels. The catheters used for RF ablation of the heart can be of different types: these catheters can be uni- or bi-directional and of different diameters (*e.g.*, 5-Fr or 7-Fr), the sizes of the ablation tip electrodes may vary, *etc.* However, their common feature is that the electrophysiologist can use the proximal handle to manipulate the distal tip. The actuation mechanism of RF ablation catheters uses pull-wires to translate the movements of the proximal handle to the flexing of the tip. Biosense Webster, Inc. [7] and Medtronic, Inc. [10] are two companies that provide a range of electrophysiology and ablation catheters.

X-ray fluoroscopy is the most commonly used medical imaging modality for visualizing catheters inside the body during RF cardiac ablation procedures. Considering that the catheter-based AF therapy is a complicated procedure that takes several hours, there is a possibility that the patient and the electrophysiologist may

be exposed to harmful X-ray radiation for significant periods of time [11].

Several studies have investigated the effect of contact force on the outcome of RF ablation [12–14] and reported that the contact force has a noticeable effect on forming lesions inside the heart and correlates with the procedure outcome. It is also shown that providing electrophysiologists with a measure of contact force reduces the procedure time remarkably [15] and that the force-time integral (FTI) can be used as a measure to quantify the quality of contact [16, 17]. If the contact force is not sufficient, the lesion formation will be incomplete and patients will experience recurrence of the arrhythmia [14]. On the other hand, excessive force may result in complications such as cardiac perforation [18].

The conventional method of performing AF ablation procedure is very challenging for a number of reasons: (1) the main feedback from the position of the catheters is the fluoroscopy imaging, which is 2D and does not provide a clear view of soft tissues, (2) the actuation mechanism of existing catheters does not provide the electrophysiologists with dexterous control of the catheter tip, (3) the electrophysiologists do not have an estimate of the contact forces between the catheter tip and the cardiac tissue. Complexity of the anatomy as well as cardiac and respiratory motions all add to these difficulties.

The popularity of catheter-based cardiac ablation for treating AF has increased during the past few decades. However, the conventional method of RF ablation is still a tedious and complicated procedure due to the aforementioned challenges and researchers seek new approaches to overcome these challenges. The ultimate goal would be designing a robot-assisted catheter system that enables electrophysiologists to manipulate the catheter tip dexterously and position the catheter tip at the target location inside the atria. The robotic system would provide haptic feedback to the clinician and would implement force control at the catheter tip to maintain the tip/tissue contact force at the desired level during the procedure. It is expected that such a system would provide better ergonomics for electrophysiologists and will help them to perform the interventional procedure in less time without compromising the outcome.

1.3 Literature Review

In this section, an overview of related work in the context of catheter-based robotic systems and their main component, *i.e.*, catheter, is presented. We have classified the proposed approaches into four categories: (1) commercial products, (2) master-slave robotic catheter systems, (3) research work that describes the behavior of catheters by mathematical or numerical modeling and (4) techniques that propose modifications to the current mechanical design of catheters.

1.3.1 Commercial Products

Recent developments in robotic technology and visualization techniques have inspired designing new products that facilitate catheter manipulation and/or visualization during electrophysiology procedures. A number of these systems are commercially available or are in clinical studies. This section gives an overview of commercial products that are developed to facilitate performing catheter-based interventional procedures.

1.3.1.1 Robotic Systems

Robotics-based catheter systems are developed to provide dexterous manipulation of flexible catheters. The main feature of these systems is that they allow the electrophysiologist to manipulate the catheter from a remote workstation and thus reduce the amount of X-ray radiations to the clinicians. The robotic catheter systems currently available are as follows in alphabetical order:

1.3.1.1.1 AmigoTM Remote Catheter System

AmigoTM (Catheter Robotics, Inc., Mount Olive, NJ) Remote Catheter System (RCS) [19] is a device designed for electrophysiology procedures. This system has two main parts:

- The catheter manipulation system that is attached to the patient's bed; into which a catheter is loaded. This system is compatible with a variety of com-

monly used electrophysiology catheters and using it within existing electrophysiology labs (EP labs) does not require any additional arrangements.

- The catheter remote controller, which looks similar to the proximal handle of a conventional catheter and provides necessary controls for inserting, retracting, rotating and deflecting the tip of the catheter loaded in the manipulation system. This controller allows the clinicians to manipulate the catheter from 30 meters away from the patient’s bed.

In a clinical study [20], the performance of Amigo in manipulating, positioning and control of catheters was assessed. This study [20] reports that Amigo is “safe and effective” and the learning curve is short, since its interface is easy to use and similar to a catheter handle. The safety and performance of Amigo for cardiac ablation is currently being investigated [19,21].

In 2012, Catheter Robotics, Inc. announced that it has received the U.S. Food and Drug Administration (FDA) approval for AmigoTM for use with two types of catheters [19].

1.3.1.1.2 CorPath[®] Vascular Robotic System

The CorPath[®] 200 Robotic System (Corindus Vascular Robotics, Inc., Waltham, MA) [22] is designed for catheter manipulation and stent delivery in coronary angioplasty. This system is compatible with standard EP lab devices and mounts on the side of standard patient tables. The electrophysiologist guides the catheter and places the stent/balloon from a remote, shielded workstation using the provided joysticks and touchscreen controls. The catheters and guidewires are visualized through X-ray images and are displayed on angiographic monitors provided in the workstation.

Clinical studies [23,24] report that performing robotic-assisted angioplasty with CorPath[®] 200 Robotic System is safe and feasible.

In 2012, Corindus Vascular Robotics, Inc. announced FDA 510(k) clearance for using Corpath[®] 200 Robotic System in percutaneous coronary interventions (PCI) [22].

1.3.1.1.3 Catheter Guidance, Control and Imaging System

The Catheter Guidance, Control and Imaging (CGCI) system (Magnetecs Corp., Inglewood, CA) [25] provides remote magnetic catheter navigation for catheter-based interventions. This system has eight large electromagnets in four robotic arms that are placed around the patient's bed. Small magnets are integrated within the tip of catheters and the catheters are steered and positioned using the magnetic field. The electrophysiologist manipulates the catheter from a remote workstation and has the option to choose between two control modes: manual and automatic. In manual mode, the physician uses a joystick to guide the catheter, while in the automatic mode, he/she clicks on the desired target and the CGCI system plans the path and moves the catheter accordingly to reach the desired location with a proper orientation. If the catheter moves away from the specified location, the system informs the operator to perform proper action [25].

The CGCI system is now undergoing human clinical trials [25]. More details on this system as well as first clinical results are reported in [26].

1.3.1.1.4 NIOBE[®] Magnetic Navigation System

The NIOBE[®] Magnetic Navigation System (Stereotaxis, Inc., St. Louis, MO) [27] provides a platform for steering and manipulating catheters inside the patient's body using a low-intensity magnetic field generated by two large permanent magnets positioned on each side of the patient's bed. The desired position and orientation of the catheters and guidewires are achieved by changing the magnetic fields through rotating the computer-controlled magnetic arms. Hence, all catheters and guidewires are equipped with magnetic tips. The electrophysiologist manipulates the catheters from a remote workstation by mouse clicks on a local display.

Magnetic navigation allows for precise positioning of the catheter and the feasibility of using this technique in clinical setting has been shown [28–30], but the procedure time might be longer than that of the manual procedure [28–30], which can be a result of insufficient lesion formation [29]. It was reported that redesigning the catheter improved the safety of magnetic AF ablation [31]. Moreover, installing

the permanent magnets in existing EP labs requires proper arrangements [32]

The NIOBE[®] Remote Magnetic Navigation system received FDA 510(k) approval in January 2003. The current generation of NIOBE[®] is now one of the main components of Stereotaxis EPOCH[™] Solution, which is a comprehensive platform for guiding and positioning of electrophysiology catheters [27]. The NIOBE[®] system is compatible with CARTO System (Biosense Webster, Inc., Diamond Bar, CA) [7].

1.3.1.1.5 Sensei[®] Robotic Catheter System

The Sensei[®] X Robotic Catheter System (Hansen Medical, Inc., Mountain View, CA) [33] provides a master/slave robotic platform control system for remote navigation and control of electrophysiology catheters in blood vessels and in the heart. The electrophysiologist's console consists of the necessary tools for manipulating the catheter as well as displays for providing visual feedback. If an Artisan catheter[®] [33] is loaded into the Sensei[®] system, the built-in pressure sensor integrated within the catheter shaft reports the contact force between the catheter and the tissue. The electrophysiologist is informed from the force information by visual as well as haptic feedback through IntelliSense[®] Fine Force Technology Interface [33]. It is reported that this technique has a better performance in measuring contact forces applied in the direction of the catheter's axis [34].

The CoHesion[™] 3D Visualization Module (Hansen Medical, Inc., Mountain View, CA) [33] integrates the abilities of the Sensei[®] platform in manipulating the catheter with those of the EnSite[™] Visualization System (St. Jude Medical, Inc., St Paul, MN, USA) [6] in providing a 3D visualization of the surgical site.

The first generation of Sensei[®] Robotic Systems obtained FDA clearance in 2007. In recent years, different clinical studies have evaluated the feasibility of using this system in electrophysiology application. References [33, 35–39] are examples of these studies.

Magellan[™] Robotic System is another product from Hansen Medical, Inc. [33] that is developed for peripheral vascular procedures. Its concept is similar to that of the Sensei[®] and it provides a robotic platform for visualization and remote manipulations of catheters [33].

An overview and comparison of different features of the aforementioned robotic systems are presented in [40]. In [41], the main features of each system are summarized and their compatibility with other systems is discussed as well.

1.3.1.2 Visualization Systems

X-ray fluoroscopy is the most commonly used medical imaging modality for visualizing the catheter-based AF ablation procedures. The X-ray imaging renders 2D images, in which the catheters and guidewires are displayed, but the visibility of soft tissue is low. Thus, it is very difficult to obtain accurate information about the 3D position and orientation of the catheter tip inside the heart chambers using these images. To help with visualizing the anatomy, locating the source of arrhythmia in the heart and positioning the catheter at the target location, a 3D visualization of the heart is reconstructed using electroanatomic mapping systems. The commercially available visualization systems are as follows:

1.3.1.2.1 CARTO[®] 3 System

Carto[®] 3 System (Biosense Webster, Inc., Diamond Bar, CA) [7] is a 3D mapping platform that provides a 3D reconstruction of heart chambers that can be merged with pre-operative CT and MR scans. To construct such a model of the heart, a mapping catheter is guided into the heart chambers. A small magnetic sensor is integrated within the catheter tip and as the catheter tip moves around in the heart chamber, its distance from the three magnetic patches under the patient's bed is recorded and then used to calculate the tip position in 3D. Studies report that the Carto[®] 3 System is accurate [42] and its ability to integrate multi-modality images and to display multiple catheters simultaneously reduces the usage of fluoroscopy imaging, but does not affect the procedure time [43, 44]. The Carto[®] 3 System is compatible with customized catheters and equipment.

1.3.1.2.2 EnSite™ Velocity™ Cardiac Mapping System

The EnSite™ Velocity™ Cardiac Mapping System (St. Jude Medical, Inc., St Paul, MN, USA) [6] provides a multi-chamber 3D visualization of the heart. To construct such spatial mapping, an electrophysiology catheter is moved inside the heart chambers. The distance of the catheter tip with respect to the reference patches mounted on patient's skin is recorded and then processed to generate a 3D view of the heart. The EnSite™ Velocity™ Cardiac Mapping System is an open platform compatible with any electrophysiology catheter and can display multiple catheters in real-time. It also provides the necessary tools for integrating preoperative CT/MRI images with the real-time imaging data [6]. Studies report that the Ensite™ visualization system provides a precise mapping of the heart and reduces the radiation exposure to the electrophysiologists [45–47]. This system also provides a feedback from catheter tip/tissue contact based on local impedance measurements [48].

Different features of these visualization systems are described and compared in [41].

1.3.1.3 Force Sensing Catheters

The importance of providing electrophysiologists with an estimate of the catheter tip/tissue contact force has been established in different studies (*e.g.*, [12–18]). These studies were made possible partly due to the development of the following two force-sensing ablation catheters:

1.3.1.3.1 TactiCath® Force-Sensing Ablation Catheter

TactiCath® Force-Sensing Ablation Catheter (Endosense™ SA, Geneva, Switzerland) [49] uses fiber optic sensor technology to measure the contact forces at the catheter tip and displays the measured force through the TactiSys Quartz™ [49]. When the catheter tip comes in contact with the tissue, the applied force causes the optical fibers to slightly deform. The small deformation of fibers affects the reflected wavelength of light and provides a means to measure the contact force. More details on the design of this catheter are given in [12]. The safety and effectiveness of using

Tacticath[®] in cardiac ablation procedures are investigated in several studies [14,49].

In 2013, St. Jude Medical[™], Inc. [6] acquired Endosense[™] SA [49] and so it is expected that new developments would be introduced in the AF ablation products.

1.3.1.3.2 THERMOCOOL[®] SMARTTOUCH[™] Catheter

THERMOCOOL[®] SMARTTOUCH[™] (Biosense Webster, Inc., Diamond Bar, CA) [7] is an ablation catheter that measures the tip/tissue contact force and provides a graphical display of the magnitude and direction of the force on the recent versions of CARTO[®] 3 System (Section 1.3.1.2.1) [7]. The force sensing ability of this catheter is based on electromagnetic location tracking technology: contact forces cause the precision spring integrated within the catheter tip to deflect slightly. Attached to the distal end of the spring, there is a magnetic transmitter which emits a location reference signal. The three magnetic sensors mounted on the other side of the spring, detect the changes in the location of the transmitter, and thus provide a means to calculate the contact force applied by the catheter tip. More details on the force sensing technique of THERMOCOOL[®] SMARTTOUCH[™] catheter are given in [18]. This catheter has been used for measuring the catheter tip/tissue contact force in several studies (*e.g.*, [15,17,18]).

THERMOCOOL[®] SMARTTOUCH[™] is the first catheter with force sensing technology that was approved by FDA for using in catheter-based cardiac ablation procedures for treating AF. Biosense Webster, Inc., a unit of Johnson & Johnson Company [50], received the FDA approval for THERMOCOOL[®] SMARTTOUCH[™] in early 2014 [50].

1.3.2 Robotics-Assisted Catheter Manipulation

Several robotic mechanisms for manipulating the catheters during endovascular interventions are developed in academia. An overview of these systems is presented in this section.

Fukuda *et al.* [51] developed one of the earliest master-slave systems for intravascular catheter manipulation during neurosurgery. The slave side included a

2-DOF catheter actuation mechanism and a catheter which was instrumented with a micro force sensor at its tip [52]. On the master side, the user manipulated the catheter using the master joystick and X-ray images from the surgical site. The user was also provided with a haptic feedback from the contact force at the catheter tip as well as the forces that the slave actuation mechanism applied to manipulate the catheter [51]. The mechanism used for steering the catheter was updated [53] and then used in developing an autonomous catheter insertion system, in which the position feedback from the catheter tip was provided through tracking magnetic tips attached to the catheter [54]. Force feedback was not provided in the latter case.

Jayender *et al.* [55] developed a robotic system for inserting a catheter into the blood vessels for angioplasty procedures. The catheter was mounted on a Mitsubishi PA 10-7C robot manipulator which was also equipped with a force sensor. The insertion mechanism monitored the force exerted for inserting the catheter into the vessel and adjusted the stroke length accordingly [55]. By instrumenting the catheter with a shape memory alloy (SMA) actuator, they also developed a master-slave catheter insertion system, in which the user manipulated the catheter remotely and received haptic feedback from the contact force at the catheter tip [56, 57]. This robotic catheter system was then enhanced by a visual servoing platform which allowed for autonomous catheter insertion: the user selected the desired path on a map showing the vasculature. Using the real-time imaging feedback and the SMA actuators to orient the catheter tip in the desired direction, the robot steered the catheter through the defined path to the target position [58].

Plicchi *et al.* [59, 60] designed a telerobotic system to navigate electrophysiology catheters through the vasculature to the heart. The catheter actuation mechanism mounted on a robotic arm near the surgical site and the user manipulated the catheter remotely. Force measurements were taken from the proximal end of the catheter to provide the user with a feedback from the forces required to insert the catheter into the blood vessel. The proposed system was tested in animal trials and showed good performance and repeatability [59, 60].

Ganji *et al.* [61] developed a teleoperated robotic system for navigating steerable catheters. A conventional catheter was loaded in a 3-Dof actuation mechanism

placed at the surgical site and it was manipulated using a remote master device with haptic feedback. The position of the catheter tip was followed by electromagnetic trackers and a kinematic model of the catheter's distal shaft was used in developing a model-based position controller to steer the catheter to the target point. The system performance was evaluated *in-vivo* [61].

In order to develop a robotic catheter system, Srimathveeravalli *et al.* [62] first studied how surgeons move their hands during catheter insertion for neurovascular procedures to identify the basic requirements for designing such robotic systems. The resulting robotic manipulator could handle guidewires and catheters at the same time and included a measurement mechanism to provide the surgeon with haptic feedback from the forces used to manipulate the catheter [62].

Park *et al.* [63] developed a force-reflecting robotic platform for remote navigation of cardiac catheters. The system consisted of a 3-DOF catheter actuation mechanism on the slave side and a remote master workstation from which the user could manipulate the catheter through a haptic device and feel the force required to insert and manipulate the catheter [63]. To improve the safety of catheter navigation, the distance between the catheter tip and the vessel wall was estimated from real-time images of the testbed and a forbidden-region virtual fixture technique was implemented to avoid collision between the catheter tip and the vessel wall [64].

Another master-slave system for guiding and positioning a catheter was proposed in [65]. In this system, a custom mechanism was developed for inserting and manipulating the catheter; the position of the catheter tip was determined through electromagnetic tracking and was displayed on a 3D virtual image of the testbed. The operator used a 3-DOF master device to steer the catheter according to this image. The insertion force was also fed back to the user [65, 66].

Payne *et al.* [67] designed a compact master-slave system for navigating the catheter during endovascular procedure. In this system, the slave mechanism replicated the motion of the master actuator to insert the catheter into the vessel. Strain gauges were mounted on the catheter tip to provide a measure of the contact between the catheter tip and the vessel walls and the user was provided with haptic feedback from the contact force information [67].

Guo *et al.* [68] developed a robotic catheter manipulator system for neurosurgery applications. This system consisted of a 2-DOF mechanism for manipulating the catheter on the slave side and a similar master mechanism on the operator's workstation. The slave mechanism replicated the axial and radial motion of the master device to steer the catheter inside the vasculature. A force measurement mechanism was implemented on the slave side to measure the forces required for inserting the catheter and the force data was provided to the user through a haptic device. To ensure the safe navigation of the catheter inside the vessels, a fiber optic force sensor was mounted on the catheter tip to measure the tip/vessel contact forces. Moreover, three custom-designed rubber sensors were mounted on the catheter's side to measure the contact force between the sides of the catheter and the vessel walls. This sensor system provided the user with real-time information of the contact force. The performance of the developed robotic system was tested with placing the master device in Japan and the slave device in China. Internet-based communication was established to transfer the data between the master and slave devices [68].

Different features of the aforementioned robotic catheter manipulation systems are summarized and compared in [69].

1.3.3 Modeling of Catheters

In order to describe the behavior of steerable catheters, several analytical and numerical models are proposed. This section provides an overview of different approaches used to model catheter behavior.

1.3.3.1 Analytical Modeling

The bending characteristics of flexible ablation catheters have been the subject of several studies. This section summarizes the analytical models proposed for describing the catheter behavior in response to proximal actuation.

Continuum robotics has become one of the main trends of research in the field of robotics. The initial motivation for studying and designing continuum robots was

the capabilities of biological manipulators such as snakes and squids in dexterous manipulation of the objects even in cluttered environments [70]. Walker *et al.* designed one of the first continuum manipulators [71]. They also developed kinematic and dynamic models to describe the behavior of these manipulators [72–75].

Steerable catheters are flexible without distinct rigid joints and they bend continuously along their length. Hence, they can be classified as continuum robots with “extrinsic actuation” [70, 76]. Several methods for modeling catheters as continuum robots have been presented in the literature. Camarillo *et al.* [77] developed a kinematic model for tendon-driven continuum robots. A steerable catheter was selected as the continuum manipulator and the proposed model was used to describe how tendon displacements affect changes in the shape of the catheter’s tip [77]. If information about the tendon actuation is not available, the model parameters can then be estimated using a vision-based approach [78]. The developed model and the proposed vision system were also used in developing a control system for controlling the position of the catheter tip [79]. In another approach, the kinematic model proposed in [74] for a continuum manipulator was used to describe the distal tip of a steerable ablation catheter [80]. Zinn *et al.* proposed a kinematic model for tendon-driven catheters in which the effect of internal frictions is taken into account [81, 82]. Based on this model, a control system for positioning the catheter tip was developed [83].

It should be noted that these models are developed based on the assumption that the catheter tip is moving in free space and is not in contact with the environment or subject to external loading.

1.3.3.2 Numerical Modeling

Numerical models of the catheters and similar mechanisms are mainly developed for use in endovascular surgical simulators, in which simulating how the catheter moves inside the vasculature is a key feature. The works presented in this section are just instances of the ongoing research in this field.

Ikuta *et al.* [84] and Dawson *et al.* [85] proposed a multibody system for modeling long flexible instruments such as catheters or endoscopes. In the proposed

technique, the flexible device is modeled as a set of rigid links connected by flexible joints. In the method suggested by Kukuk *et al.* [86], all possible shapes for a discretized flexible instrument are found and then the shape which complies best with the physical and mechanical constraints, is selected. Niessen *et al.* [87,88] considered the guidewire as a series of small rigid segments connected with joints. The shape of the guidewire within the vasculature was then found based on the principle of minimization of energy, where energy is defined as a function of the positions of all joints. Finite element method (FEM) is another technique to numerical modeling of flexible catheters, which assumes that a wire-like object is composed of multiple beams [89–91]. Tang *et al.* [92] modeled the guidewire as connected elastic rods. Observing that the mechanical properties of the guidewire’s tip are different from those of the guidewire’s body, they also proposed a modeling technique based on Cosserat theory which accounted for these differences [93].

1.3.4 Catheter Prototypes

With the goal of facilitating the use of current catheters in performing endovascular procedures, several prototypes of new catheters are proposed and tested. The designed prototypes are mainly classified into two categories: (1) active catheters designed to improve the maneuverability in steering the catheter and (2) catheters with integrated force sensors that measure the contact forces at the distal tip. This section provides an overview of these catheter prototypes.

1.3.4.1 Active Catheters

Current steerable catheters use remote actuation, *i.e.*, the catheter’s distal tip is manipulated using the proximal handle. Considering the flexibility of the catheter and the complexity of the environment within which the catheter is used, steering the catheter and accurate positioning of the tip requires considerable skill and experience. To increase the maneuverability of the catheter tip, active catheters are designed. The actuators integrated within the distal shaft of these catheters provide a means to control the shape and the position of the catheter with more degrees of freedom.

Different actuation mechanisms have been used in developing active catheters, including: (1) tendon-driven, (2) shape memory alloys, (3) conductive polymers, (4) hydrodynamics and (5) magnetic driven. A very brief overview of these catheters is presented in this section. A more detailed review is provided in [94].

Artisan ExtendTM Control Catheter (Hansen Medical, Inc., Mountain View, CA) [33] is a tendon-driven active catheter that uses a system of pulleys and four tendons to actuate the tip with six degrees of freedom [36]. Using smart materials, such as shape memory alloy (SMA), is another choice for designing active catheters. Haga *et al.* [95] used SMA coils as the tip actuators. Jayender *et al.* [58] integrated SMA actuators at the tip of a catheter and used it in a robotic system to autonomously navigate the catheter through the vasculature. Using such catheters facilitates choosing blood vessel branches in vascular bifurcations. In [58] it was also noted that since the SMA actuators are activated by heat, they must be properly insulated and sufficient time between two consecutive actuation should be allowed to prevent causing harm to the vasculature. Conductive polymers (CP) are another smart material that have been used for actuating a catheter's distal tip [96].

Another group of active catheters are magnetic-driven ones. These catheters are equipped with small magnetic implants at the distal tip and are manipulated by external magnetic fields. NIOBE[®] (Stereotaxis, Inc., St. Louis, MO) Magnetic Navigation System [27] uses such magnetic catheters. Using hydraulic actuation mechanism led to the development of hydraulically-driven catheters. Examples of this type of active catheters are proposed in [97, 98]. One of the challenges in designing these catheters is that in order to improve the dexterity of the catheter, the number of driving tubes should increase. The small diameter of the catheter poses certain limitations in this regard. It must also be ensured that there is no blockage inside the driving tubes and there is no air/fluid leakage.

1.3.4.2 Force Sensing Catheters

The flexibility and length of catheters limit the user's perception of the contact forces at the catheter tip. Moreover, considering the fact that the catheters are steered through the vasculature, the forces that the user perceives during the catheter ma-

nipulation are mainly due to the frictional forces between the catheter body and its environment. It is very difficult for the user to distinguish how much of the perceived force is due to the contact at the catheter tip. In order to overcome this issue, several research projects have addressed the design of force sensors that can be integrated at the tip of the catheters.

Tanimoto *et al.* [52] designed one of the first force sensing catheter prototypes for neurosurgical applications. In order to measure contact forces, a micro pressure sensor was placed inside the catheter tip and the performance of this sensor was evaluated through *in-vivo* experiments. Polygerinos *et al.* [99–101] designed an MRI-compatible fiber optic force sensor and integrated it within the tip of an ablation catheter. The performance of this sensor was evaluated in several phantom and *in-vivo* studies. Kesner and Howe [102] designed an inexpensive but accurate 3D printed force sensor that was placed inside the catheter tip. This force sensor was then used in developing a robotic catheter system to maintain a constant force between the catheter tip and the heart tissue during annuloplasty procedures [103].

The material presented in this section is a general overview of the state-of-the-art in the research towards improving the efficacy of catheter-based interventional procedures. Each chapter of this thesis presents a detailed literature review of the topic under discussion in that chapter. Therefore, some overlap between the reviews in the chapters may exist.

To conclude this section, we note that the topic of controlling the catheter tip/tissue contact force during catheter-based cardiac ablation procedures has not been discussed previously. This fact constitutes the main motivation of this thesis.

1.4 Research Statement

The work presented in this thesis establishes the basis for developing a robotics-assisted catheter manipulation system with force control at the catheter tip. In this study, it is assumed that the catheter has been manually steered through the vascula-

ture, guided to the atrium and placed in proximity of the myocardium. Thus, how the catheter moves inside the vasculature and its interaction with the environment during the insertion phase, which have been topics of several research papers (*e.g.*, [87,88]), are not the primary concern. The main focus of this research project is to:

1. study how the catheter tip deflects when it interacts with tissue;
2. model the static deflection of the catheter tip;
3. find a method to measure the contact force at the catheter tip without using a force sensor; and
4. design a control system for maintaining a constant contact force at the catheter tip.

The research project presented in this thesis is defined as part of a larger project which aims at developing an image-guided robotics-assisted system for cardiac ablation. A schematic of this system is illustrated in Figure 1.1. The highlighted sections are those that are studied in this work. The proposed system is designed to have the following features:

- Compatible with conventional steerable ablation catheters.
- Teleoperated master-slave control of steerable catheters.
- Capable of tool/tissue contact force control or display (haptic/visual).
- Intra-operative 3D visualization of the distal part of the catheter within the beating heart.

In the proposed design, the user controls the motion of the catheter tip. The user's commands are sent from the master computer to the slave side where the slave computer controls a robot manipulator. The robot steers the catheter through a specifically designed actuation mechanism. The steerable ablation catheter is actuated using pull wires while the position and orientation of its tip is tracked in real time. The contact force and tip position data are fed back to the controller to ensure that the catheter tip does not move away from the target location and an adequate level of force between the tip and the tissue is always maintained. An imaging modality will provide intraoperative images to the user's display and the user can feel the contact force through the haptic device.

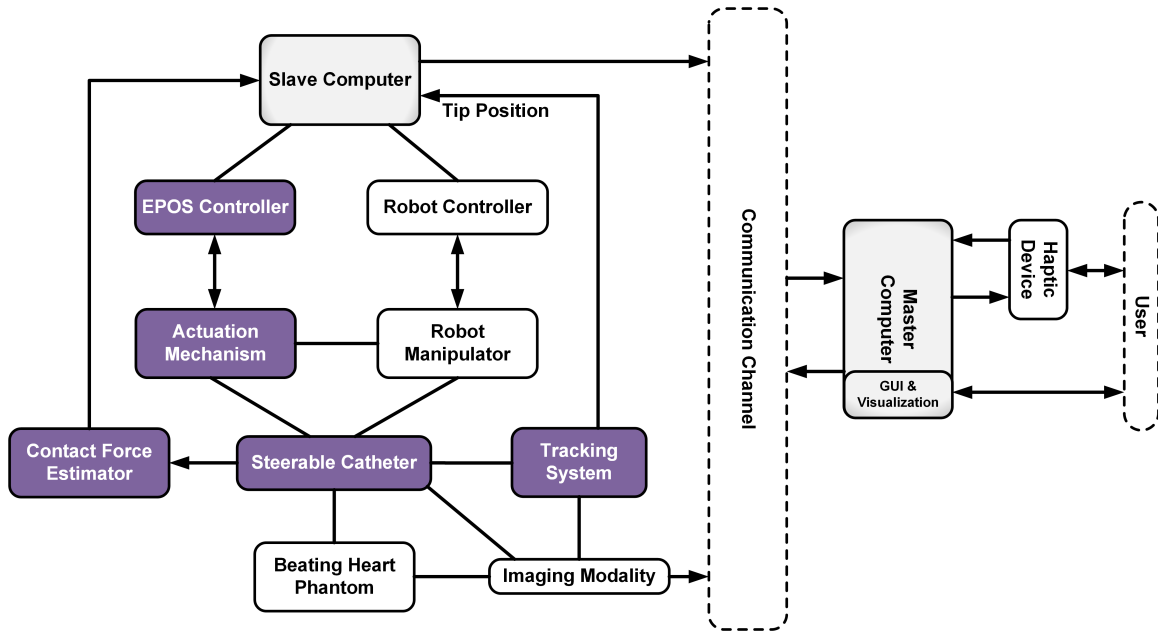


Figure 1.1: Schematic of the master-slave robotic system for catheter-based cardiac ablation.

It should be noted that although the existing robotic catheter manipulation systems (Section 1.3.1.1) improve dexterity and facilitate catheter navigation through the vasculature, many of them do not provide the electrophysiologist with an estimate of the contact force at the catheter tip, and none of them implements force control to ensure a consistent contact between the catheter tip and cardiac tissue. The available force sensing catheters (Section 1.3.1.3) are compatible only with certain equipment, which is not necessarily commonly available. The emerging techniques for placing force sensors at the tip of the catheters (Section 1.3.4.2) either call for significant changes in the current structure of the catheters, or are not well suited for the case of ablation catheters due to the presence of ablation electrode at the catheter tip and/or temperature variations during the ablation procedure. On the other hand, the kinematic models for describing the behavior of continuum manipulators (Section 1.3.3.1) are generally developed based on the assumption that the manipulator is not in contact with the environment and thus actuating the driving tendons causes the manipulator to bend in the form of an arc with constant curvature. This assumption is not valid during the ablation procedure, where not only is the catheter

in contact with the myocardium, but it is also required to apply sufficient force on cardiac tissue to produce the desirable outcome. Not meeting this requirement may lead to poor model performance and inaccurate results.

A robotic system that is capable of manipulating the commonly used ablation catheters and implementing force control at their tip is currently not available. It is evident that in such a robotic system, a measure of the contact force should be provided by techniques other than direct force measurement.

1.5 Thesis Structure and Contributions

This section summarizes the main contributions of this thesis. The outline of the thesis and corresponding contributions in each chapter are as follows.

In Chapter 2, the behavior of the catheter tip in contact with the environment is investigated. The objective of this study is to investigate how the shape of the catheter changes when external forces are applied. A model is proposed to provide a mapping between the contact force and the catheter shape. The main advantage of the suggested approach is that it does not require information about tendon actuation.

- The force-deflection relationship of the catheter tip is described using a large deflection beam model based on Euler-Bernoulli beam theory.
- Two different techniques for including the initial bending of the tip in the calculations are proposed.
- The performance of the proposed model is validated experimentally for both techniques and is compared to that of an FEM-based model.

Chapter 3 proposes an improved static model for the catheter's distal shaft. The well-established static equations are simple to understand and solve, and yield more accurate results.

- The force-deflection relationship of the catheter tip is described with a pseudo-rigid-body (PRB) 3R model originally proposed for a cantilever beam.
- It is shown that the performance of the PRB model is similar to that of the beam model, but the equations are tractable and the model inverse can be easily obtained.

- An algorithm is presented for obtaining the parameters of the PRB 3R model for the catheter.
- The performance of the customized PRB 3R model is validated experimentally and is compared to that of the large deflection beam model used in Chapter 2.
- A more realistic setup is used to further evaluate the performance. Analyses of the results show the superiority of the PRB 3R model.
- A mapping between the proximal handle displacement and the catheter tip angle is obtained.
- It is shown that estimating the contact force using the proposed force-deflection model and the obtained handle displacement-tip angle mapping is feasible.

In Chapter 4, the results of our first attempts to apply force control at the catheter tip are presented. In the designed control system, a custom-designed strain sensor provides an estimate of the contact forces at the catheter tip.

- The control system and the experimental setup are designed.
- The mappings between the proximal handle displacement, the tip angle and the sensor output are derived.
- The controller parameters are tuned using force feedback from a force sensor.
- The full setup including the strain sensor, the controller and the static model is tested to evaluate its performance.

The work in Chapter 5 is inspired by the results in Chapter 4. Observing the limitations in the strain sensor's performance, a thorough analysis on the shape of the catheter's distal shaft in free space and in contact with the environment is carried out.

- An algorithm for extracting the catheter shape from images is developed. This algorithm detects the smallest changes in the curvature of the catheter.
- The curvature of the catheter in free space is analyzed.
- A kinematic model for describing the distal shaft in free space is proposed and the Denavit-Hartenberg (D-H) parameters are derived.
- The Performance of the proposed kinematic model is compared to that of the model presented in Chapter 3 and a constant curvature model from the literature.

- The curvature of the distal tip is analyzed for the cases when the catheter is in contact with the environment.
- A force index that quantifies the effect of contact force on the tip curvature is proposed.
- A Gaussian-Mixture Model (GMM) is used to associate the obtained force index with a force range.
- A framework is suggested for determining where to mount strain sensors on the catheter tip to have the best sensor performance.
- The proposed framework is also used to evaluate the performance of multiple sensors.

In Chapter 6, a robotics-assisted catheter manipulation system is presented. The proposed robotic system maintains a constant force at the catheter tip by compensating for the motion of the moving target.

- An image-based algorithm for obtaining the position and orientation of the catheter tip in real-time is proposed.
- The frequency response of the catheter is analyzed.
- A control system for achieving a desired tip angle in free space is developed.
- A technique for online estimation of the motion frequency is proposed.
- A control system that compensates for the motion of the tissue is developed.
- It is shown that the proposed approach improves the quality of contact between the catheter tip and the moving environment.
- A discussion on the limitations of the system and how the system can be used in a clinical environment is provided.

Chapter 7 summarizes the work presented in this thesis and provides guidelines and suggestions for future work.

References

- [1] “WHO — World Health Organization.” [Online]. Available: www.who.int/mediacentre/factsheets/fs317/en
- [2] “Statistics Canada.” [Online]. Available: www.statcan.gc.ca/pub/84f0209x/84f0209x2009000-eng.pdf
- [3] “The Heart and Stroke Foundation.” [Online]. Available: www.heartandstroke.com
- [4] A. Natale and J. Jalife, *Atrial Fibrillation: From Bench to Bedside*, ser. Contemporary Cardiology. Humana Press, 2008.
- [5] M. Haïssaguerre, P. Sanders, M. Hocini, P. Jaïs, and J. Clémenty, “Pulmonary veins in the substrate for atrial fibrillation: The “venous wave” hypothesis,” *Journal of the American College of Cardiology*, vol. 43, pp. 2290–2292, Jun 2004.
- [6] “St. Jude Medical, Inc.” [Online]. Available: www.sjm.com
- [7] “Biosense Webster, Inc.” [Online]. Available: www.biosensewebster.com
- [8] P.A. Friedman, “Novel mapping techniques for cardiac electrophysiology,” *Heart*, vol. 87, no. 6, pp. 575–582, Jun 2002.
- [9] F. Morady, “Radio-frequency ablation as treatment for cardiac arrhythmias,” *New England Journal of Medicine*, vol. 340, no. 7, pp. 534–544, Feb 1999.
- [10] “Medtronic, Inc.” [Online]. Available: www.medtronic.com

-
- [11] D. Lakkireddy *et al.*, “Impact of a comprehensive safety program on radiation exposure during catheter ablation of atrial fibrillation: a prospective study,” *Journal of Interventional Cardiac Electrophysiology*, vol. 24, pp. 105–112, Mar 2009.
- [12] K. Yokoyama *et al.*, “Novel contact force sensor incorporated in irrigated radiofrequency ablation catheter predicts lesion size and incidence of steam pop and thrombus,” *Circulation: Arrhythmia and Electrophysiology*, vol. 1, no. 5, pp. 354–362, Dec 2008.
- [13] A. Thiagalingam *et al.*, “Importance of catheter contact force during irrigated radiofrequency ablation: Evaluation in a porcine *ex vivo* model using a force-sensing catheter,” *Journal of Cardiovascular Electrophysiology*, vol. 21, no. 7, pp. 806–811, Jul 2010.
- [14] V.Y. Reddy *et al.*, “The relationship between contact force and clinical outcome during radiofrequency catheter ablation of atrial fibrillation in the TOCCATA study,” *Heart Rhythm*, vol. 9, no. 11, pp. 1789 – 1795, Nov 2012.
- [15] M. Martinek *et al.*, “Clinical impact of an open-irrigated radiofrequency catheter with direct force measurement on atrial fibrillation ablation,” *Pacing and Clinical Electrophysiology*, vol. 35, no. 11, pp. 1312–1318, Nov 2012.
- [16] D.C. Shah *et al.*, “Area under the real-time contact force curve (force-time integral) predicts radiofrequency lesion size in an in vitro contractile model,” *Journal of Cardiovascular Electrophysiology*, vol. 21, no. 9, pp. 1038–1043, Sept 2010.
- [17] G. Stabile *et al.*, “Catheter-tissue contact force for pulmonary veins isolation: a pilot multicentre study on effect on procedure and fluoroscopy time,” *Europace*, vol. 16, no. 3, pp. 335–340, Mar 2014.
- [18] F. Perna *et al.*, “Assessment of catheter tip contact force resulting in cardiac perforation in swine atria using force sensing technology,” *Circulation: Arrhythmia and Electrophysiology*, vol. 4, no. 2, pp. 218–224, Apr 2011.

- [19] “Catheter Robotics, Inc.” [Online]. Available: www.catheterrobotics.com
- [20] E. Khan *et al.*, “First experience with a novel robotic remote catheter system: AmigoTM mapping trial,” *Journal of Interventional Cardiac Electrophysiology*, vol. 37, no. 2, pp. 121–129, Aug 2013.
- [21] M. López-Gil *et al.*, “Cavo-tricuspid isthmus radiofrequency ablation using a novel remote navigation catheter system in patients with typical atrial flutter,” *Europace*, Sept 2013.
- [22] “Corindus, Inc.” [Online]. Available: <http://www.corindus.com>
- [23] J.F. Granada *et al.*, “First-in-human evaluation of a novel robotic-assisted coronary angioplasty system,” *Journal of the American College of Cardiology: Cardiovascular Interventions*, vol. 4, no. 4, pp. 460 – 465, Apr 2011.
- [24] G. Weisz *et al.*, “Safety and feasibility of robotic percutaneous coronary intervention - PRECISE (Percutaneous Robotically-Enhanced Coronary Intervention) study,” *Journal of the American College of Cardiology: Cardiovascular Interventions*, vol. 61, no. 15, pp. 1596–1600, Apr 2013.
- [25] “Magnetecs Corp.” [Online]. Available: www.magnetecs.com
- [26] D. Filgueiras-Rama *et al.*, “Remote magnetic navigation for accurate, real-time catheter positioning and ablation in cardiac electrophysiology procedures,” *Journal of Visualized Experiments*, vol. 6, no. 74, pp. e3658–56, Apr 2013.
- [27] “Stereotaxis, Inc.” [Online]. Available: www.stereotaxis.com
- [28] C. Pappone *et al.*, “Robotic magnetic navigation for atrial fibrillation ablation,” *Journal of the American College of Cardiology*, vol. 47, no. 7, pp. 1390–1400, Apr 2006.
- [29] L. Di Biase *et al.*, “Remote magnetic navigation: Human experience in pulmonary vein ablation,” *Journal of the American College of Cardiology*, vol. 50, no. 9, pp. 868 – 874, Aug 2007.

-
- [30] S. Miyazaki *et al.*, “Remote magnetic navigation with irrigated tip catheter for ablation of paroxysmal atrial fibrillation,” *Circulation: Arrhythmia and Electrophysiology*, vol. 3, no. 6, pp. 585–589, Oct 2010.
- [31] K.R. Julian-Chun *et al.*, “Remote-controlled magnetic pulmonary vein isolation using a new irrigated-tip catheter in patients with atrial fibrillation,” *Circulation: Arrhythmia and Electrophysiology*, vol. 3, no. 5, pp. 458–464, Jul 2010.
- [32] B. Schmidt *et al.*, “Remote navigation systems in electrophysiology,” *Europace*, vol. 10, no. suppl 3, pp. iii57–iii61, Nov 2008.
- [33] “Hansen Medical, Inc.” [Online]. Available: www.hansenmedical.com
- [34] S.K. Hussain, J.M. Hobby, D. Harari, and J.M. Mangrum, “Complementary techniques and location of excessive contact force detection in the left atrium with robotic catheter navigation.” [Online]. Available: www.endosense.com – Retrieved on 2014-03-04.
- [35] W. Saliba *et al.*, “Atrial fibrillation ablation using a robotic catheter remote control system: Initial human experience and long-term follow-up results,” *Journal of the American College of Cardiology*, vol. 51, no. 25, pp. 2407 – 2411, Jun 2008.
- [36] P. Kanagaratnam *et al.*, “Experience of robotic catheter ablation in humans using a novel remotely steerable catheter sheath,” *Journal of Interventional Cardiac Electrophysiology*, vol. 21, no. 1, pp. 19–26, Jan. 2008.
- [37] L. Di Biase *et al.*, “Relationship between catheter forces, lesion characteristics, popping, and char formation: experience with robotic navigation system,” *Journal of Cardiovascular Electrophysiology*, vol. 20, no. 4, pp. 436–40, Apr 2009.
- [38] S. Willems *et al.*, “Persistence of pulmonary vein isolation after robotic remote-navigated ablation for atrial fibrillation and its relation to clinical outcome,” *Journal of Cardiovascular Electrophysiology*, vol. 21, no. 10, pp. 1079–1084, Oct 2010.

- [39] R. Bai *et al.*, “Worldwide experience with the robotic navigation system in catheter ablation of atrial fibrillation: Methodology, efficacy and safety,” *Journal of Cardiovascular Electrophysiology*, vol. 23, no. 8, pp. 820–826, Aug 2012.
- [40] B.L. Nguyen, J.L. Merino, and E.S. Gang, “Remote navigation for ablation procedures a new step forward in the treatment of cardiac arrhythmias,” *European Cardiology Review*, vol. 6, no. 3, pp. 50–56, 2010.
- [41] M. Shenasa *et al.*, *Cardiac Mapping*. Wiley-Blackwell, 2012.
- [42] L. Gepstein, G. Hayam, and S.A. Ben-Haim, “A novel method for nonfluoroscopic catheter-based electroanatomical mapping of the heart: In vitro and in vivo accuracy results,” *Circulation*, vol. 95, no. 6, pp. 1611–1622, Mar 1997.
- [43] S. Willems *et al.*, “Catheter ablation of atrial flutter guided by electroanatomic mapping (carto): a randomized comparison to the conventional approach,” *Journal of cardiovascular electrophysiology*, vol. 11, no. 11, pp. 1223–1230, Nov 2000.
- [44] M. Scaglione *et al.*, “Visualization of multiple catheters with electroanatomical mapping reduces x-ray exposure during atrial fibrillation ablation,” *Europace*, vol. 13, no. 7, pp. 955–962, Mar 2011.
- [45] R. Ventura *et al.*, “Catheter ablation of common-type atrial flutter guided by three-dimensional right atrial geometry reconstruction and catheter tracking using cutaneous patches: a randomized prospective study,” *Journal of Cardiovascular Electrophysiology*, vol. 15, no. 10, pp. 1157–1161, Oct 2004.
- [46] H.L. Estner *et al.*, “Electrical isolation of pulmonary veins in patients with atrial fibrillation: reduction of fluoroscopy exposure and procedure duration by the use of a non-fluoroscopic navigation system (navx®),” *Europace*, vol. 8, no. 8, pp. 583–587, Aug. 2006.
- [47] G. Stabile *et al.*, “Reduced fluoroscopy exposure during ablation of atrial fibrillation using a novel electroanatomical navigation system: a multicentre experience,” *Europace*, vol. 14, no. 1, pp. 60–65, Jan. 2012.

-
- [48] B.R. Andrea, C. Piorkowski, T. Gaspar, and G. Hindricks, “A novel method for catheter-tissue contact assessment during atrial fibrillation ablation: The electrical coupling index,” *The Journal of Innovations in Cardiac Rhythm Management*, vol. 2, pp. 118–124, Jan 2011.
- [49] “Endosense SA.” [Online]. Available: www.endosense.com
- [50] “Johnson & Johnson Company.” [Online]. Available: www.jnj.com
- [51] M. Tanimoto *et al.*, “Telesurgery system for intravascular neurosurgery,” in *Medical Image Computing and Computer-Assisted Intervention (MICCAI)*, 2000, vol. 1935, pp. 29–39.
- [52] M. Tanimoto *et al.*, “Micro force sensor for intravascular neurosurgery,” in *IEEE International Conference on Robotics and Automation (ICRA)*, vol. 2, 1997, pp. 1561–1566.
- [53] F. Arai, R. Fujimura, T. Fukuda, and M. Negoro, “New catheter driving method using linear stepping mechanism for intravascular neurosurgery,” in *IEEE International Conference on Robotics and Automation (ICRA)*, vol. 3, 2002, pp. 2944–2949.
- [54] C. Tercero *et al.*, “Autonomous catheter insertion system using magnetic motion capture sensor for endovascular surgery,” *International Journal of Medical Robotics and Computer Assisted Surgery*, vol. 3, no. 1, pp. 52–58, Mar 2007.
- [55] J. Jayender, R.V. Patel, and S. Nikumb, “Robot-assisted catheter insertion using hybrid impedance control,” in *IEEE International Conference on Robotics and Automation (ICRA)*, 2006, pp. 607–612.
- [56] J. Jayender and R.V. Patel, “Wave variables based bilateral teleoperation of an active catheter,” in *IEEE RAS & EMBS International Conference on Biomedical Robotics and Biomechatronics (BioRob)*, 2008, pp. 27–32.

- [57] J. Jayender, M. Azizian, and R.V. Patel, “Bilateral telemanipulation of a flexible catheter in a constrained environment,” in *IEEE International Conference on Robotics and Automation (ICRA)*, 2008, pp. 649–654.
- [58] J. Jayender, M. Azizian, and R.V. Patel, “Autonomous image-guided robot-assisted active catheter insertion,” *IEEE Transactions on Robotics*, vol. 24, no. 4, pp. 858–871, Aug. 2008.
- [59] L. Cencenelli, E. Marcelli, and G. Plicchi, “Initial experience with a telerobotic system to remotely navigate and automatically reposition standard steerable ep catheters,” *ASAIO Journal*, vol. 53, no. 5, pp. 523–529, Sept 2007.
- [60] E. Marcelli, L. Cencenelli, and G. Plicchi, “A novel telerobotic system to remotely navigate standard electrophysiology catheters,” in *Computers in Cardiology*, 2008, pp. 137–140.
- [61] Y. Ganji, F. Janabi-Sharifi, and A. Cheema, “Robot-assisted catheter manipulation for intracardiac navigation,” *International Journal of Computer Assisted Radiology and Surgery*, vol. 4, no. 4, pp. 307–315, Jun. 2009.
- [62] G. Srimathveeravalli, T. Kesavadas, and X. Li, “Design and fabrication of a robotic mechanism for remote steering and positioning of interventional devices,” *International Journal of Medical Robotics and Computer Assisted Surgery*, vol. 6, no. 2, pp. 160–170, Feb 2010.
- [63] J.W. Park *et al.*, “Development of a force-reflecting robotic platform for cardiac catheter navigation,” *Artificial Organs*, vol. 34, no. 11, pp. 1034–1039, Nov 2010.
- [64] J. W. Park, J. Choi, Y. Park, and K. Sun, “Haptic virtual fixture for robotic cardiac catheter navigation,” *Artificial Organs*, vol. 35, no. 11, pp. 1127–1131, Nov 2011.
- [65] Y. Fu, A. Gao, H. Liu, K. Li, and Z. Liang, “Development of a novel robotic catheter system for endovascular minimally invasive surgery,” in *IEEE/ICME International Conference on Complex Medical Engineering (CME)*, 2011, pp. 400–405.

- [66] Y. Fu, A. Gao, H. Liu, and S. Guo, “The master-slave catheterisation system for positioning the steerable catheter,” *International Journal of Mechatronics and Automation*, vol. 1, nos. 3/4, pp. 143–152, 2011.
- [67] C.J. Payne, H. Rafii-Tari, and G.-Z. Yang, “A force feedback system for endovascular catheterisation,” in *IEEE/RSJ International Conference on Intelligent Robots and Systems (IROS)*, 2012, pp. 1298–1304.
- [68] S. Guo, N. Xiao, and B. Gao, “A novel robot-assisted catheter surgery system with force feedback,” in *Selected Topics in Micro/Nano-robotics for Biomedical Applications*. Springer New York, 2013, pp. 175–190.
- [69] H. Rafii-Tari, C. Payne, and G.-Z. Yang, “Current and emerging robot-assisted endovascular catheterization technologies: A review,” *Annals of Biomedical Engineering*, pp. 1–19, Nov 2013.
- [70] G. Robinson and J. Davies, “Continuum robots - a state of the art,” in *IEEE International Conference on Robotics and Automation (ICRA)*, vol. 4, 1999, pp. 2849–2854.
- [71] M.W. Hannan and I.D. Walker, “Analysis and experiments with an elephant’s trunk robot,” *Advanced Robotics*, vol. 15, no. 8, pp. 847–858, Dec. 2001.
- [72] I.A. Gravagne and I.D. Walker, “On the kinematics of remotely-actuated continuum robots,” in *IEEE International Conference on Robotics and Automation (ICRA)*, vol. 3, 2000, pp. 2544–2550.
- [73] M.W. Hannan and I.D. Walker, “Novel kinematics for continuum robots,” in *7th Int. Symp. Advances in Robot Kinematics*. Piran, Slovenia: Kluwer Academic Publishers, 2000, pp. 227–238.
- [74] M.W. Hannan and I.D. Walker, “Kinematics and the implementation of an elephant’s trunk manipulator and other continuum style robots,” *Journal of Robotic Systems*, vol. 20, pp. 45–63, Sept 2003.

-
- [75] B.A. Jones and I.D. Walker, “Kinematics for multisection continuum robots,” *IEEE Transactions on Robotics*, vol. 22, no. 1, pp. 43–55, Feb 2006.
- [76] R.J. Webster and B.A. Jones, “Design and kinematic modeling of constant curvature continuum robots: A review,” *The International Journal of Robotics Research*, vol. 29, no. 13, pp. 1661–1683, Jun 2010.
- [77] D.B. Camarillo, C.F. Milne, C.R. Carlson, M.R. Zinn, and J.K. Salisbury, “Mechanics modeling of tendon-driven continuum manipulators,” *IEEE Transactions on Robotics*, vol. 24, no. 6, pp. 1262–1273, Dec 2008.
- [78] D.B. Camarillo, K.E. Loewke, C.R. Carlson, and J.K. Salisbury, “Vision based 3-D shape sensing of flexible manipulators,” in *IEEE International Conference on Robotics and Automation (ICRA)*, 2008, pp. 2940–2947.
- [79] D.B. Camarillo, C.R. Carlson, and J.K. Salisbury, “Task-space control of continuum manipulators with coupled tendon drive,” in *Experimental Robotics*, 2009, vol. 54, pp. 271–280.
- [80] Y. Ganji and F. Janabi-Sharifi, “Catheter kinematics for intracardiac navigation,” *IEEE Transactions on Biomedical Engineering*, vol. 56, no. 3, pp. 621–632, Mar 2009.
- [81] J. Jung, R.S. Penning, N.J. Ferrier, and M. Zinn, “A modeling approach for continuum robotic manipulators: Effects of nonlinear internal device friction,” in *IEEE/RSJ International Conference on Intelligent Robots and Systems (IROS)*, 2011, pp. 5139–5146.
- [82] J. Jung, R.S. Penning, and M.R. Zinn, “A modeling approach for robotic catheters: effects of nonlinear internal device friction,” *Advanced Robotics*, vol. 28, no. 8, pp. 557–572, Jan 2014.
- [83] R.S. Penning, J. Jung, J. Borgstadt, N.J. Ferrier, and M.R. Zinn, “Towards closed loop control of a continuum robotic manipulator for medical applications,” in *IEEE International Conference on Robotics and Automation (ICRA)*, 2011, pp. 4822–4827.

- [84] K. Ikuta, K. Iritani, and J. Fukuyama, “Mobile virtual endoscope system with haptic and visual information for non-invasive inspection training,” in *IEEE International Conference on Robotics and Automation (ICRA)*, vol. 2, 2001, pp. 2037–2044.
- [85] S.L. Dawson, S. Cotin, D. Meglan, D.W. Shaffer, and M.A. Ferrell, “Designing a computer-based simulator for interventional cardiology training,” *Catheterization and Cardiovascular Interventions*, vol. 51, no. 4, pp. 522–527, Dec 2000.
- [86] M. Kukuk and B. Geiger, “A real-time deformable model for flexible instruments inserted into tubular structures,” in *Medical Image Computing and Computer-Assisted Intervention (MICCAI)*, 2002, vol. 2489, pp. 331–338.
- [87] M.K. Konings, E. van de Kraats, T. Alderliesten, and W.J. Niessen, “Analytical guide wire motion algorithm for simulation of endovascular interventions,” *Medical and Biological Engineering and Computing*, vol. 41, pp. 689–700, Nov 2003.
- [88] T. Alderliesten, M.K. Konings, and W.J. Niessen, “Modeling friction, intrinsic curvature, and rotation of guide wires for simulation of minimally invasive vascular interventions,” *IEEE Transactions on Biomedical Engineering*, vol. 54, no. 1, pp. 29–38, Jan 2007.
- [89] W. Lawton, R. Raghavan, S.R. Ranjan, and R. Viswanathan, “Ribbons and groups : a thin rod theory for catheters and filaments,” *Journal of Physics A: Mathematical and General*, vol. 32, pp. 1709–1735, Mar 1999.
- [90] S. Cotin, C. Duriez, J. Lenoir, P. Neumann, and S. Dawson, “New approaches to catheter navigation for interventional radiology simulation,” in *Medical Image Computing and Computer-Assisted Intervention (MICCAI)*, 2005, vol. 3750, pp. 534–542.
- [91] J. Lenoir, S. Cotin, C. Duriez, and P. Neumann, “Interactive physically-based simulation of catheter and guidewire,” *Computers & Graphics*, vol. 30, no. 3, pp. 416–422, Jun 2006.

- [92] W. Tang *et al.*, “A realistic elastic rod model for real-time simulation of minimally invasive vascular interventions,” *The Visual Computer*, vol. 26, no. 9, pp. 1157–1165, Sept 2010.
- [93] W. Tang, T.R. Wan, D.A. Gould, T. How, and N.W. John, “A stable and real-time nonlinear elastic approach to simulating guidewire and catheter insertions based on cosserat rod,” *IEEE Transactions on Biomedical Engineering*, vol. 59, no. 8, pp. 2211–2218, Aug 2012.
- [94] Y. Fu, H. Liu, W. Huang, S. Wang, and Z. Liang, “Steerable catheters in minimally invasive vascular surgery,” *International Journal of Medical Robotics and Computer Assisted Surgery*, vol. 5, no. 4, pp. 381–391, Dec. 2009.
- [95] Y. Haga, Y. Tanahashi, and M. Esashi, “Small diameter active catheter using shape memory alloy,” in *International Workshop on Micro Electro Mechanical Systems*, 1998, pp. 419–424.
- [96] T. Shoa, J.D. Madden, N. Fekri, N.R. Munce, and V.X.D. Yang, “Conducting polymer based active catheter for minimally invasive interventions inside arteries,” in *International Conference of the IEEE Engineering in Medicine and Biology Society (EMBS)*, 2008, pp. 2063–2066.
- [97] Y. Bailly and Y. Amirat, “Modeling and control of a hybrid continuum active catheter for aortic aneurysm treatment,” in *IEEE International Conference on Robotics and Automation (ICRA)*, 2005, pp. 924–929.
- [98] Y. Haga, Y. Muyari, T. Mineta, T. Matsunaga, H. Akahori, and M. Esashi, “Small diameter hydraulic active bending catheter using laser processed super elastic alloy and silicone rubber tube,” in *IEEE/EMBS Special Topic Conference on Microtechnology in Medicine and Biology*, 2005, pp. 245–248.
- [99] P. Polygerinos *et al.*, “Novel miniature MRI-compatible fiber-optic force sensor for cardiac catheterization procedures,” in *IEEE International Conference on Robotics and Automation (ICRA)*, 2010, pp. 2598–2603.

-
- [100] P. Polygerinos *et al.*, “MRI-compatible intensity-modulated force sensor for cardiac catheterization procedures,” *IEEE Transactions on Biomedical Engineering*, vol. 58, no. 3, pp. 721–726, Mar 2011.
- [101] P. Polygerinos, L.D. Seneviratne, R. Razavi, T. Schaeffter, and K. Althofer, “Triaxial catheter-tip force sensor for mri-guided cardiac procedures,” *IEEE/ASME Transactions on Mechatronics*, vol. 18, no. 1, pp. 386–396, Feb 2013.
- [102] S.B. Kesner and R.D. Howe, “Design principles for rapid prototyping forces sensors using 3-d printing,” *IEEE/ASME Transactions on Mechatronics*, vol. 16, no. 5, pp. 866–870, Oct 2011.
- [103] S.B. Kesner and R.D. Howe, “Force control of flexible catheter robots for beating heart surgery,” *IEEE International Conference on Robotics and Automation (ICRA)*, pp. 1589–1594, 2011.

Chapter 2

Static Modeling Based on Beam Theory

2.1 Introduction

Catheter-based cardiac ablation has gained increasing popularity in the treatment of heart arrhythmias during the past two decades. It has become the most widely accepted interventional treatment for cardiac arrhythmias with a high success rate [2], [3]. However, it is considered a challenging interventional procedure which may take up to 4 hours [4]. The major complexity arises from the fact that guidance and control of the distal tip of a catheter inside a beating heart is difficult without proper 3D visualization, dexterous control of the flexible catheter and a sense of touch at the catheter tip. There are commercial software packages which provide 3D visualization of the heart and catheter using electro-anatomical mappings and/or pre-operative CT/MRI images of a patient's heart. Azizian and Patel [5] proposed the use of online 3D ultrasound-based visualization of the heart and ablation catheter using transthoracic echocardiography (TTE) images.

Robotic catheter control systems have also been developed to provide dexterous manipulation of flexible ablation catheters. The Sensei[®] robotic catheter system (Hansen Medical, Mountain View, CA) provides a master/slave control system for remote navigation and control of an ablation catheter using a steerable sheath [6]; It also displays a rough estimation of the tip contact forces on the screen [2]. The NIOBE[®] magnetic navigation system (Stereotaxis, St. Louis, MO) provides magnetic navigation of a soft catheter [7]. Jayender *et al.* [8] proposed a master-slave

A version of this chapter has been presented in *IEEE International Conference on Robotics and Automation (ICRA)*, 2012 and has been published in [1]. [©2012 IEEE]

robotic system which guides an active catheter instrumented with Shape Memory Alloy (SMA) actuators through the vasculature. However, none of these systems provide haptic feedback or any sort of force/impedance control of the catheter tip.

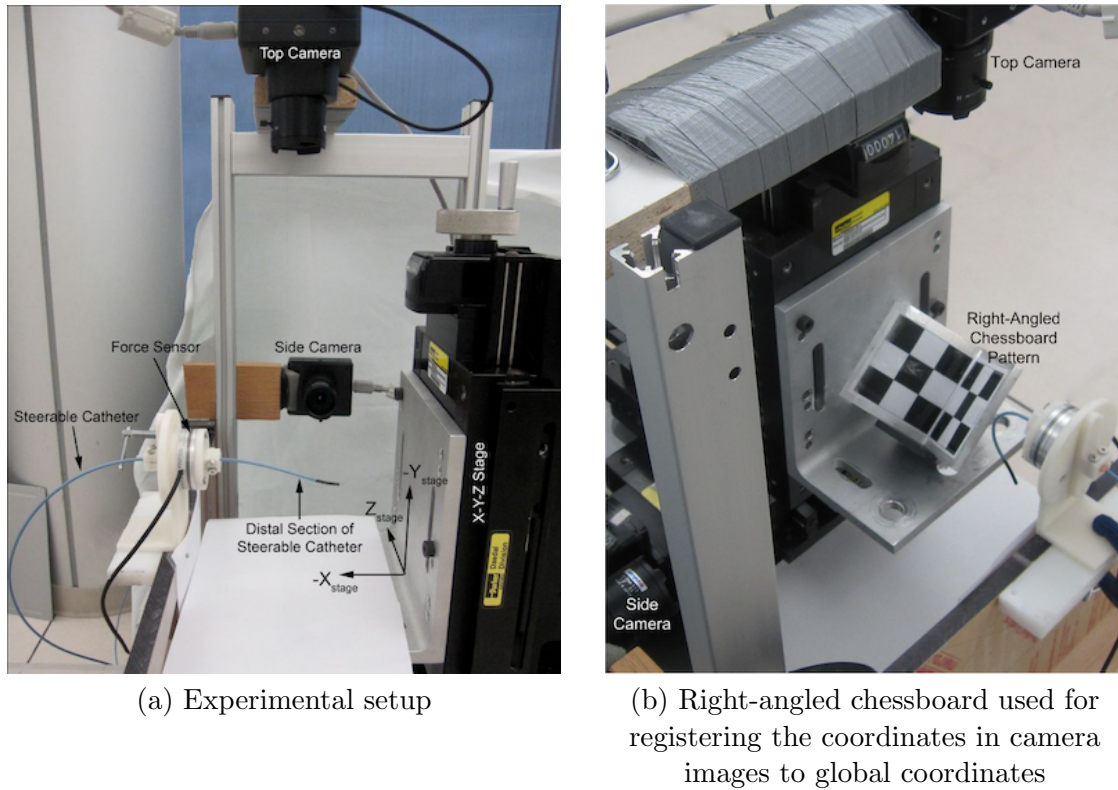
Studies show that the forces applied by the catheter tip to the heart tissue have a great impact on the outcome of the ablation procedure [2]. Insufficient force could lead to incomplete ablation, while excessive forces could result in complications such as cardiac perforation. Therefore, it would be very useful to provide the cardiologist with a measure of the contact force at the distal tip of the catheter to help him/her perform a faster and more reliable interventional procedure with less complications due to improper catheter/endocardium contact during ablation. It would also be useful to perform a hybrid position/force or impedance control on the catheter tip in order to regulate the applied force at a desired level while keeping contact at a target location on the beating heart wall. Recent work by Kesner and Howe [9] has proposed a robotic catheter system to assist with surgery performed inside the beating heart such as mitral valve annuloplasty. The proposed system benefits from a force sensor mounted right at the tip of the catheter and a force controller which aids in maintaining a constant contact force at the catheter tip during the procedure in spite of the beating heart motion.

Control of the contact force or impedance at the tip of a steerable catheter requires a model of its distal section. The problem of modeling a catheter has been studied by a number of research groups and several different methods have been proposed. Numerical approaches have been used for modeling and simulating a catheter inside the vasculature. Ikuta *et al.* [10] and Dawson *et al.* [11] proposed a multibody system for modeling long flexible instruments, such as catheters or endoscopes, in which the flexible device is modeled as a set of rigid links connected by flexible joints. Another technique was suggested by Kukuk *et al.* [12], where all possible shapes for a discretized flexible instrument are found and then the shape which complies best with the physical and mechanical constraints is selected. Another approach was proposed by Konings *et al.* [13]. It considers a guidewire as a series of small rigid segments connected with joints and finds the shape of the guidewire within the vasculature based on the principle of minimization of energy, where energy is defined as a function of the

positions of all joints. Another category of numerical methods assumes that a wire-like object is composed of multiple beams and uses a finite element method (FEM) to model it [14–16]. Although FEM can be used to model the behavior of long flexible instruments, it is computationally expensive and may lead to inaccurate results if all the constraints are not known.

Continuum robot theory is another approach to modeling a catheter [17]. The behavior of continuum robots has been well studied and different models have been proposed [18–20]. Camarillo *et al.* [21] developed a model for tendon-driven continuum robots which can also be used for pull-wire catheters. In this model, a single section of the manipulator is considered as a cantilever beam which undergoes large deflection due to actuation by a single tendon. The displacements of tendons are employed to determine the shape of the manipulator using a mapping between tendon displacements and the shape of the beam. However, this approach requires detailed information of the actuators of a continuum robot which is not available for a catheter.

We model the distal section of a steerable ablation catheter as a beam that undergoes large deflections and investigate the performance of such a model. The developed model describes the in-plane bending of a catheter when the applied forces are also in the catheter plane. The pull-wire bending of the catheter is modeled with two different approaches and the results are compared. Notably, the proposed model does not require extensive knowledge of the internal structure of the catheter and it can be applied to an arbitrary steerable ablation catheter with a fairly simple calibration step. An experimental setup is used to validate the proposed model empirically. This setup is described in Section 2.2. The mathematical model of a beam with large deflections along with the approaches taken to describe the pull-wire bending of the catheter tip is presented in Section 2.3. Section 2.4 reports experimental results which are then discussed in Section 2.5. Section 2.6 concludes the chapter with suggestions for future research.



(a) Experimental setup

(b) Right-angled chessboard used for registering the coordinates in camera images to global coordinates

Figure 2.1: Experimental setup.

2.2 Experimental Setup

The experimental setup is shown in Figure 2.1. A conventional 5-Fr catheter, which can bend only in one direction, is used in the experiments for collecting force-deflection data. The adopted force sensor is Nano43 from ATI Industrial Automation. This is a multi-axis force/torque sensor that measures all six components of the force and torque. The force sensor is mounted on the catheter at 60 mm from the ablation tip. Two cameras (Dragonfly from Point Grey) capture 640×480 resolution images and record the shape of the catheter for each applied force. An X-Y-Z linear stage is used to apply force to the catheter tip and hence deflect it in different directions. Global coordinates are considered along the three directions of the linear stage, as shown in Figure 2.1.

2.2.1 Camera Registration

The two cameras are positioned perpendicularly, one on the side and the other above the catheter tip and are used for generating the 3D shape of the catheter tip for each applied force. A right-angled chessboard pattern (Figure 2.1b) is fixed to the linear stage. Since the position of points on the chessboard are known in its local coordinates and the chessboard is in a known position with respect to the linear stage, describing the chessboard points in global coordinates is straightforward and the chessboard can be used to register the two cameras to global coordinates. The registration process is as follows [8]:

1. The coordinates of the corners of the chessboard in global coordinates are determined. The set of these points is denoted by C .
2. Using the linear stage, the chessboard is moved step-by-step in each direction. In each step, images of the chessboard are captured from both views. I_s and I_t represent the images for side and top cameras, respectively.
3. Corner points in images I_s and I_t are extracted and arranged in two set points C_s and C_t in the same order as the points in C for side and top images, respectively.
4. The transformation that describes the coordinates of image points in global coordinates is determined by the least-squares method.

For obtaining the transformation relating the image points to global coordinates, three sets of points are defined: $C_s = \{(x_{s_k}, z_{s_k}) | k = 1, \dots, j\}$, $C_t = \{(x_{t_k}, y_{t_k}) | k = 1, \dots, j\}$ and $C = \{(x_k, y_k, z_k) | k = 1, \dots, j\}$, where j is the number of points used for registration. These points may be rearranged in matrix form as:

$$Q = \begin{bmatrix} x_{t1} & \dots & x_{tj} \\ y_{t1} & \dots & y_{tj} \\ x_{s1} & \dots & x_{sj} \\ z_{s1} & \dots & z_{sj} \end{bmatrix}, \quad C = \begin{bmatrix} x_1 & \dots & x_j \\ y_1 & \dots & y_j \\ z_1 & \dots & z_j \end{bmatrix} \quad (2.1)$$

The transformation that maps Q into C is a 3×4 matrix, namely T , which is obtained by solving the following optimization problem:

$$\min_T ||TQ - C|| \quad (2.2)$$

The optimization problem has a unique solution when there are at least four nonplanar points. In our case, 8 nonplanar points can be extracted from the chessboard, so a unique transformation matrix, T_0 , can be calculated. The matrix T_0 can then be used for determining the 3D coordinates of a point, based on the images from the side and top cameras. If a point c_p has the coordinates $c_{ps} = [x_{ps} \ z_{ps}]^T$ and $c_{pt} = [x_{pt} \ y_{pt}]^T$ in the side and top cameras, respectively, then its 3D coordinates in global coordinate frame, will be:

$$c_p = \begin{bmatrix} x_p \\ y_p \\ z_p \end{bmatrix} = T_0 \begin{bmatrix} c_{pt} \\ \dots \\ c_{ps} \end{bmatrix} \quad (2.3)$$

For registration, the chessboard was moved by 2-mm steps in each direction for 10 steps using the linear stage. In each step, images of the chessboard are captured by each of the cameras, resulting in 31 images for each of them. Hence, 248 points are used for registration. The standard deviation of the registration error is 0.6 mm, 0.38 mm and 0.35 mm in x , y and z directions, respectively.

2.3 2D Static Model for the Catheter tip

The goal is to develop a static model which describes the mapping between the force sensor readings and the ablation tip deflection for the catheter. We assume that the catheter is positioned inside the heart chamber manually. The focus is on the distal deflectable shaft of the catheter that comes out of its sheath. It is assumed that this shaft cannot move in and out of the sheath and cannot rotate from its base. With these assumptions, the catheter tip inside the heart chamber is similar to a cantilever beam and the same boundary conditions apply, *i.e.*, the catheter tip is fixed at one end and the other end is free and experiences applied forces. It is also assumed that the catheter is adjusted such that the applied forces and the bending of the tip all

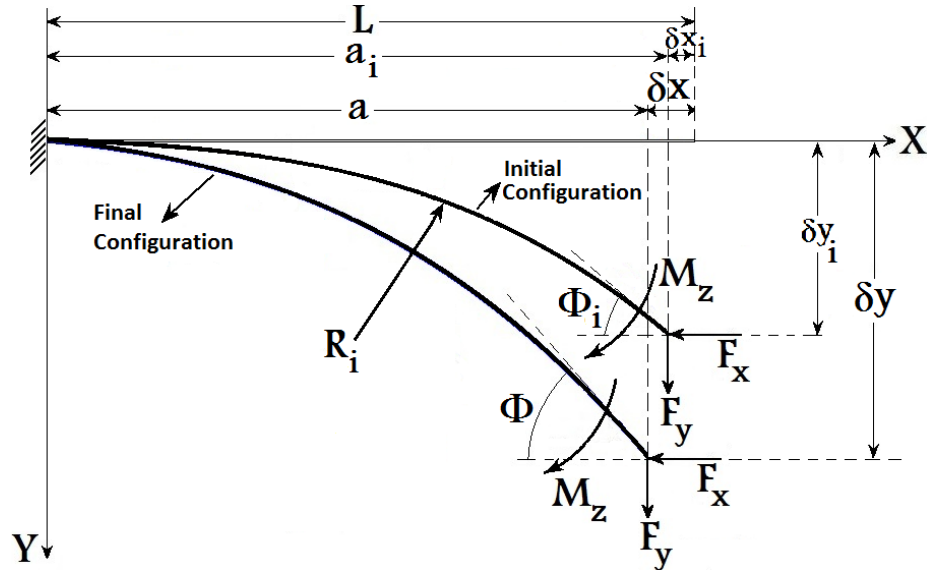


Figure 2.2: Deflection of an initially curved cantilever beam caused by external loads concentrated at the free end

occur in a 2D plane.

2.3.1 Large Deflection Beam Model

Figure 2.2 shows a uniform thickness initially curved cantilever beam that is loaded with three end loads: F_x , F_y and M_z . To derive the load-displacement relations for this beam, it is assumed that Euler-Bernoulli assumptions are valid and hence the curvature κ at any point of the beam is proportional to the bending moment M at that point, i.e.,

$$EI\kappa = M \quad (2.4)$$

where E is the Young's modulus and I is the moment of inertia of the beam cross-section around the natural axis. It is also assumed that bending does not change the length of the beam.

In Figure 2.2, L denotes the length of the beam, δx and δy are the horizontal and vertical components of displacement at the loaded end, respectively, R_i is the radius of curvature in the undeflected beam shape and $\Phi = \phi_{tip}$ is the maximum deflection angle of the beam that occurs at the loaded tip. Parameters with subscript "i" relate

to the initial configuration of the beam. The origin of the Cartesian coordinate system is assumed to be at the fixed end of the beam. The exact equation for the curvature is stated in terms of arc length s and slope angle ϕ as:

$$\kappa = \frac{d\phi}{ds} \quad (2.5)$$

For small deflections, δx (Figure 2.2) is negligible and the curvature at any point of the beam can be approximated by [22]

$$\kappa = \frac{d^2y}{dx^2} \quad (2.6)$$

Hence in the case of small deflections, the load-displacement relation is reduced to a linear one. However, since the catheter tip can bend from zero to over 90° , a small-deflection model will not yield accurate results. Moreover, the catheter tip is deflected before it comes in contact with the tissue, implying that a more comprehensive model should be sought for the catheter. The bending moment M at an arbitrary point (x, y) along the beam is

$$M = F_x(\delta y - y) + F_y(L - x - \delta x) \quad (2.7)$$

Substituting Equations (2.7) and (2.5) in Equation (2.4) and differentiating both sides with respect to s yields

$$EI \frac{d^2\phi}{ds^2} = -F_x \frac{dy}{ds} - F_y \frac{dx}{ds} \quad (2.8)$$

From Figure 2.2, $\frac{dx}{ds} = \cos \phi$ and $\frac{dy}{ds} = \sin \phi$, resulting in

$$EI \frac{d^2\phi}{ds^2} = -F_x \sin \phi - F_y \cos \phi \quad (2.9)$$

$$\Rightarrow \frac{d}{ds} \left\{ \frac{1}{2} EI \left(\frac{d\phi}{ds} \right)^2 - F_x \cos \phi + F_y \sin \phi \right\} = 0 \quad (2.10)$$

$$\Rightarrow \frac{1}{2} EI \left(\frac{d\phi}{ds} \right)^2 - F_x \cos \phi + F_y \sin \phi = C \quad (2.11)$$

The constant of integration, C , is determined by observing that at the free end

$$\left. \frac{d\phi}{ds} \right|_{s=L} = \frac{M_z}{EI} + \frac{1}{R_i} \quad (2.12)$$

$$\Rightarrow C = \frac{1}{2}EI \left(\frac{M_z}{EI} + \frac{1}{R_i} \right)^2 + F_y \sin \Phi - F_x \cos \Phi \quad (2.13)$$

For simplicity, the following notations are used:

$$F_y = P \quad , \quad F_x = nP \quad , \quad \alpha^2 = \frac{PL^2}{EI} \quad , \quad \eta = \sqrt{1+n^2} \quad , \quad \Theta_F = \tan^{-1} \frac{1}{-n} \quad (2.14)$$

then the following holds:

$$\alpha = \frac{1}{\sqrt{2}} \int_0^\Phi \frac{d\phi}{\sqrt{\sin \Phi - n \cos \Phi - \sin \phi + n \cos \phi + \left(\frac{M_z}{EI} + \frac{1}{R_i} \right)^2 \frac{EI}{2P}}} \quad (2.15)$$

After some trigonometric manipulation, Equation (2.15) can be rewritten as

$$\alpha = \frac{1}{\sqrt{2}} \int_0^\Phi \frac{d\phi}{\sqrt{\eta [\cos(\Theta_F - \Phi) - \cos(\Theta_F - \phi)] + \frac{1}{2} \left(\frac{M_z}{EI} + \frac{1}{R_i} \right)^2 \frac{L^2}{\alpha^2}}} \quad (2.16)$$

Taking into account that $\cos \phi = \frac{dx}{ds}$ and $\sin \phi = \frac{dy}{ds}$, the horizontal and vertical deflection of the tip are found as

$$a = L - \delta x = \frac{L}{\alpha\sqrt{2}} \int_0^\Phi \frac{\cos \phi d\phi}{\sqrt{\eta [\cos(\Theta_F - \Phi) - \cos(\Theta_F - \phi)] + \frac{1}{2} \left(\frac{M_z}{EI} + \frac{1}{R_i} \right)^2 \frac{L^2}{\alpha^2}}} \quad (2.17)$$

$$\delta y = \frac{L}{\alpha\sqrt{2}} \int_0^\Phi \frac{\sin \phi d\phi}{\sqrt{\eta [\cos(\Theta_F - \Phi) - \cos(\Theta_F - \phi)] + \frac{1}{2} \left(\frac{M_z}{EI} + \frac{1}{R_i} \right)^2 \frac{L^2}{\alpha^2}}} \quad (2.18)$$

In Equations(2.16)-(2.18), the parameters α, M_z, Θ_F define the loads applied at the

tip and the parameters $\Phi, a, \delta y$ describe the tip deflection. Unfortunately, it is not convenient to solve for deflection parameters when the load parameters are known, since the parameter Φ is one of the integration limits. A number of techniques have been proposed to solve large-deflection beam equations; *e.g.*, Howell [23] suggested a solution based on elliptic integrals and Saxena and Kramer [24] solved the problem using numerical methods.

2.3.2 Modeling the Initial Bending of the Catheter Tip

Using the proximal handle, the catheter tip may be bent into different angles before the external forces are applied. In pull-wire catheters, the pull-wires are coaxial with the hollow catheter body and are extended from the proximal handle to the distal tip, where they are attached. Manipulating the proximal handle will put tension on just one of the pull wires, resulting in the in-plane deflection of the distal tip. With such a mechanism, the tension force in a pull-wire creates a moment at the catheter tip, which causes tip deflection.

The load-displacement relations derived in the previous section are valid when $\alpha \neq 0$. To estimate the moment that causes the initial bending of the catheter, Equations (2.4) and (2.5) can be used to obtain:

$$\frac{d\phi}{ds} = \frac{1}{EI} M_z \quad (2.19)$$

Integrating Equation (2.19) over the beam length yields:

$$M_z = \frac{EI}{L} \Phi \quad (2.20)$$

Based on the large deflection model presented in the previous section and the end moment load-tip deflection angle relation (Equation (2.20)), the initial bending of the catheter can be modeled with two different approaches:

1. Initial curvature approach: It is assumed that the bent catheter is an “initially curved beam” with the initial radius of curvature R_i , on which the external forces with arbitrary in-plane directions are applied.

2. Moment approach: The bending of the catheter tip before applying the external forces is used to calculate the moment at the tip using Equation (2.20). The external forces are then applied in arbitrary in-plane directions and measured by the force sensor.

In both approaches, the tip deflection caused by external loads is calculated and then compared to the actual tip deflection obtained from images.

2.3.3 Analysing the Effect of Beam Rigidity on the Load-Displacement Relation

To investigate how the large deflections of a cantilever beam relate to the applied end loads, an estimate of the rigidity of the beam is required. Figure 2.3 shows how the value of the product $E * I$ affects the load-displacement relation of a cantilever beam. The resulting curves shown in this figure are obtained using the following arbitrarily chosen nominal values for parameters:

$$\begin{aligned} n = 0 \quad , \quad L = 60 \text{ mm} \quad , \quad R_i = 120 \text{ mm} \\ M_z = 0 \text{ gf.mm}^2 \quad , \quad EI_0 = 60000 \text{ g.mm}^2 \end{aligned} \quad (2.21)$$

From Figure 2.3, in the range of applied loads, if the value of $E * I$ is not estimated correctly, there will be an increasing error between the real value of the deflection angle and the calculated one obtained from the beam model equations (Equations (2.16)-(2.18)). This fact does not depend on the nominal values for the other parameters (Equation (2.21)).

2.3.4 Finite Element Analysis of the Catheter Tip

Numerical methods provide a different approach to finding the deflection of the catheter tip when the loads are applied to its free end. Herein, the performance of the finite element method in describing the load-deflection relation of the catheter tip is compared to that of the analytical beam model.

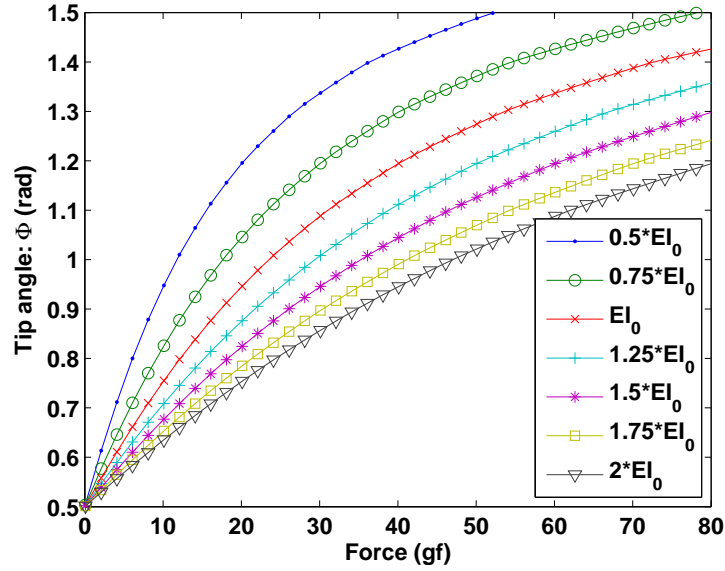


Figure 2.3: Relation between the beam tip deflection Φ and the end force P for different values of $E * I$

The catheter tip is decomposed into a number of two-dimensional beam elements shown in Figure 2.4, where L_e is the length of the beam element, f_x is the axial force, f_y is the transverse force and f_θ is the bending moment at each node. The beam has three degrees of freedom for each node, namely horizontal displacement (u_x), transverse displacement (u_y) and angular rotation (u_θ).

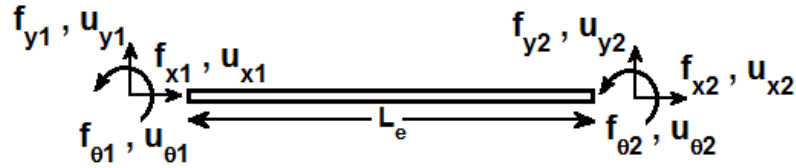


Figure 2.4: A beam element

For each of the beam elements, the elementary stiffness matrix K_e is a 6×6 symmetric matrix that relates the position of each node to the loads applied to the

element

$$K_e = \begin{bmatrix} \frac{AE}{L_e} & 0 & 0 & -\frac{AE}{L_e} & 0 & 0 \\ 0 & \frac{12EI}{L_e^3} & \frac{6EI}{L_e^2} & 0 & -\frac{12EI}{L_e^3} & \frac{6EI}{L_e^2} \\ 0 & \frac{6EI}{L_e^2} & \frac{4EI}{L_e} & 0 & -\frac{6EI}{L_e^2} & \frac{2EI}{L_e} \\ -\frac{AE}{L_e} & 0 & 0 & \frac{AE}{L_e} & 0 & 0 \\ 0 & -\frac{12EI}{L_e^3} & -\frac{6EI}{L_e^2} & 0 & \frac{12EI}{L_e^3} & -\frac{6EI}{L_e^2} \\ 0 & \frac{6EI}{L_e^2} & \frac{2EI}{L_e} & 0 & -\frac{6EI}{L_e^2} & -\frac{4EI}{L_e} \end{bmatrix} \quad (2.22)$$

where A is the beam cross-section area, L_e is the length of the beam element, E is the Young's modulus and I is the moment of inertia of the beam cross-section. The global stiffness matrix, K is then calculated by combining the contribution of each beam element toward the overall displacement. The equation that describes the relation between the applied forces and the position of the beam ends is

$$KU = F \quad , \quad U = \begin{bmatrix} u_{x1} \\ u_{y1} \\ u_{\theta1} \\ u_{x2} \\ u_{y2} \\ u_{\theta2} \end{bmatrix} \quad , \quad F = \begin{bmatrix} f_{x1} \\ f_{y1} \\ f_{\theta1} \\ f_{x2} \\ f_{y2} \\ f_{\theta2} \end{bmatrix} \quad (2.23)$$

The catheter tip is assumed to be a cantilever beam and hence the boundary conditions for the base node (the clamped end of the tip) will be

$$u_{x1} = u_{y1} = u_{z1} = 0 \quad (2.24)$$

This linear formulation cannot be used directly to obtain the tip deflection, since in the case of the catheter, tip deflections are large and hence nonlinear. To solve this problem, in a method similar to that used in [14], the applied force is increased gradually upto its final value (measured by the force sensor) and the stiffness matrix K is updated at each step.

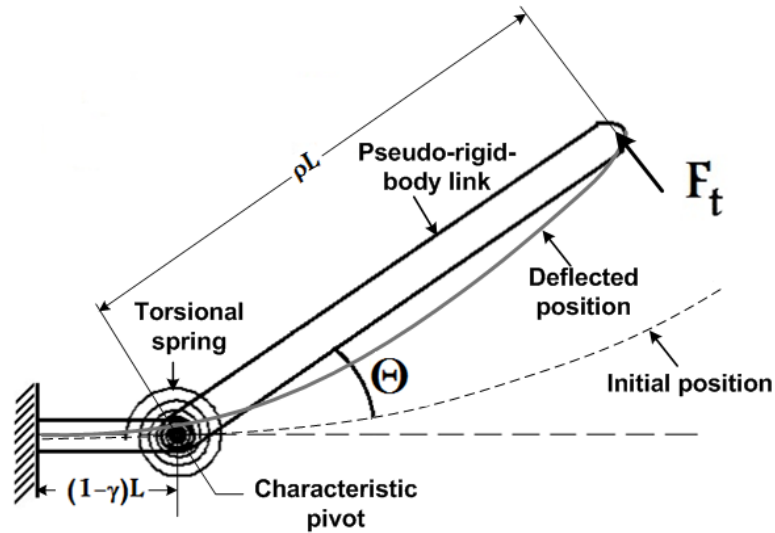


Figure 2.5: Pseudo-rigid-body model for an initially curved cantilever beam

2.4 Experimental Results

The performance of the large deflection beam model for describing the behavior of the catheter tip is evaluated experimentally. It should be noted that the forces applied at the tip of the catheter are equal to those read by the mounted force sensor. This fact, theoretically proved by the static equilibrium equations for the catheter tip, is also validated experimentally. Another force sensor was placed right at the tip of the catheter and it was verified that the difference between the readings of the force sensors does not exceed 0.1 gram-force (gf). The catheter tip mass is estimated to be 1 g and it was verified experimentally that it does not contribute to the tip deflection. Nevertheless, the weight can be easily included in the applied loads without the need for altering the model.

2.4.1 Rigidity of the Catheter Tip

A pseudo-rigid-body model can be used to determine the rigidity of the catheter tip at each deflection angle. Using this model for describing the large deflections of an initially curved beam (Figure 2.5), the deflection angle Θ depends on the applied transverse force F_t through [25]:

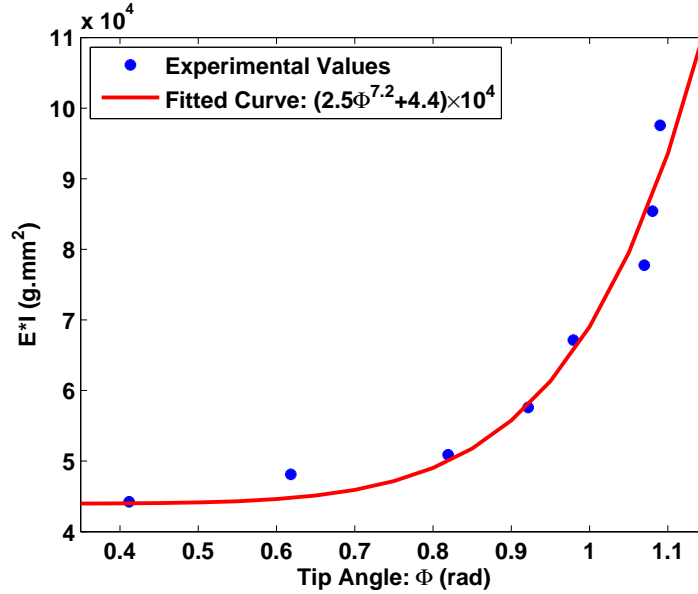


Figure 2.6: Relation between the catheter tip deflection Φ and the value of EI for the catheter tip

$$\Theta = \frac{L^2}{K_{\Theta} EI} F_t \quad (2.25)$$

where L is the length of the beam, γ is the characteristic radius, K_{Θ} is the stiffness coefficient and ρ is a function of γ and the curvature [25].

Using Equation (2.25), the value of the product $E * I$ is determined experimentally for a number of bending angles. Figure 2.6 shows the experimental results and the curve to which the points are fitted. For each bending angle at the catheter tip, the corresponding value for EI is used in the beam equations (Equations (2.16)-(2.18)) to predict the final shape of the catheter from the initial bending and force data.

2.4.2 Evaluating Model Performance

Using the experimental setup described in Section 2.2, force and deflection data are collected with three different approaches. These three approaches will be helpful in observing how the previous shape of the catheter affects its current shape:

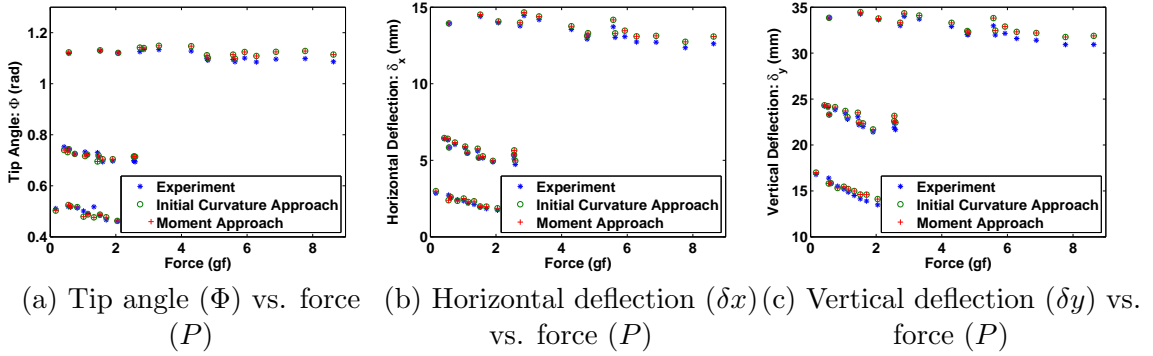


Figure 2.7: Estimation of Φ , δx and δy for dataset \mathcal{A} , when P is measured using the force sensor and $n = 0$.

1. The catheter tip is bent to an initial angle. A concentrated vertical force ($n = 0$) is applied at the tip and force data and the catheter shape are recorded. The force is released and the catheter restores its initial bent shape before force is applied for the next sample. The data collected using this approach is stored as dataset \mathcal{A} .
2. The catheter tip is bent to an initial angle and a concentrated vertical force ($n = 0$) is applied at the tip. The force and deflection data are recorded consecutively without restoring the catheter to its initial bent shape between each two samples. Moreover, the tip angle may change during data collection using the catheter handle at the proximal end. The dataset \mathcal{B} includes the data points collected at different tip angles.
3. The catheter tip is bent to an initial angle and a series of increasing concentrated axial loads ($n = -\cot \Phi$) are applied. Using the catheter's proximal handle, the catheter tip is returned to its straight position before the tip is bent to reach a new deflection angle. The force and deflection data collected using this approach are stored as dataset \mathcal{C} .

For all datasets, the beam model takes the initial bending angle of the tip and the force data to calculate the final deflection angle, which is then compared to the actual value measured experimentally. The results are shown in Figures 2.7-2.9 for both the initial curvature and moment approaches.

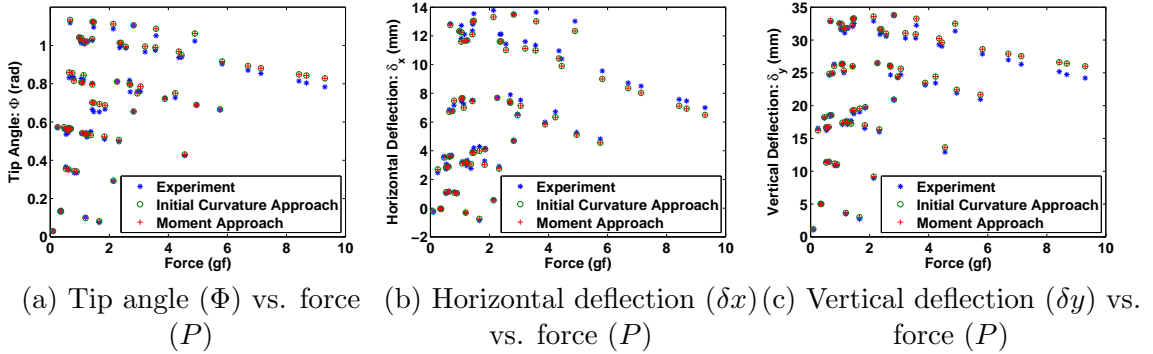


Figure 2.8: Estimation of Φ , δx and δy for dataset \mathcal{B} , when P is measured using the force sensor and $n = 0$.

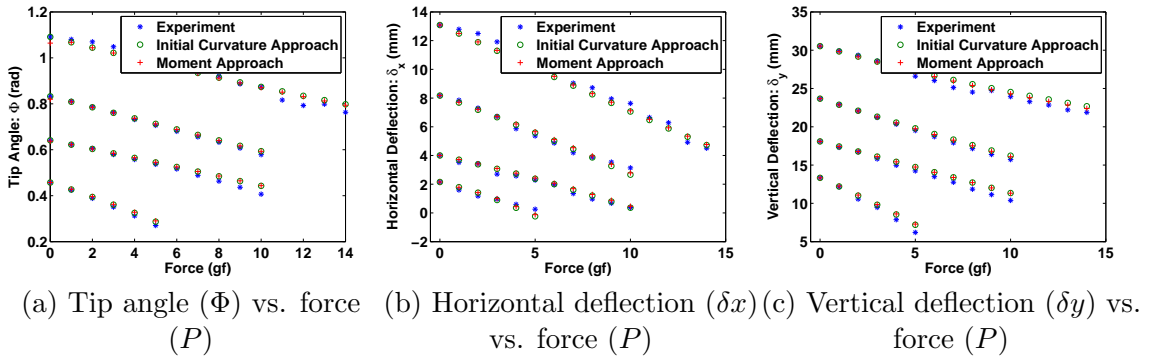


Figure 2.9: Estimation of Φ , δx and δy for dataset \mathcal{C} , when P is measured using the force sensor and $n = -\cot \Phi$.

Table 2.1 provides statistical measures that show the model performance. In this table, MAE and RMSE denote the mean absolute error and the root mean square error. The tip angle was measured in radians and all deflection measurements were in millimeters.

The model predicts the tip deflection angle with an error less than 0.0197 rad ($\approx 1.13^\circ$). The error in estimating the horizontal and vertical components of the displacement is less than 0.6 mm (Table 2.1). Considering that the catheter diameter is 1.67 mm, this error is acceptable since the position of the catheter tip is estimated with an error of the order of the tip radius. From Table 2.1, the performance of the analytical beam model is almost the same as that of the FE-based model. Moreover,

Table 2.1: Statistical measures showing model performance for the datasets \mathcal{A} , \mathcal{B} and \mathcal{C} evaluated for all results shown in Figures 2.7, 2.8 and 2.9 (Appr.1: Initial Curvature Approach; Appr.2: Moment Approach, FEM: FE-based Model)

	MAE								
	Dataset \mathcal{A}			Dataset \mathcal{B}			Dataset \mathcal{C}		
	Appr.1	Appr.2	FEM	Appr.1	Appr.2	FEM	Appr.1	Appr.2	FEM
ϕ (rad)	0.013	0.013	0.015	0.015	0.015	0.021	0.012	0.013	0.007
δ_x (mm)	0.184	0.182	0.138	0.227	0.228	0.201	0.228	0.228	0.233
δ_y (mm)	0.423	0.421	0.216	0.432	0.43	0.388	0.435	0.383	0.326

	RMSE								
	Dataset \mathcal{A}			Dataset \mathcal{B}			Dataset \mathcal{C}		
	Appr.1	Appr.2	FEM	Appr.1	Appr.2	FEM	Appr.1	Appr.2	FEM
ϕ (rad)	0.017	0.017	0.019	0.02	0.02	0.025	0.017	0.018	0.009
δ_x (mm)	0.223	0.221	0.167	0.299	0.3	0.259	0.287	0.279	0.283
δ_y (mm)	0.495	0.493	0.269	0.599	0.597	0.472	0.546	0.483	0.3902

modeling the initial bending of the catheter with a moment that could have caused such a deflection leads to slightly more accurate results. Furthermore, the model performs better in predicting the final tip angle for Datasets \mathcal{A} and \mathcal{C} . This is mostly due to the different approaches in collecting data samples and shows that the previous shape of the catheter introduces some error in the results. Finally, the results suggest that the model can predict the final tip angle accurately for axial loads as well as vertical ones.

2.5 Discussion

In the previous section, the performance of the beam model in estimating the shape of the catheter tip was evaluated and statistical measures for model performance were provided in Table 2.1. The factors that contribute to errors for all approaches include:

1. Error in measuring the tip angle and the horizontal and vertical components of the displacement due to camera registration error.
2. The catheter wears down during the experiments, causing the characteristics

of the catheter to change gradually over time. This effect is best seen by a closer look at the results for dataset \mathcal{B} (Figure 2.8). In this dataset, the earlier the sample is collected, the closer it is to the value predicted by the proposed model. A complete study of how the stiffness of a catheter changes over time is beyond the scope of this chapter. However, the rigidity analysis of the catheter tip (Section 2.3.3) reveals that if the value of EI varies within $\pm 10\%$ of its original value, the introduced error in predicting the final tip deflection angle will be less than 3.5%.

3. Internal structure of the catheter: The catheter tip may look like a cantilever beam; however its internal structure is quite different and consists of different parts. For example, bending is caused by pulling one of the plates. Since the catheter structures can be quite different, including this information in the static model leads to model complexity and restricts the model to specific catheters only. Moreover, it is worthwhile noting that when the tip angle is changed by the proximal handle, there is a delay until the catheter reaches a specified angle. This is also true when the catheter is restored to its straight position. This effect could be due to friction in the internal structure of the pull-wire catheter.

In proposing the beam model, it is assumed that the catheter bends in the plane of the applied force; however this assumption is not generally true. The next step in verifying the beam model for the catheter tip would be to extend the 2D model to a 3D one and repeat the experiments for a more general set of data.

2.6 Conclusions

In this chapter, using a large deflection beam model for describing the behavior of the distal section of a steerable catheter under applied tip forces was investigated. To the best of our knowledge, this is the first attempt to provide an analytical mapping between the forces applied at the tip of a steerable ablation catheter and its shape without using any knowledge of the catheter internal structure. This is the key issue in modeling the behavior of a steerable catheter when its tip is in contact with tissue.

The suggested model was validated through experiments on a conventional pull-wire ablation catheter under different conditions and it was shown that the developed model is capable of estimating the shape of the distal section of a steerable catheter based on the forces applied at the distal tip.

This work presented an analytical static model for an ablation catheter which can be a first step towards designing a model-based force-position control of the catheter tip. Setting our sights on designing such a controller, we have focused on developing a general static model that can describe the behavior of conventional steerable ablation catheters. Extending the proposed model to a 3-dimensional model by considering out-of-plane bending and providing real-time force-deflection calculations will lead to a generalized model that could potentially be used to design a hybrid force/position or impedance controller for a robot-assisted catheter control system.

References

- [1] M. Khoshnam, M. Azizian, and R.V. Patel, “Modeling of a steerable catheter based on beam theory,” in *IEEE International Conference on Robotics and Automation (ICRA)*, 2012, pp. 4681–4686.
- [2] L. Di Biase *et al.*, “Relationship between catheter forces, lesion characteristics, popping, and char formation: experience with robotic navigation system.” *Journal of Cardiovascular Electrophysiology*, vol. 20, no. 4, pp. 436–40, Apr 2009.
- [3] D. Lakkireddy *et al.*, “Impact of a comprehensive safety program on radiation exposure during catheter ablation of atrial fibrillation: a prospective study.” *Journal of Interventional Cardiac Electrophysiology : An International Journal of Arrhythmias and Pacing*, vol. 24, no. 2, pp. 105–12, Mar 2009.
- [4] J.M. Miller, “Catheter ablation of arrhythmias,” *Circulation*, vol. 106, no. 25, pp. 203e–205, Dec 2002.
- [5] M. Azizian and R.V. Patel, “Intraoperative 3D stereo visualization for image-guided cardiac ablation,” in *Proceedings of SPIE Medical Imaging*, vol. 7964, 2011, pp. 79 640F–79 640F–8.
- [6] W. Saliba *et al.*, “Novel robotic catheter remote control system: feasibility and safety of transseptal puncture and endocardial catheter navigation.” *Journal of Cardiovascular Electrophysiology*, vol. 17, no. 10, pp. 1102–5, Oct 2006.
- [7] C. Pappone *et al.*, “Robotic magnetic navigation for atrial fibrillation ablation.” *Journal of the American College of Cardiology*, vol. 47, no. 7, pp. 1390–400, Apr 2006.

-
- [8] J. Jayender, M. Azizian, and R.V. Patel, “Autonomous image-guided robot-assisted active catheter insertion,” *IEEE Transactions on Robotics*, vol. 24, no. 4, pp. 858–871, Aug 2008.
- [9] S.B. Kesner and R.D. Howe, “Force Control of flexible catheter robots for beating heart surgery,” in *International Conference on Robotics and Automation (ICRA)*, 2011.
- [10] K. Ikuta, K. Iritani, and J. Fukuyama, “Mobile virtual endoscope system with haptic and visual information for non-invasive inspection training,” *IEEE International Conference on Robotics and Automation (ICRA)*, pp. 2037–2044, 2001.
- [11] S.L. Dawson, S. Cotin, D. Meglan, D.W. Shaffer, and M.A. Ferrell, “Designing a computer-based simulator for interventional cardiology training,” *Catheterization and Cardiovascular Interventions*, vol. 51, no. 4, pp. 522–527, Dec 2000.
- [12] M. Kukuk and B. Geiger, “A real-time deformable model for flexible instruments inserted into tubular structures,” *Medical Image Computing and Computer-Assisted Intervention (MICCAI)*, pp. 331–338, 2002.
- [13] M.K. Konings, E.B. van de Kraats, T. Alderliesten, and W.J. Niessen, “Analytical guide wire motion algorithm for simulation of endovascular interventions.” *Medical & Biological Engineering & Computing*, vol. 41, no. 6, pp. 689–700, Nov 2003.
- [14] S. Cotin, C. Duriez, J. Lenoir, P. Neumann, and S. Dawson, “New approaches to catheter navigation for interventional radiology simulation.” *Medical Image Computing and Computer-Assisted Intervention (MICCAI)*, vol. 8, no. Pt 2, pp. 534–42, Jan 2005.
- [15] J. Lenoir, S. Cotin, C. Duriez, and P. Neumann, “Interactive physically-based simulation of catheter and guidewire,” *Computers & Graphics*, vol. 30, no. 3, pp. 416–422, Jun 2006.

-
- [16] W. Lawton, R. Raghavan, S.R. Ranjan, and R. Viswanathan, “Ribbons and groups : a thin rod theory for catheters and filaments,” *Journal of Physics A: Mathematical and General*, vol. 32, pp. 1709–1735, Mar 1999.
- [17] G. Robinson and J. Davies, “Continuum robots - a state of the art,” *IEEE International Conference on Robotics and Automation (ICRA)*, pp. 2849–2854, 1999.
- [18] A.A. Transeth, K.Y. Pettersen, and P.l. Liljebäck, “A survey on snake robot modeling and locomotion,” *Robotica*, vol. 27, no. 07, pp. 999–1015, Mar 2009.
- [19] M. Hannan and I. Walker, “Novel kinematics for continuum robots,” in *International Symposium on Advances in Robot Kinematics*. Piran, Slovenia: Kluwer Academic Publishers, 2000, pp. 227–238.
- [20] B. Jones and I. Walker, “Kinematics for multisection continuum robots,” *IEEE Transactions on Robotics*, vol. 22, no. 1, pp. 43–55, Feb 2006.
- [21] D.B. Camarillo, C.F. Milne, C.R. Carlson, M.R. Zinn, and J.K. Salisbury, “Mechanics modeling of tendon-driven continuum manipulators,” *IEEE Transactions on Robotics*, vol. 24, no. 6, pp. 1262–1273, Dec 2008.
- [22] O. Bauchau and J. Craig, *Structural Analysis: With Applications to Aerospace Structures*. Dordrecht Heidelberg London New York: Springer Verlag, 2009.
- [23] L. Howell, *Compliant Mechanisms*, ser. A Wiley-Interscience publication. Wiley, 2001, ch. 2, pp. 45–55.
- [24] A. Saxena and S.N. Kramer, “A simple and accurate method for determining large deflections in compliant mechanisms subjected to end forces and moments,” *Journal of Mechanical Design*, vol. 120, no. 3, pp. 392–400, Sept 1998.
- [25] L. Howell, *Compliant Mechanisms*, ser. A Wiley-Interscience publication. Wiley, 2001, ch. 5, pp. 166–170.

Chapter 3

Static Pseudo-Rigid-Body 3R Model

3.1 Introduction

Heart arrhythmias correspond to abnormal electrical activity in heart chambers, resulting in irregular heartbeat or abnormal heart rhythm. Over the past two decades, catheter-based cardiac ablation has been increasingly offered as a curative procedure to patients suffering from cardiac arrhythmias [2, 3]. In the conventional method of catheter ablation, a thin flexible tube, called a catheter, is inserted through small incisions in the neck, arm or groin area and is guided through the blood vessels to reach inside the heart. The catheter is then steered under image guidance (most commonly X-ray fluoroscopy) to be positioned properly on the target location and a form of energy (usually radio frequency) is delivered to burn appropriate cardiac tissue and restore normal heart rhythm. Due to the heart beat and respiratory movements, not only is the accurate positioning of the catheter under 2D X-ray fluoroscopic image guidance a challenging task, but also without having an estimate of catheter tip/tissue contact force, the need to maintain a sufficient and consistent force introduces new difficulties. Hence, new techniques are being sought to improve the efficacy of the ablation procedure by offering 3D visualization, dexterous control of the flexible catheter and a sense of touch at the catheter tip.

Steering catheter through blood vessels and inside the heart chambers can be facilitated by a robotic catheter control system which provides dexterous manipulation of a flexible ablation catheter. The Sensei[®] robotic catheter system

A version of this chapter has been presented in *IEEE International Conference on Robotics and Automation (ICRA)*, 2013 and has been published in [1]. [©2013 IEEE]

(Hansen Medical[®], Mountain View, CA, USA), the NIOBE[®] magnetic navigation system (Stereotaxis, St. Louis, MO, USA) and the Amigo[®] Remote Catheter System (Catheter Robotics, Mount Olive, NJ, USA) are commercial robotic systems that provide remote navigation and control of flexible ablation catheters [2,4–8]; However, they do not provide haptic feedback or force/impedance control of the catheter tip. Moreover, both Sensei[®] and NIOBE[®] work with custom-designed catheters. The two master-slave force-reflecting robotic systems presented in [9–11] reflect a measure of the force at the slave side to the user via a haptic interface. However, the force reflected to the master side is the force that the slave actuator applies for inserting and manipulating the catheter. Hence, although the user is provided with force feedback from the slave side, the contact forces at the catheter tip are still unknown. In the ideal case, a catheter control system should provide the user with hybrid force/position control of the catheter tip, such that maintaining a certain force at the desired location is always guaranteed.

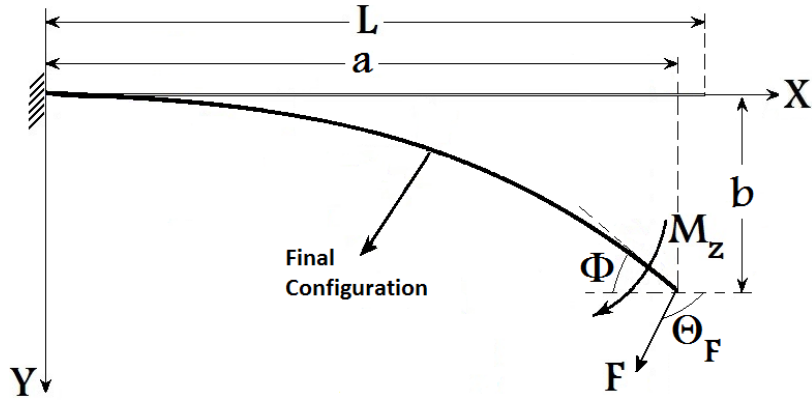
This chapter studies how the shape of the catheter distal tip changes when forces are applied. The problem of modeling catheters and similar mechanisms has been studied by several researchers [12–17]. Numerical models are mainly developed for simulating the catheter behavior inside the vasculature [18–22]. While these methods provide powerful tools for simulation purposes, in most cases, it is not convenient to use them in designing control systems. It is worthwhile noting that one of the limitations in modeling the conventional steerable ablation catheters is that detailed information about the internal structure, pull-wires and internal friction is not often available. Moreover, because of tip electrodes, placing force sensors right at the distal tip is challenging.

A large deflection beam model is based on the Euler-Bernoulli beam theory and describes the nonlinear displacement of the beam when it is bending beyond the linear range. Pseudo-rigid-body (PRB) models provide an easier and more efficient method of describing the force-deflection relationships of a compliant system that undergoes large deflections [23]. A cantilever beam is modeled as a pseudo-rigid-body with two rigid links connected with a revolute joint and a torsional spring. The PRB of a cantilever beam has been studied extensively to comply with different

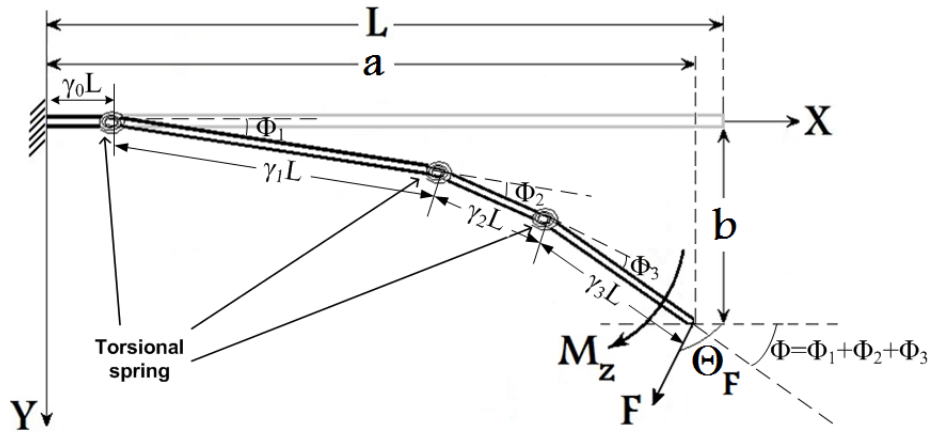
loading conditions with high accuracy [24, 25]. Su suggested a PRB 3R model of a cantilever beam to further improve the model accuracy for different load modes [26]. To calculate the parameters of this model, the link lengths and spring stiffness values are optimized such that the model can always estimate the path that the tip of a cantilever beam would follow under applied loads. In our previous work, we showed that a large deflection beam model can estimate the shape of the bending section of a steerable catheter, if the applied force is known [27]. In this chapter, a PRB 3R model for the catheter tip is introduced to describe the force-deflection relationship of the catheter tip. The model parameters are determined such that the model will estimate the path that the catheter tip follows when loads are applied. The model performance is evaluated empirically and it is shown that the proposed model can define the force-deflection relation of different catheters with a calibration step. The model described in this chapter has a number of significant advantages over that in our previous work: It substantially improves the accuracy in estimating the position of the catheter tip. Unlike the model in [27], the model proposed herein is numerically stable (it does not require solving nonlinear integrals), its inverse model is well-defined, its equations are simpler and can be implemented in real-time. These factors make the proposed model a convenient choice for use in developing a control strategy. In Section 3.2, the pseudo-rigid-body 3R model for a cantilever beam is briefly reviewed. Section 3.3 gives an overview of how the catheter tip shape is estimated using a beam model and its pseudo-rigid-body equivalent. Details of defining a pseudo-rigid-body 3R model for a steerable catheter are given in Section 3.4. Empirical results evaluating the proposed model performance are found in Section 3.5 and finally, Section 3.6 concludes the chapter with suggestions for future research.

3.2 Pseudo-Rigid-Body 3R Model of a Cantilever Beam

Figure 3.1 shows a cantilever beam and its equivalent PRB 3R model. The cantilever beam is initially straight with length L and the origin of the Cartesian coordinate



(a) Deflection of a cantilever beam with applying end loads



(b) Equivalent pseudo-rigid-body 3R model

Figure 3.1: Deflection of a loaded cantilever beam and its pseudo-rigid-body model equivalent.

system is assumed to be at the fixed end of the beam. Loads are applied in such a way that the beam deflection occurs in the xy plane. The applied loads include end moment M_z and end force F which has components in both x and y directions, where Θ_F denotes the direction of the end force F . Horizontal and vertical components of tip deflection at the loaded end are represented with a and b , respectively, and Φ is the maximum deflection angle of the beam that occurs at the loaded tip.

The PRB 3R model replaces a flexible cantilever beam with four rigid links connected by three revolute joints and three torsional springs [26] and is an improvement on the PRB 1R model [23] with higher accuracy. From Figure 3.1, the following

equation holds for the characteristic radius $\gamma_i, i = 0, 1, 2, 3$:

$$\gamma_0 + \gamma_1 + \gamma_2 + \gamma_3 = 1 \quad (3.1)$$

Denoting the deflection angle of joints by $\Phi_i, i = 1, 2, 3$, the equations describing the forward kinematics of a 3R serial chain can be written as:

$$\begin{cases} P_x = \gamma_0 + \gamma_1 c_1 + \gamma_2 c_{12} + \gamma_3 c_{123} \\ P_y = \gamma_1 s_1 + \gamma_2 s_{12} + \gamma_3 s_{123} \\ \Phi = \Phi_1 + \Phi_2 + \Phi_3 \end{cases} \quad (3.2)$$

where $P = \begin{pmatrix} P_x \\ P_y \end{pmatrix} = \begin{pmatrix} a/L \\ b/L \end{pmatrix}$ is the normalized tip point and $c_1 = \cos \Phi_1, s_1 = \sin \Phi_1, c_{12} = \cos(\Phi_1 + \Phi_2), s_{12} = \sin(\Phi_1 + \Phi_2), c_{123} = \cos(\Phi_1 + \Phi_2 + \Phi_3), s_{123} = \sin(\Phi_1 + \Phi_2 + \Phi_3)$.

Tip loads in Cartesian space are mapped into equivalent joint torques via the Jacobian transpose:

$$\begin{pmatrix} \tau_1 \\ \tau_2 \\ \tau_3 \end{pmatrix} = J^T \begin{pmatrix} FL \cos \Theta_F \\ FL \sin \Theta_F \\ M_z \end{pmatrix} \quad (3.3)$$

where J^T is the transpose of the Jacobian of a 3R manipulator derived by differentiating Equation (3.2). Let's assume:

$$\tau_i = k_i \Phi_i \quad , \quad i = 1, 2, 3 \quad (3.4)$$

i.e., the joint torques are proportional to the joint deflection angles. The optimal link lengths for a 3R serial chain to follow the path of the free end of a cantilever beam under applied loads are found to be [26]:

$$\gamma_0 = 0.1, \quad \gamma_1 = 0.35, \quad \gamma_2 = 0.4, \quad \gamma_3 = 0.15 \quad (3.5)$$

and the equivalent spring stiffness values are [26]:

$$k_1 = 3.51 \frac{EI}{L}, \quad k_2 = 2.99 \frac{EI}{L}, \quad k_3 = 2.58 \frac{EI}{L} \quad (3.6)$$

where E is the Young's modulus and I is the moment of inertia of the beam cross-section around the neutral axis. A detailed discussion of the optimization algorithm and how the optimal values are determined can be found in [26].

3.3 Experimental Evaluation of the Beam PRB 3R Model for the Catheter Tip

In this section, the performance of the beam PRB 3R model in estimating the angle and position of the catheter tip under applied loads is evaluated experimentally and is compared to the performance of a large deflection beam model.

3.3.1 Evaluating Model Performance

The performance of the PRB 3R model in estimating the large deflections of a catheter is evaluated by examining the tip deflection with applying loads, using the experimental setup described in Section 2.2. Since different loading conditions may affect the load-displacement relation, two different approaches are used to collect force and deflection data:

1. For dataset \mathcal{A} , the catheter tip is bent to an initial angle. A concentrated vertical force ($F_x = 0$) is applied at the tip. The force is released and the catheter returns to its initial bent shape before another force is applied.
2. Dataset \mathcal{B} is collected using the same method as for dataset \mathcal{A} , but with applying a series of increasing concentrated end loads acting in the direction of the tip ($\Theta_F = \pi + \Phi$), *i.e.*, the applied force has components in both x and y directions.

For both datasets, the PRB 3R model takes the initial bending angle of the tip and the force data to calculate the final deflection angle, which is then compared

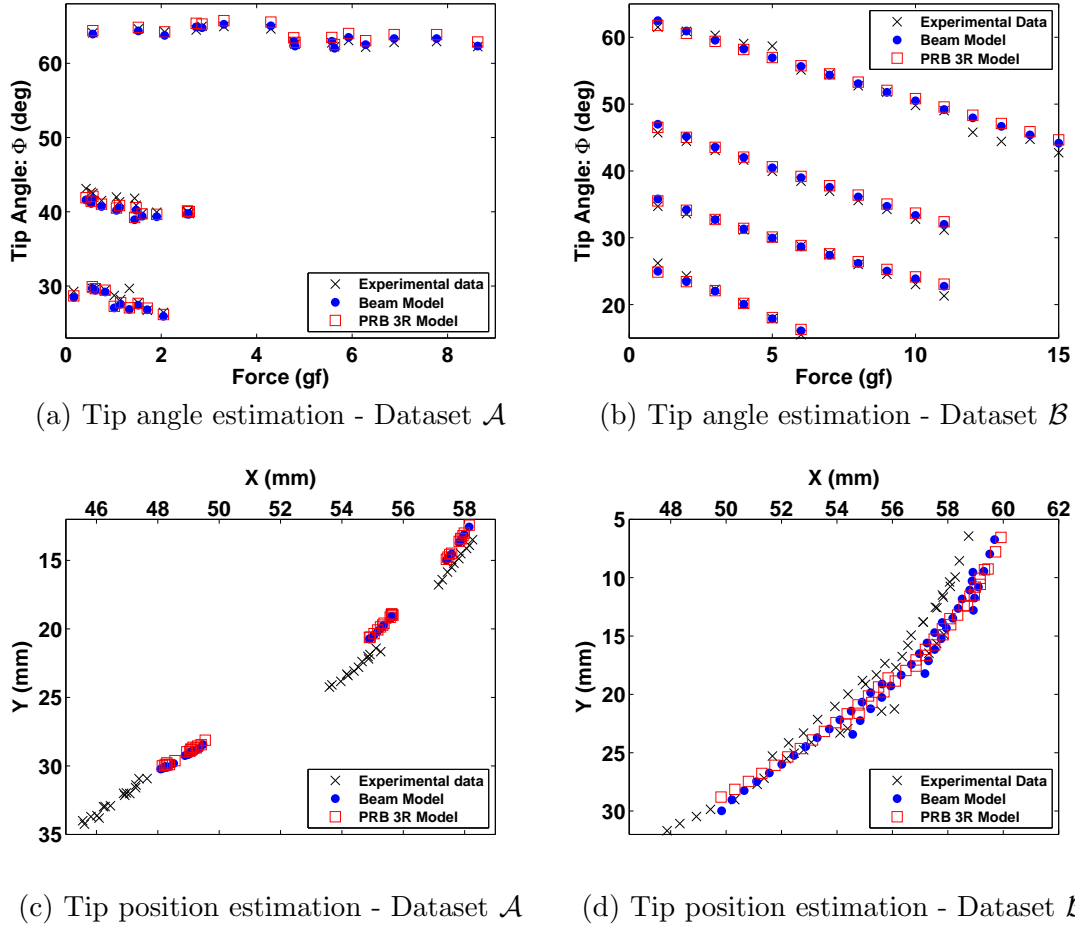


Figure 3.2: Performance of the large deflection beam model and the PRB 3R model in estimating the shape of the catheter tip under applied loads.

to the actual value measured experimentally and the value obtained from the large deflection beam model [27] (Table 3.1). It is observed that although the tip angle is estimated accurately, there is an offset between the actual and estimated position of the tip. This variable offset depends on the initial bending of the catheter and is partially due to the inaccurate estimation of the tip rigidity.

Statistical measures of model performance are given in Table 3.1. In this table, MAE and RMSE denote the mean absolute error and the root mean squared error. The tip angle is measured in degrees and all position measurements are in millimetres. From Table 3.1, the performance of the PRB 3R model and the large deflection beam

Table 3.1: Statistical measures showing model performance for datasets \mathcal{A} and \mathcal{B} evaluated for the large deflection beam model and the PRB 3R model.

		Beam Model		PRB 3R Model	
		MAE	RMSE	MAE	RMSE
Dataset \mathcal{A}	Tip angle (deg)	0.6203	0.92	0.6324	0.8761
	Tip position (mm)	2.9356	3.178	3.1026	3.3468
Dataset \mathcal{B}	Tip angle (deg)	0.6441	0.8452	0.7646	0.9813
	Tip position (mm)	1.9778	2.0978	2.3967	2.5193

model are similar. This is expected as the PRB 3R model provides an approximation to the large deflection beam model. The tip angle has been estimated with an error less than one degree, however the variable position offset leads to noticeable error in position estimation (an error greater than the radius of the catheter). Previously in [27], the offset was calculated by observing the first two collected data points at each bending angle; the model was not convenient to use in real-time estimations. To solve this problem and to ensure model performance for a range of applied loads and bending angles, hereinafter, a 3R rigid manipulator is proposed using the catheter force-deflection data. The parameters of this model are optimized such that the manipulator follows the path of the catheter tip with the correct orientation. Without the need to remove any position or angle offsets, the proposed model is simple and convenient to use in real-time applications and control structures.

3.4 Pseudo-Rigid-Body 3R Model of a Catheter Tip

To find the PRB 3R model of the catheter tip, link lengths γ_i , $i = 0, 1, 2, 3$ and spring stiffness values should be determined in such a way that the model follows the catheter tip position and orientation for different load modes with an acceptable error. The search algorithm is adapted from [26] with minor changes:

- $\gamma_i \in [0.05, 0.5]$, $i = 0, 1, 2, 3$ is chosen such that: $\sum_{i=0}^3 \gamma = 1$.
- For each set of γ_i , the spring stiffness k_{init} is calculated for dataset points

defining the initial shape of the catheter tip, *i.e.*, the catheter is bent, but no force is applied and the load at the tip is a pure moment load.

- For each set of γ_i , the spring stiffness k_{fin} is calculated for dataset points defining the final shape of the catheter tip in dataset \mathcal{A} , *i.e.*, the catheter is bent, and a vertical force is applied.
- The optimal set of γ_i is the set for which $\|k_{init} - k_{fin}\|$ is minimum, *i.e.*, k_{init} is closest to k_{fin} .

With this optimization procedure, the optimal characteristic radius factors were found to be:

$$\gamma_0 = 0.05, \quad \gamma_1 = 0.4, \quad \gamma_2 = 0.5, \quad \gamma_3 = 0.05 \quad (3.7)$$

for which:

$$k_{init} = [3.2258 \quad 2.1349 \quad 4.3986] * \frac{EI}{L}$$

$$k_{fin} = [3.1655 \quad 2.0373 \quad 4.2401] * \frac{EI}{L}$$

Let's define:

$$k_{\theta_i} = k_i \frac{L}{EI}, \quad i = 1, 2, 3$$

as the normalized spring stiffness values. Setting the link lengths to their optimal values (Equation (3.7)), best k_{θ_i} , $i = 1, 2, 3$ for a range of different load modes should be determined. Figure 3.3 shows value of k_{θ_i} , $i = 1, 2, 3$ versus load ratio which is defined as [26]:

$$\kappa = \frac{M_z^2}{2F(EI)^2} \quad (3.8)$$

By averaging over $\kappa \in (0, 32)$, optimal values for normalized stiffness k_{θ} , are obtained:

$$k_{\theta_1} = 3.298, \quad k_{\theta_2} = 2.052, \quad k_{\theta_3} = 4.515 \quad (3.9)$$

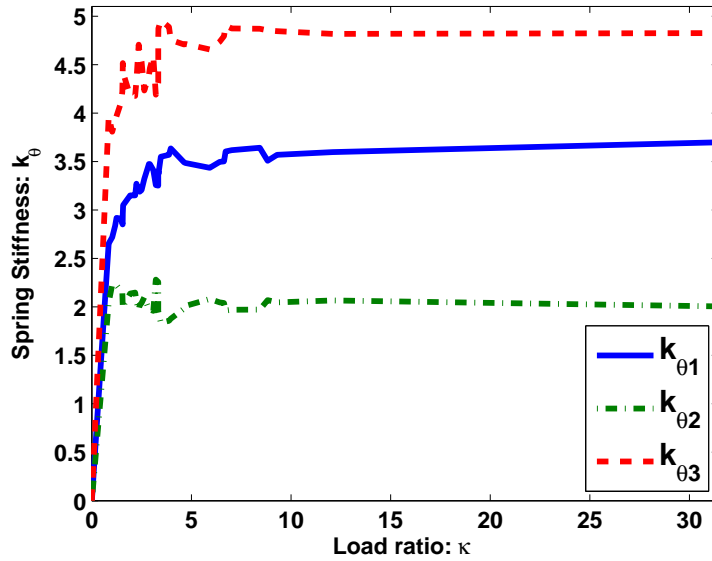


Figure 3.3: k_{θ_i} vs. load ratio $\kappa \in (0, 32)$ for $\Theta_F = -\frac{\pi}{2}$.

Table 3.2: Statistical measures showing the model performance for datasets \mathcal{A} and \mathcal{B} evaluated for the PRB 3R model of the catheter tip.

	Dataset \mathcal{A}		Dataset \mathcal{B}	
	MAE	RMSE	MAE	RMSE
Tip angle (deg)	0.671	0.911	0.6863	0.8018
Tip position (mm)	0.6883	0.7831	0.8057	0.8586

Figure 3.4 shows how the obtained model estimates the final shape of the catheter tip. The configuration of the 3R manipulator is shown for a number of tip points. Statistical measures are given in Table 3.2. It is observed that with the catheter tip PRB 3R model, the offset is removed and the accuracy is improved.

It is worthwhile noting that since in most cases the catheter is bent before it touches the heart tissue, the load modes used to obtain the model parameters are pure moment (bent catheter) and a combination of moment and vertical end force (force applied on the bent catheter). Pure force loads were applied on the initially straight catheter and data points were collected to ensure model performance, but this data was not used in obtaining optimal parameters for the proposed model.

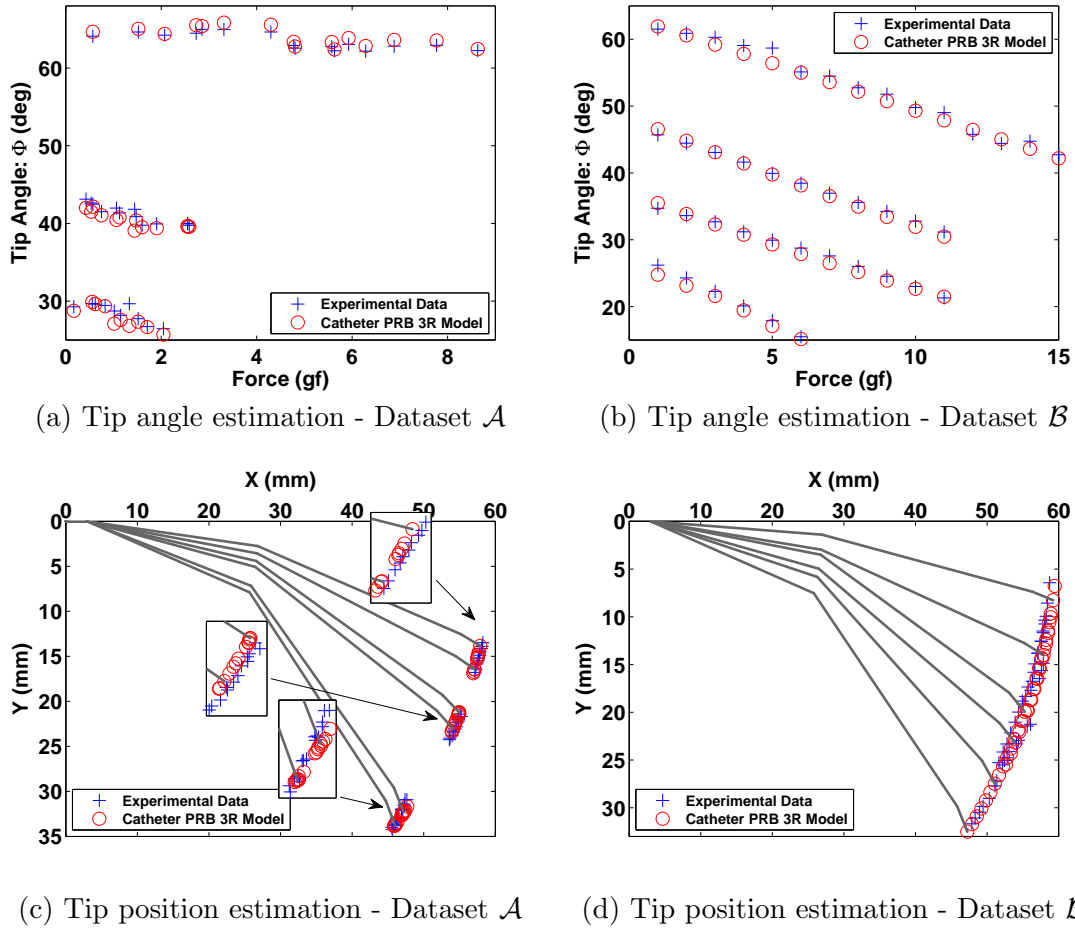


Figure 3.4: Performance of the catheter PRB 3R model in estimating the shape of the catheter tip under applied loads (solid grey: link configuration).

3.5 Performance Evaluation of the Catheter PRB 3R Model in a More Realistic Environment

The Performance of the catheter tip PRB 3R model is further studied in a second experimental setup, which is more realistic in the sense that the catheter is passed through a standard sheath and it is no longer clamped and fixed at one end. Hence, as the loads are applied on the free end, the base of the bending section may move as well. Herein, it is investigated if the model parameters can be determined such that the model accurately describes the relation between the applied loads and the

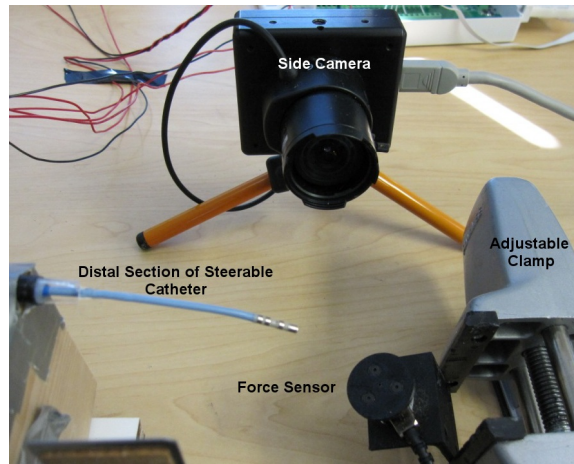


Figure 3.5: A view of catheter tip in the second experimental setup.

catheter tip angle.

3.5.1 Experimental Setup

In the experimental setup for this part, the base of a motorized linear stage (Zaber Technologies Inc., Vancouver, BC, Canada) is fixed to the table and the catheter handle is fixed to the sliding stage by an ABS rapid prototyped adaptor piece. The catheter is a conventional 7-Fr radio frequency ablation catheter that can bend in only one direction. The catheter is passed through a standard catheter sheath which is fixed in place along its length, so there is no out-of-plane bending. The distal 8 cm of the catheter, which is the bending section, is free in space. A camera (Dragonfly[®], Point Grey Research Inc., Richmond, BC, Canada) is placed on the side to record 640×480 resolution images of the catheter tip. A force sensor (Nano17, ATI Industrial Automation, Apex, NC, USA) is used to apply forces on the tip (Figure 3.5).

3.5.2 Evaluating Model Performance

By actuating the catheter handle with the motorized linear stage, the catheter tip is bent to different angles and its shape is recorded before and after the force is applied. The catheter tip rigidity in different bending angles is estimated by the method described in [27]. To determine the parameters of the PRB 3R model for

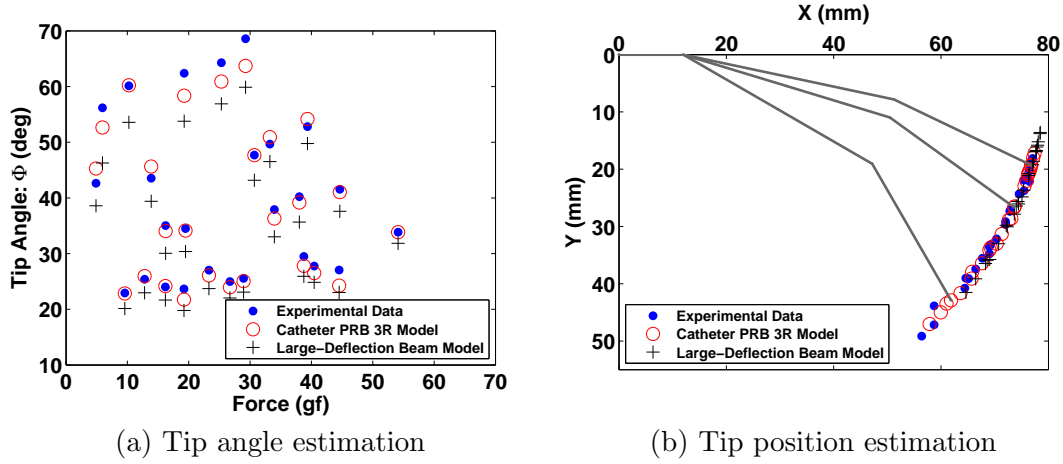


Figure 3.6: Performance of the catheter PRB 3R model and the large deflection beam model when the tip end is not fixed (solid grey: link configurations - catheter PRB 3R model).

Table 3.3: Statistical measures showing the performance of the catheter PRB 3R model and the large deflection beam model when the tip end is not fixed.

	Catheter PRB 3R Model		Beam Model	
	MAE	RMSE	MAE	RMSE
Tip angle (deg)	1.083	1.4203	4.4352	4.8957
Tip position (mm)	1.2404	2.002	7.0644	7.4211

this catheter, vertical forces are applied on the bent catheter and the tip angle data is recorded. The optimization algorithm from Section 3.4 is then used to obtain the optimal link parameters and spring stiffness values for this catheter, which are found to be:

$$\gamma_0 = 0.15, \quad \gamma_1 = 0.25, \quad \gamma_2 = 0.25, \quad \gamma_3 = 0.35 \quad (3.10)$$

and

$$k_{\theta_1} = 2.1546, \quad k_{\theta_2} = 8.6564e3, \quad k_{\theta_3} = 1.6886 \quad (3.11)$$

The large value of k_{θ_2} shows that the corresponding joint angle is nearly zero. It means that the catheter in this special case can also be modeled with three links and two revolute joints.

To ensure model performance for different loads, forces are applied on the bent catheter in various in-plane directions and shape data is collected. A comparison of the empirical data and the model results is given in Figure 3.6. Table 3.3 provides the statistical measures of model performance. It is noticeable that although in this experimental setup, the catheter tip is not fixed at one end, the model follows the position and angle of the catheter tip, but with a larger error compared to the previous case, where the tip was fixed at one end. This result suggests that with optimizing the model parameters based on force-deflection data of the catheter tip, it is possible to have basic information about the shape of the catheter tip. To confirm that the catheter PRB 3R model shows a better performance in estimating the tip shape, in Figure 3.6 and Table 3.3, we have also provided the results of estimating the shape using the large deflection beam model. It is evident that the PRB 3R model has significantly improved the estimation accuracy.

3.5.3 Estimating Contact Force from Catheter Shape and Handle Displacement

Observing that the catheter tip PRB 3R model can describe the relation between catheter tip deflection and applied forces, we now investigate the performance of the inverse model in estimating the contact force from the actuation information, *i.e.*, if the forces applied at the catheter tip can be calculated by observing the tip angle and the displacement at the catheter proximal handle.

3.5.3.1 Mapping Handle Displacement to Tip Angle

Using the motorized linear stage, the catheter proximal handle is moved by 1 mm in each step and the catheter tip shape is recorded. This procedure has been done 8 times forth and back. A mapping between the handle displacement and the catheter shape is achieved by fitting a two-term power series model to the data from all runs (Figure 3.7):

$$\Phi(d) = 0.0144(d + 1)^{3.535} + 1.256 \quad (3.12)$$

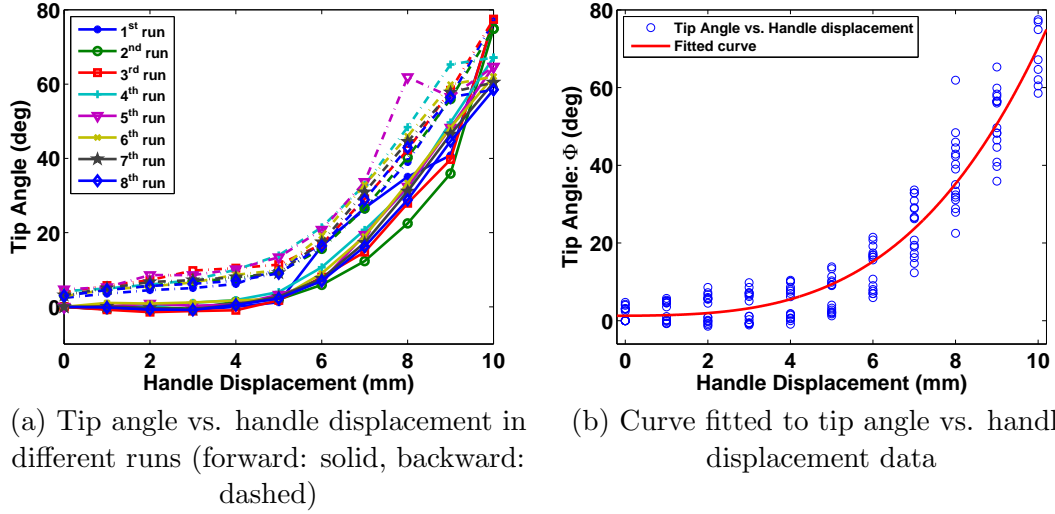


Figure 3.7: Relation between handle displacement and tip angle in different runs.

where Φ and d represent the tip angle and the handle displacement respectively.

3.5.3.2 Data Collection and Experimental Results

The force sensor is placed under the catheter tip such that as the tip bends the sensor exerts a vertical force on it. The catheter proximal handle is actuated using the motorized linear stage. For each handle displacement, the force and tip shape data are collected. Using Equation (3.12), the initial bending angle of the catheter is calculated for each displacement. This is the angle that the tip would have if the force was not applied, *i.e.*, if the tip was being moved in free space. The contact force is estimated based on the difference between the initial angle (calculated) and the final angle (measured) using the catheter PRB 3R model. The estimated force value is then compared to the reading of the force sensor.

Figure 3.8 shows the estimation results. It is observed that the model follows the increasing/decreasing trend of the contact force, but the difference between the measured and the estimated force values is about 2 gf (RMSE = 1.66 gf). This error is noticeable, taking into account that the applied force does not exceed 10 gf and that the contact force between the heart tissue and the catheter tip should be 20 to 30 gf for an effective ablation [2]. A part of this error is due to inaccuracies in mapping

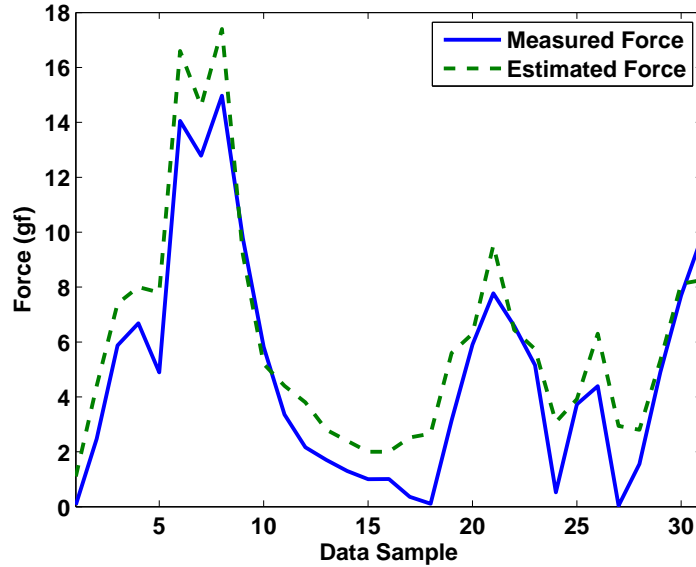


Figure 3.8: Estimation of contact force based on the tip angle.

the handle displacement to the tip angle. Work is continuing on investigating other sources of error in force estimation.

3.6 Conclusions

In this chapter, a 2-dimensional pseudo-rigid-body 3R model is proposed for describing how the shape of the bending section of a steerable ablation catheter relates to the applied contact force. The model parameters are optimized for each catheter based on the path that the catheter tip follows when loads are applied. Extensive experiments on conventional pull-wire ablation catheters show that the proposed model is capable of estimating the shape of the catheter's distal section if force data is available. A mapping is defined between the proximal handle displacement and the tip angle, and is used together with the proposed force-deflection model to evaluate the performance of the inverse model and to show that the contact force can be estimated by observing the tip angle. This technique might be a reasonable alternative to placing force sensors at the catheter tip to monitor the contact force. Moreover, the simple equations of the proposed model and its accuracy make it a convenient choice for performing

force-deflection calculations in real-time.

This work is a step towards understanding and modeling the catheter behavior and designing a model-based force-position control of the catheter tip. Evaluating the model in more realistic settings and extending the model to include cases where the catheter tip undergoes out-of-plane bending are parts of our ongoing work towards designing hybrid force/position or impedance controllers for a robot-assisted catheter control system.

References

- [1] M. Khoshnam and R.V. Patel, “A pseudo-rigid-body 3R model for a steerable ablation catheter,” in *IEEE International Conference on Robotics and Automation (ICRA)*, 2013, pp. 4412–4417.
- [2] L. Di Biase *et al.*, “Relationship between catheter forces, lesion characteristics, popping, and char formation: experience with robotic navigation system.” *Journal of Cardiovascular Electrophysiology*, vol. 20, no. 4, pp. 436–40, Apr 2009.
- [3] D. Lakkireddy *et al.*, “Impact of a comprehensive safety program on radiation exposure during catheter ablation of atrial fibrillation: a prospective study.” *Journal of Interventional Cardiac Electrophysiology : An International Journal of Arrhythmias and Pacing*, vol. 24, no. 2, pp. 105–12, Mar 2009.
- [4] “Hansen Medical Sensei X Robotic Catheter System.” [Online]. Available: www.hansenmedical.com/sensei
- [5] W. Saliba *et al.*, “Novel robotic catheter remote control system: feasibility and safety of transseptal puncture and endocardial catheter navigation.” *Journal of Cardiovascular Electrophysiology*, vol. 17, no. 10, pp. 1102–5, Oct 2006.
- [6] “Stereotaxis NIOBE Magnetic Navigation.” [Online]. Available: www.stereotaxis.com
- [7] C. Pappone *et al.*, “Robotic magnetic navigation for atrial fibrillation ablation.” *Journal of the American College of Cardiology*, vol. 47, no. 7, pp. 1390–400, Apr 2006.
- [8] “Catheter Robotics Amigo RCS.” [Online]. Available: www.catheterrobotics.com/rcs-main.htm

-
- [9] J.W. Park *et al.*, “Development of a force-reflecting robotic platform for cardiac catheter navigation,” *Artificial Organs*, vol. 34, no. 11, Nov 2010.
- [10] Y. Fu, A. Gao, H. Liu, and S. Guo, “The master-slave catheterisation system for positioning the steerable catheter,” *International Journal of Mechatronics and Automation*, vol. 1, nos. 3/4, pp. 143–152, 2011.
- [11] Y. Fu, A. Gao, H. Liu, K. Li, and Z. Liang “Development of a novel robotic catheter system for endovascular minimally invasive surgery,” in *IEEE/ICME International Conference on Complex Medical Engineering (CME)*, May 2011, pp. 400–405.
- [12] I.A. Gravagne, C.D. Rahn, and I.D. Walker, “Large deflection dynamics and control for planar continuum robots,” *IEEE/ASME Transactions on Mechatronics*, vol. 8, no. 2, pp. 299–307, Jun 2003.
- [13] D.B. Camarillo, C.F. Milne, C.R. Carlson, M.R. Zinn, and J.K. Salisbury, “Mechanics modeling of tendon-driven continuum manipulators,” *IEEE Transactions on Robotics*, vol. 24, no. 6, pp. 1262–1273, Dec 2008.
- [14] R.J. Webster, J.M. Romano, and N.J. Cowan, “Mechanics of precurved-tube continuum robots,” *IEEE Transactions on Robotics*, vol. 25, no. 1, pp. 67–78, Feb 2009.
- [15] P. Dupont, J. Lock, B. Itkowitz, and E. Butler, “Design and control of concentric-tube robots,” *IEEE Transactions on Robotics*, vol. 26, no. 2, pp. 209–225, Apr 2010.
- [16] K. Xu and N. Simaan, “Intrinsic wrench estimation and its performance index for multisegment continuum robots,” *IEEE Transactions on Robotics*, vol. 26, no. 3, pp. 555–561, Jun 2010.
- [17] K. Xu and N. Simaan, “Analytic formulation for kinematics, statics and shape restoration of multi-backbone continuum robots via elliptic integrals,” *Journal of Mechanisms and Robotics*, vol. 2, no. 1, pp. 011 006–1,011 006–13, Feb 2010.

-
- [18] W. Lawton, R. Raghavan, S.R. Ranjan, and R. Viswanathan, “Ribbons and groups : a thin rod theory for catheters and filaments,” *Journal of Physics A: Mathematical and General*, vol. 32, pp. 1709–1735, Mar 1999.
- [19] S.L. Dawson, S. Cotin, D. Meglan, D.W. Shaffer, and M.A. Ferrell, “Designing a Computer-Based Simulator for Interventional Cardiology Training,” *Catheterization and Cardiovascular Interventions*, vol. 51, no. 4, pp. 522–527, Dec 2000.
- [20] K. Ikuta, K. Iritani, and J. Fukuyama, “Mobile virtual endoscope system with haptic and visual information for non-invasive inspection training,” *IEEE International Conference on Robotics and Automation (ICRA)*, pp. 2037–2044, 2001.
- [21] S. Cotin, C. Duriez, J. Lenoir, P. Neumann, and S. Dawson, “New approaches to catheter navigation for interventional radiology simulation.” *Medical Image Computing and Computer-Assisted Intervention (MICCAI)*, vol. 8, no. Pt 2, pp. 534–42, 2005.
- [22] J. Lenoir, S. Cotin, C. Duriez, and P. Neumann, “Interactive physically-based simulation of catheter and guidewire,” *Computers & Graphics*, vol. 30, no. 3, pp. 416–422, Jun 2006.
- [23] L. Howell, *Compliant Mechanisms*, ser. A Wiley-Interscience publication. Wiley, 2001.
- [24] A. Saxena and S.N. Kramer, “A simple and accurate method for determining large deflections in compliant mechanisms subjected to end forces and moments,” *Journal of Mechanical Design*, vol. 120, no. 3, pp. 392–400, Sept 1998.
- [25] C. Kimball and L.-W. Tsai, “Modeling of flexural beams subjected to arbitrary end loads,” *Journal of Mechanical Design*, vol. 124, no. 2, pp. 223–235, 2002.
- [26] H.-J. Su, “A pseudorigid-body 3R model for determining large deflection of cantilever beams subject to tip loads,” *Journal of Mechanisms and Robotics*, vol. 1, no. 2, pp. 021 008.1–021 008.9, Jan 2009.

- [27] M. Khoshnam, M. Azizian, and R.V. Patel, “Modeling of a steerable catheter based on beam theory,” in *IEEE International Conference on Robotics and Automation (ICRA)*, May 2012, pp. 4681–4686.

Chapter 4

Force Control in Contact with a Static Environment

4.1 Introduction

Ablative therapy for cardiac arrhythmias has evolved from invasive open thoracotomy surgeries to minimally invasive catheter-based ablation procedures over the last few decades [2]. Catheters are long flexible tubes that are guided through the blood vessels to the heart in order to deliver some source of energy to heart tissue [2]. One of the factors that affects the efficacy of an ablation procedure is the quality of contact between the catheter tip and tissue [2]. Excessive force may result in perforating the heart wall, while insufficient force results in incomplete ablation and recurrence of arrhythmia. Recently, several studies have shown that the contact force has a great impact on the outcome of an ablation procedure. Therefore, developing catheters with integrated force sensors that are capable of reporting contact forces has become of interest [3–5]. The TactiCath[®] force sensing irrigated ablation catheter (Endosense[™], Switzerland) [6] uses optical fiber sensors to measure the slightest deformation of the catheter tip. The magnitude and direction of the applied force are then calculated based on deformation measurements. However, with the Endosense catheter, only one-axis axial forces can be sensed. The Thermocool[®] SMARTTOUCH[™] Catheter (Biosense Webster, Diamond Bar, CA) [7] is another force sensing catheter. In this catheter, magnetic signal emitters and sensors are

A version of this chapter has been presented in *IEEE International Conference on Robotics and Automation (ICRA)*, 2013 and has been published in [1]. [©2013 IEEE]

integrated within the tip. The change in the position of these sensors provides a means of measuring the contact force as well as the catheter angle. This information can then be graphically displayed on the Carto[®]3 Electroanatomic Mapping and Navigation System. Both these catheters provide clinicians with a measure of the tool/tissue contact force and its direction, hence improving the efficacy of the ablation procedure [4, 5].

Catheter navigation and manipulation can be facilitated with the help of robotic catheter control systems. The Sensei[®] robotic catheter system (Hansen Medical[®], Mountain View, CA, USA), the NIOBE[®] magnetic navigation system (Stereotaxis, St. Louis, MO, USA) and the Amigo[™] Remote Catheter System (Catheter Robotics, Mount Olive, NJ, USA) are the robotic systems that improve dexterity and reduce the amount of X-ray exposure by providing remote navigation and control of flexible ablation catheters [4, 8–12]; however, they do not provide haptic feedback or force/impedance control of the catheter tip.

Equipping a steerable ablation catheter with a force sensor and using it together with a robotic catheter actuation system are efforts towards developing force-reflecting robotic catheter systems. The two master-slave robotic systems developed in [13–15] present a measure of the force at the slave side to the user via a haptic interface. However, the force reflected to the master side is the force that the slave actuator applies for inserting and manipulating the catheter and hence it should be studied how this force relates to the forces at the catheter tip. Kesner and Howe [16, 17] implemented robot-assisted force and position control of flexible cardiac catheters. In this system, which can help with the surgeries performed inside the heart, *e.g.*, mitral valve annuloplasty, the heart motion is compensated for by position control at the catheter tip. The force sensor is integrated right at the distal tip and the force measurements are fed back to a control loop that ensures a constant contact force. Such a system would be ideal for providing assistance during cardiac ablation as well. However, in the case of ablation catheters, integrating the force sensors right at the tip is a challenge because of tip electrodes. Hence, an alternative technique is required.

Modeling a steerable ablation catheter and similar mechanisms has been stud-

ied by a number of groups, *e.g.*, [18–21]. Unfortunately, not all these modeling approaches can be readily applied to model and control a conventional steerable ablation catheter, since the exact information about the actuation mechanism, pull-wires, is not available.

With the aim of proposing a model-based control system for steerable catheters, this chapter first studies how the catheter distal tip responds to proximal handle actuation. The resulting displacement-tip angle mapping is then combined with a previously developed model that relates the shape of the catheter tip to contact force [22]. A custom designed force sensor is proposed for detecting the bending angle at the catheter tip. This optical strain sensor together with the obtained mappings provide an overall model that is then used in designing a control system for maintaining a certain contact force at the catheter tip *without directly measuring the applied force*. The models and the control system are developed under the assumption that the applied forces act in the plane of the bent catheter. It is also assumed that the forces are static and there is enough time for the catheter to reach its final state before the applied force changes. The control system performance is evaluated empirically using the experimental setup presented in Section 4.2. The design of the strain sensor and the corresponding mappings are explained in Section 4.3. Section 4.4 studies how the catheter shape changes by actuating the proximal handle and applying forces. The control system structure and experimental results are presented in Section 4.5 followed by a discussion in Section 4.6. Section 4.7 concludes the chapter with suggestions for future directions.

4.2 Experimental Setup

The setup is shown schematically in Figure 4.1. The base of a motorized linear stage (Zaber Technologies Inc., Vancouver, BC, Canada) is mounted on a table and the catheter handle is fixed to the sliding stage by an ABS rapid prototyped adaptor piece. The catheter used for these experiments is a conventional unidirectional 7-Fr radio frequency ablation catheter. The catheter is passed through a standard catheter sheath which is fixed in place along its length, so there is no out-of-plane

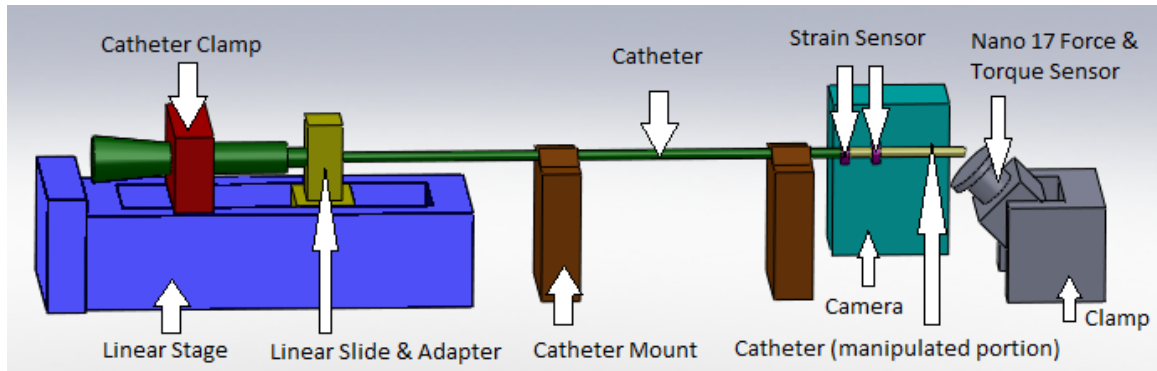


Figure 4.1: Schematic of the experimental setup.

bending. The distal 8 cm of the catheter, which is the bending section, is free in space. A camera (Dragonfly[®], Point Grey Research Inc., Richmond, BC, Canada) is positioned to show a planar view of the catheter during the catheter tip bending, and captures 640×480 resolution images. The optical force sensor plates are mounted on the catheter tube at distances of 8 cm and 7.4 cm from the catheter tip. The first sensor plate is located at the distance where the catheter slope is zero in order to correspond to the catheter's flexible body model. The second plate is placed at the distance where the range of analog voltage output is high between catheter tip angles of 0 to 120 degrees (Design details are given in Section 4.3). Another force sensor (Nano17, ATI Industrial Automation, Apex, NC, USA) is used to measure the force applied on the catheter tip. The readings of this force sensor provide a measure of the actual forces acting on the catheter tip.

4.3 Optical Strain Sensor

The optical strain sensor is comprised of five components, a transmitter/receiver plate, a reflector plate, transmitting/receiving fibers, red LED's and photodiodes. The transmitter/receiver plate is a 6 mm diameter, 2 mm thickness elastomeric plate with eight outer holes for mounting the fiber optic. The jacket of fiber optic cable used has been removed and the cable consists only of the core and cladding, with a diameter of 1 mm. The eight holes are in pairs, one hole for the light transmitting fiber and one hole for the receiving fiber. One central hole is included for the catheter tube to pass

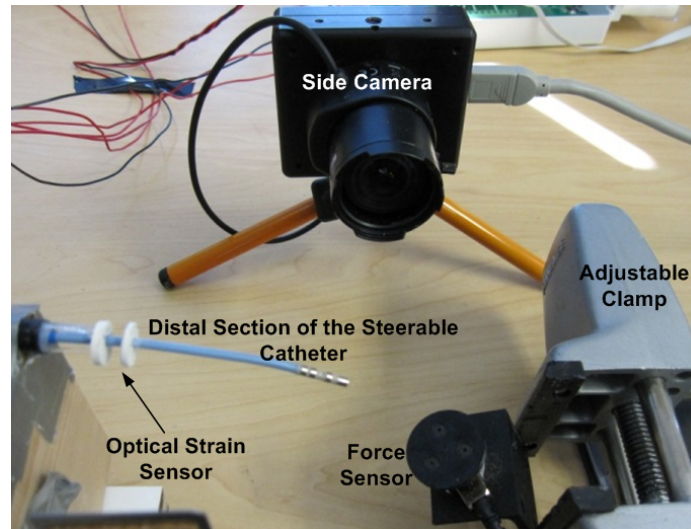


Figure 4.2: A view of the catheter tip, camera and strain sensor in the experimental setup.

through. The reflector plate, of the same material, diameter and thickness, is coated with a layer of 3M engineering grade reflective tape. One central hole is made for the catheter. The red LED light passes through the light-transmitting fiber; the light reflects off the reflector plate and some of it is sent back through the light-receiving fiber. The light-receiving fiber leads back to the photodiode, which detects the change in light intensity captured by the light-receiving fiber and relays a corresponding analog voltage to the data acquisition card. As the catheter bends the plates become off plane with respect to each other, changing the angle of reflection and the amount of light received by the light-receiving fiber. This change in the plane principal, coupled with the distance changes between the fibers and the reflecting plate during bending, creates large (0-5 Volt) changes in the analog voltage with negligible noise and drift. The sensors used show a linear correlation between the analog voltage and the tip angle, and approximately 5 mV changes in signal per degree of tip angle change. The data acquisition card easily detects these voltage changes without any signal filtering, or amplification on the controls or electrical side. The benefit of this optical sensor is that the final model slides over the sheath of the unaltered conventional steerable ablation catheter. The design and construction of a commercially produced catheter will not need to be altered and the final product will not be much larger in diameter,

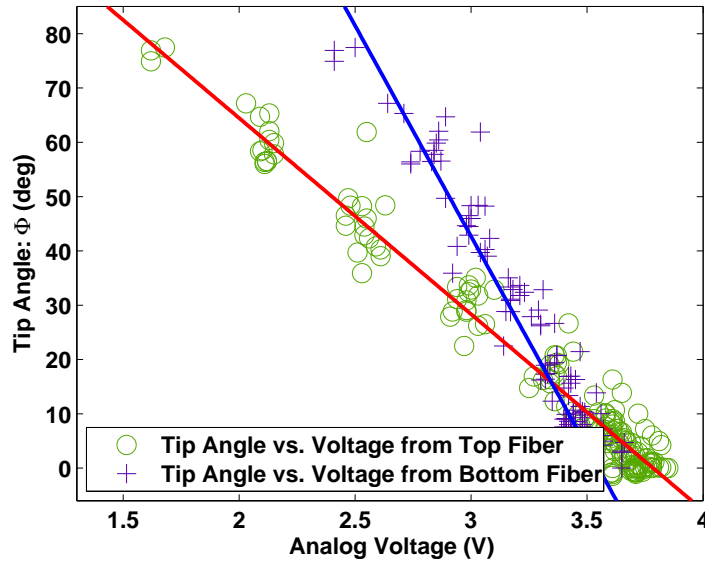


Figure 4.3: Relation between analog voltage and tip angle (solid lines are fitted curves)

therefore should not restrict blood flow during catheter insertion. This allows for easy installation and a cost effective and efficient solution for position feedback and force feedback. The use of four light-receiving fibers allows the sensor to provide 3-axis force and 3-axis torque measurements through relative light intensity values between the fibers. The final model of the sensor will be approximately 2.8 mm in diameter for a 7-Fr catheter. Since the diameter of the fibers used are smaller ($250 \mu\text{m}$), signal amplification and filtering may be necessary to improve the accuracy of the sensor. It is worth noting that although the fiber bragg grating (FBG) technology is a means to monitor and track the shape of a flexible tool, *e.g.* a catheter, along its length [23,24], the noticeable costs currently associated with this technology hinders its extensive use in experimental setups/clinical applications.

4.3.1 Mapping Analog Voltage to Tip Angle

The purpose of our first experiment with the optical strain sensor was to find an experimental correlation between the analog voltage input and the catheter tip angle in single plane bending. For this experiment, a light transmitting fiber and light receive-

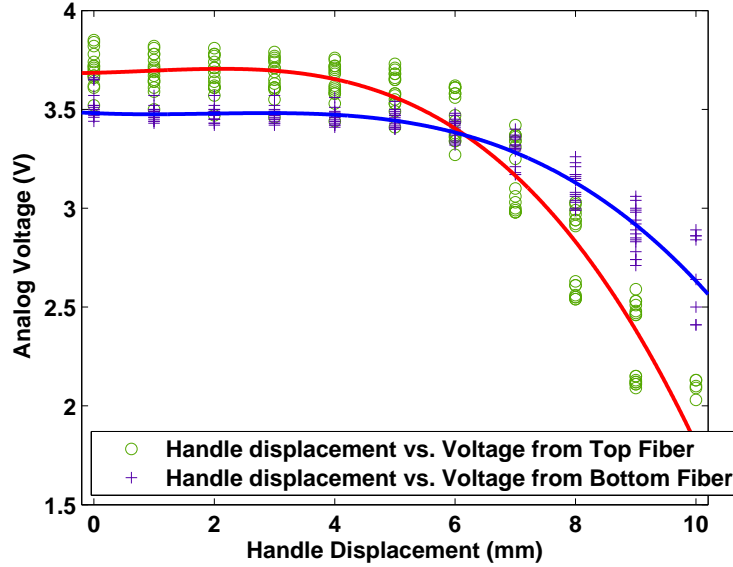


Figure 4.4: Relation between handle displacement and analog voltage (solid lines are fitted curves)

ing fiber were fixed in both the top and bottom portions of the fiber mounting plate. In Figure 4.3, the catheter tip angle is shown versus values taken from the receiving fibers mounted on the top and bottom portions of the plate. The experimental results show that the unloaded catheter tip angle varies linearly with analog input voltage using the criterion of R-squared value above 0.98:

$$\begin{aligned}\phi(v_t) &= -36.12v_t + 136.7 \\ \phi(v_b) &= -77.61v_b + 275.5\end{aligned}\tag{4.1}$$

where Φ is the catheter tip angle, and v_t and v_b represent the voltage values read from the top and bottom fibers respectively.

Moreover, it is shown that the angle information provided by the top receiving fiber of the strain sensor is accurate to 0.36 degrees using an acquisition system, such as PCI 6224 with millivolt accuracy. Lastly, it is shown that the sensitivity of the upper portion of the system is higher, which is because as the tip bends the angle of reflection increases and the distance between the top portion of the mounting and reflection plates increases. Both of these factors diminish the analog voltage values.

4.3.2 Mapping Handle Displacement to Analog Voltage

The optical sensor output voltages were also mapped against the catheter handle displacement in order to create a usable correlation for feedback position control during tele-robotic surgery:

$$\begin{aligned} v_t(d) &= -0.002618d^3 + 0.006711d^2 + 0.007023d + 3.685 \\ v_b(d) &= -0.001666d^3 + 0.009509d^2 - 0.01346d + 3.481 \end{aligned} \quad (4.2)$$

where d is the handle displacement, and v_t and v_b represent the voltage values read from the top and bottom fibers respectively. Figure 4.4 shows that once the handle reaches 4 mm the optical sensor is able to track the handle displacement to within 0.01 mm with a data acquisition system having an accuracy of 1 mV.

4.4 Modeling Catheter Behavior

A model that describes different features of the catheter has been developed for designing a model-based control system. In this section, we investigate how actuating the proximal handle changes the catheter angle and how this angle responds to applied loads.

4.4.1 Mapping Handle Displacement to Tip Angle

Using the motorized linear stage, the catheter proximal handle is moved by 1 mm in each step and the catheter tip shape is recorded. This procedure was done 8 times forth and back. Figure 4.5 shows the results. Since the catheter does not go back to a completely straight shape after each run, there is an angle offset at the beginning. Removing this offset shows that the trend is very similar for all runs (Figure 4.5-a). A mapping between the handle displacement and the catheter shape is achieved by fitting a curve to the data from all runs (Figure 4.5-b):

$$\Phi(d) = 0.0144(d + 1)^{3.535} + 1.256 \quad (4.3)$$

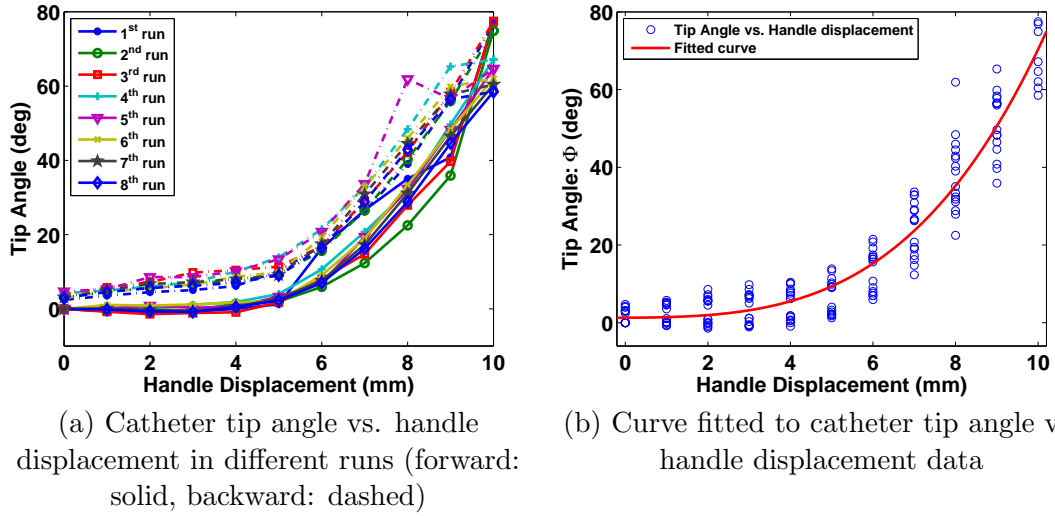


Figure 4.5: Relation between the catheter tip angle and the handle displacement.

where Φ and d represent the tip angle and handle displacement respectively.

4.4.2 Mapping Tip Angle to Applied Loads

It was previously shown [22] that a large deflection beam model based on Euler-Bernoulli beam theory can describe the shape of the bending section of a steerable catheter, if the applied loads are known. In this method, a catheter tip is modeled as a cantilever beam that undergoes large deflections when the loads are applied. Figure 4.6 shows an initially curved cantilever beam with length L . In this figure, R_i denotes the initial curvature of the beam. F_x , F_y and M_z are the loads applied at the free end, and δx and δy represent the horizontal and vertical displacements at the tip respectively. Φ is the maximum deflection angle of the beam that occurs at the loaded tip. The origin of the Cartesian coordinate system is assumed to be at the fixed end of the beam. The deflection of the beam and the applied loads are related through the following equation [25]:

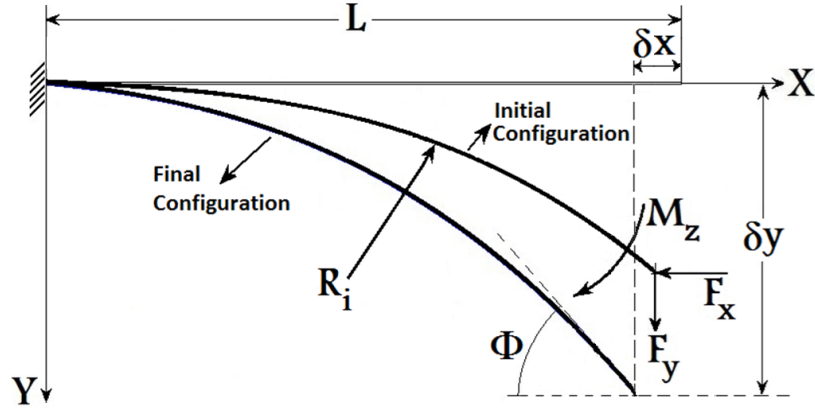


Figure 4.6: Deflection of an initially curved cantilever beam under applied loads.

$$F_y = \frac{EI}{2L^2} \left[\int_0^\Phi \left(\frac{1}{2} \left(\frac{M_z}{EI} + \frac{1}{R_i} \right)^2 \frac{EI}{F_y} + \sin \Phi - \frac{F_x}{F_y} \cos \Phi - \sin \phi + \frac{F_x}{F_y} \cos \phi \right)^{\frac{-1}{2}} d\phi \right]^2 \quad (4.4)$$

To evaluate the performance of such a model for describing the catheter behavior in current experiments, the catheter is first bent to different angles and then forces with arbitrary in-plane directions are applied at the tip of the catheter. The catheter tip shape as well as force magnitude and direction are recorded at each step. Figure 4.7 shows the collected shape and force data together with the values estimated by the model. Using force measurements, we can use the model to accurately estimate the final shape of the catheter with an error less than 1.5 degrees. It is worthwhile noting that the catheter tip rigidity and the initial bending of the catheter are estimated using the method in [22].

4.5 Experimental Results

Sections 4.3 and 4.4 provide a knowledge of how the catheter tip responds to the handle actuation and how the data from the strain sensor relates to the tip angle. In this section, this information is used to develop and evaluate a model-based control system to achieve a desired contact force at the catheter tip.

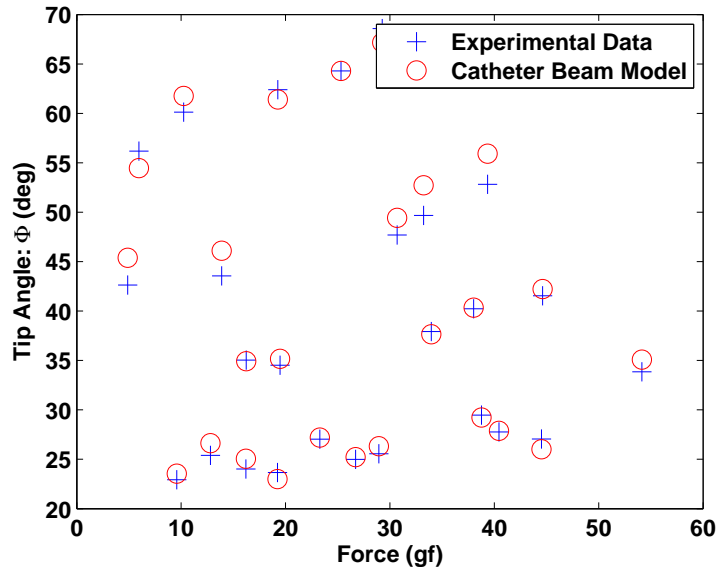


Figure 4.7: Estimating catheter tip angle from applied loads.

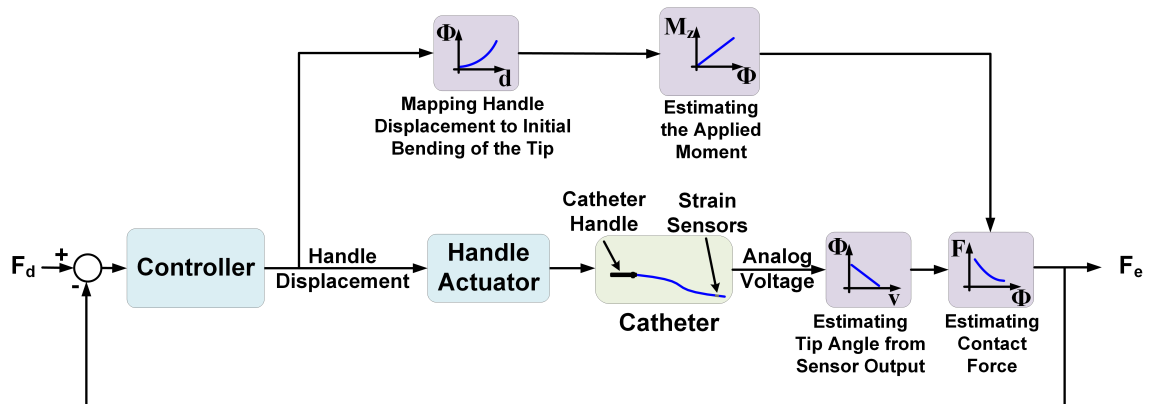


Figure 4.8: A schematic of the control system.

A schematic of the control system structure is shown in Figure 4.8. Receiving the control commands from the controller, the actuator (motorized linear stage) moves the catheter handle and bends the catheter tip, changing the readings of the optical strain sensor accordingly. The initial bending of the catheter is modeled as a moment load which is linearly related to the catheter tip angle. This angle is the one that

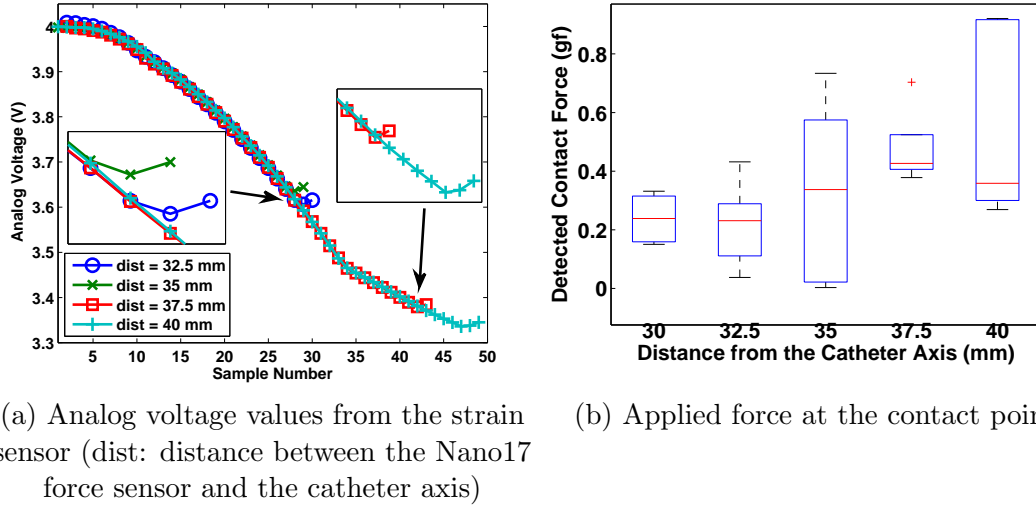


Figure 4.9: Performance of the system in detecting catheter tip/environment contact

the catheter tip would have in free space, if it did not come into contact with the environment and is calculated based on the handle displacement (Equation (4.3)). Using the force-deflection model for the catheter tip (Equation (4.4)), the contact force at the catheter tip is determined from the moment load and the tip angle estimated from the strain sensor data (Equation (4.1)). By adjusting the position of the catheter proximal handle, the PID controller maintains a desired contact force. Several sets of experiments are performed to evaluate the performance of different parts in this structure. The Nano17 force sensor is placed under the catheter tip and is used to provide a measure of the actual value of loads applied on the catheter tip. In a number of experiments, the force feedback is also closed using the data from this force sensor and the results are compared to those obtained by an estimation of the contact force. The parameters of the controller are tuned experimentally and remain the same through all the experiments.

4.5.1 Detecting Tip/Environment Contact

The purpose of our first experiment was to find if by monitoring the analog voltage from the top fiber of the strain sensor, we can detect that the catheter tip has come into contact with its environment. By actuating the proximal handle, the catheter

tip is bent until it touches the Nano17 force sensor. This point is marked by a change in the tip angle and thus by a sudden change in the trend of voltages read from the strain sensor. This deviation is observable in the voltage trend shown in Figure 4.9-a. The controller stops the handle actuation at this point. Placing the force sensor at different distances from the catheter axis, this procedure was repeated 5 times in each case and the contact force was recorded. The results are summarized in Figure 4.9-b. It can be seen that at the contact point, the force at the tip is less than 1 gf which verifies that observing the changes in the catheter tip angle can be an accurate measure to detect tip/environment contact.

4.5.2 Regulation Performance

In this set of experiments, the objective was to maintain a desired contact force at the tip. Following the control signal commands, the position of the proximal handle was finely adjusted such that a desired contact force was achieved at the catheter tip. This procedure was repeated for different values of the desired contact force and with placing the force sensor at different distances from the catheter axis. The contact force values and the control signals are shown in Figures 4.10 and 4.11. It was also tested if the desired contact force can be maintained when load disturbances are present (Figures 4.12 and 4.13) and when it is required to apply a varying force on the environment (Figures 4.14 and 4.15).

4.5.3 Estimating Contact Force from the Tip Shape

Visual feedback was used as an alternative to force feedback. Images from the catheter tip were captured consecutively; the tip angle was extracted from the images and the contact force was estimated from the tip angle. Figure 4.16 shows the results. This experiment was done to evaluate the accuracy of performing force-deflection calculations in real-time. The steady-state error in this case was 0.7 gf.

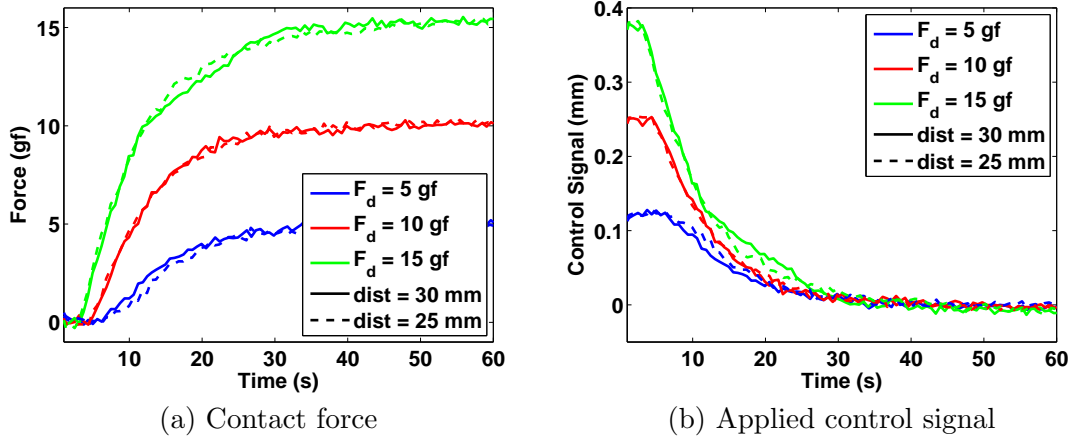


Figure 4.10: Regulation performance of the system with measured force feedback for different distances and desired contact force values ($F_d = 5, 10, 15$ gf; dist: distance between the Nano17 force sensor and the catheter axis)

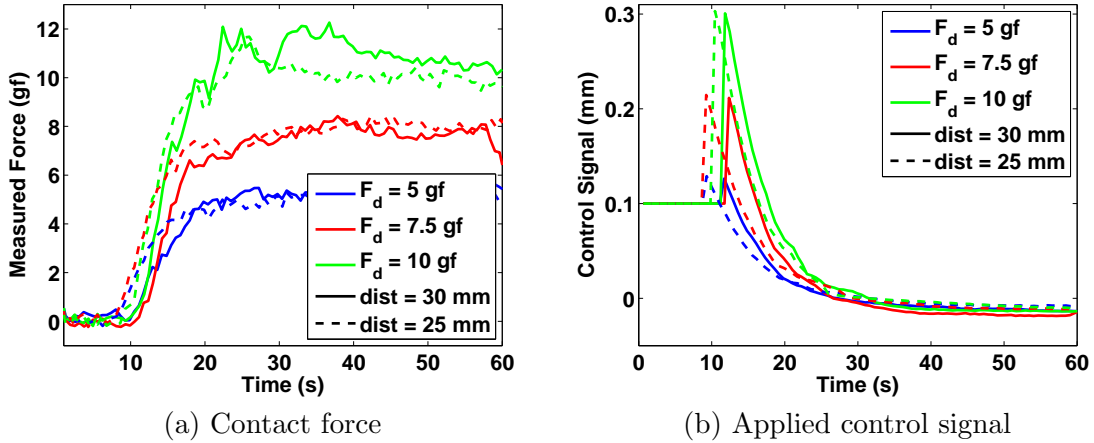


Figure 4.11: Regulation performance of the system with estimated force feedback (using strain sensor data) for different distances and desired contact force values ($F_d = 5, 10, 15$ gf; dist: distance between the Nano17 force sensor and the catheter axis).

4.6 Discussion

Section 4.5 presented the experimental results evaluating the performance of the proposed model-based control system for maintaining a desired force at the catheter tip in different scenarios. The control is implemented by precise manipulation of the catheter proximal handle, without involving inserting/retracting motions. Moreover,

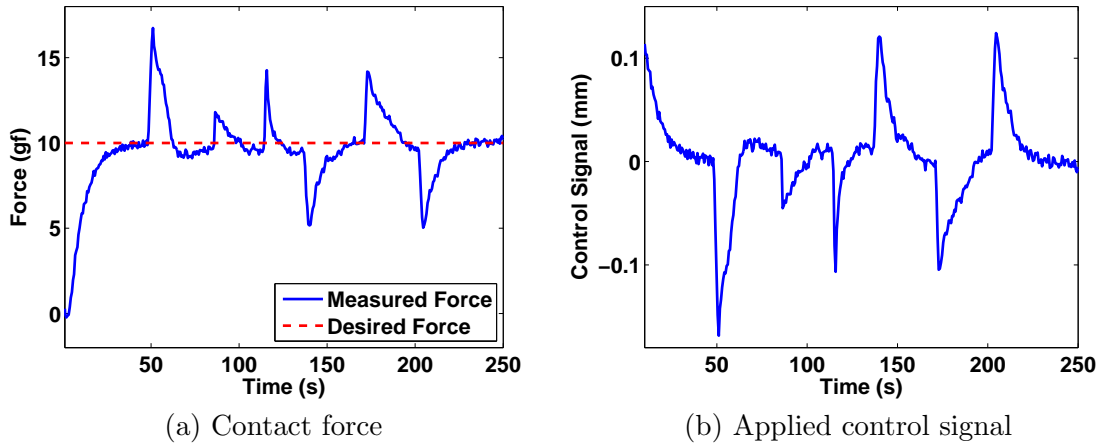


Figure 4.12: Performance of the system with measured force feedback in maintaining the desired contact force value.

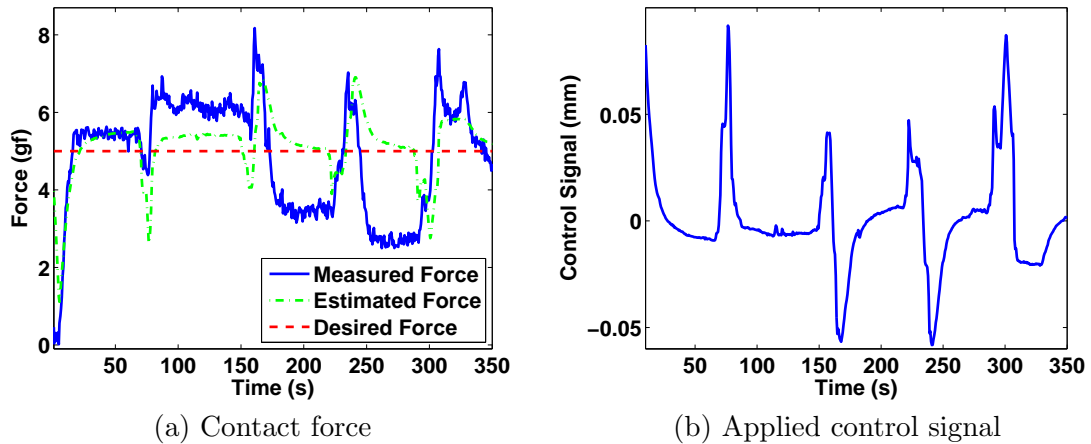


Figure 4.13: Performance of the system with estimated force feedback (using strain sensor data) in maintaining the desired contact force value.

since there are no out-of-plane deflections/loads, twisting the catheter handle is not required. To better analyze the system performance and the sources of errors, the designed experiments were in three different categories: with measured force feedback, with estimated force feedback and with visual feedback. The system shows good performance with the measured force feedback in all cases and the steady-state error is less than 1 gf. The strain sensor provides an accurate estimate of the tip angle

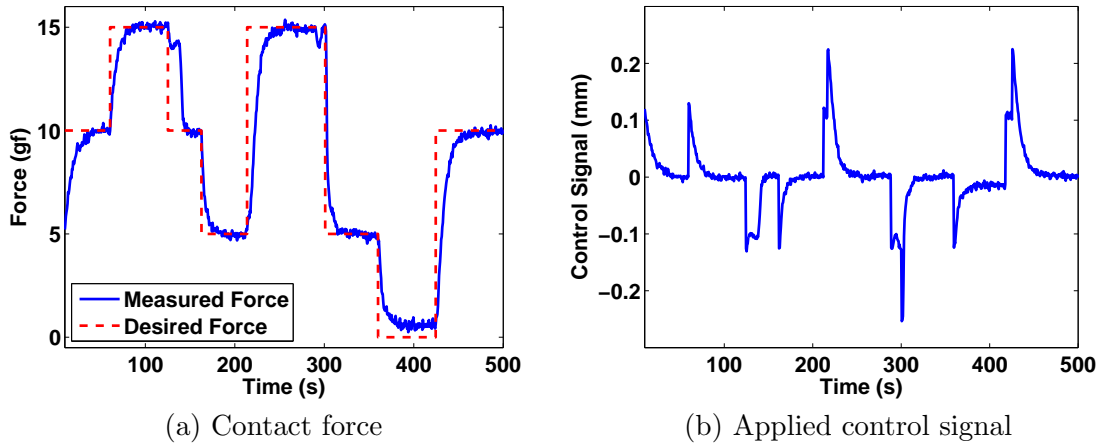


Figure 4.14: Performance of the system with measured force feedback in tracking the desired contact force values.

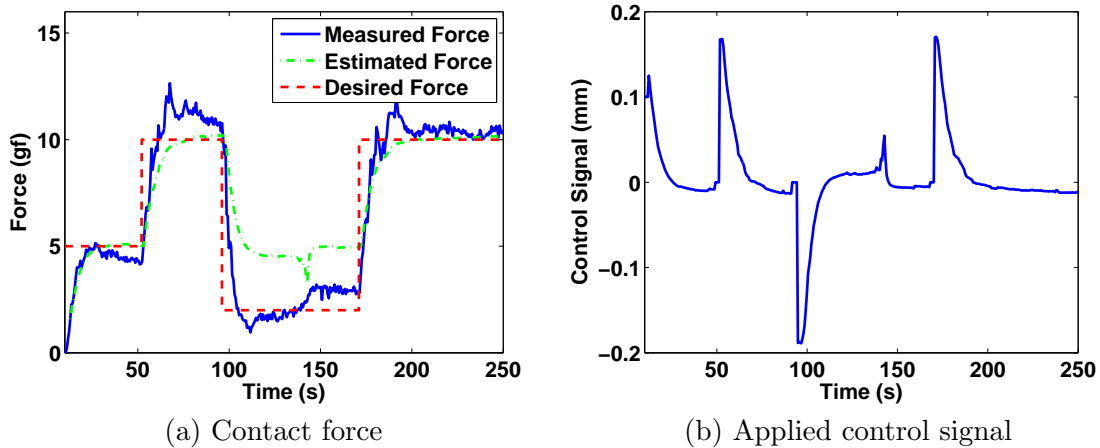


Figure 4.15: Performance of the system with estimated force feedback (using strain sensor data) in tracking the desired contact force values.

when the catheter tip is bending in free space. However, it is observed that its readings become much less accurate when the catheter tip is applying forces on the environment. Figure 4.17 shows the performance of the sensor in contact with the environment. In this figure, the measured tip angle and the measured contact force are shown with marker symbols. The handle displacement is the same for marker symbols with the same color and shape. Figure 4.17a shows the tip angle estimated from the

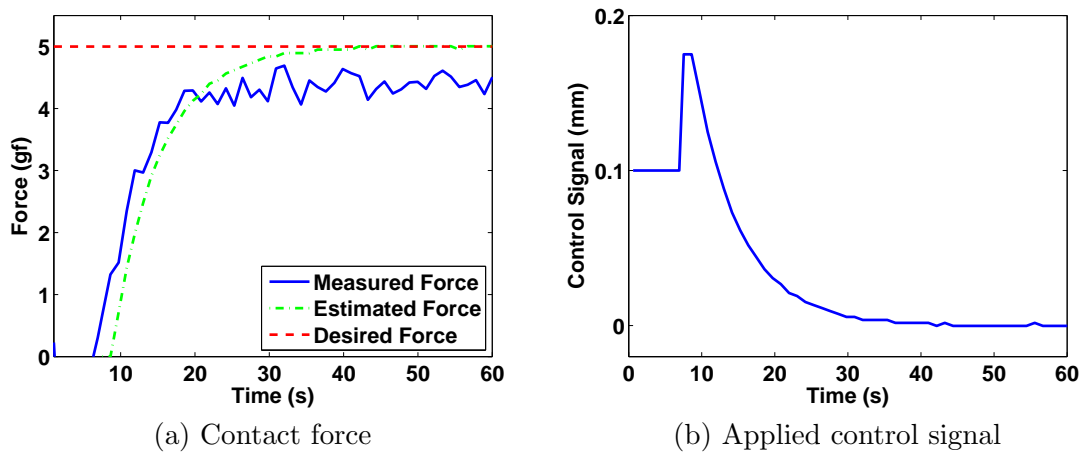


Figure 4.16: Performance of the system with estimated force feedback (using image data) in tracking the desired contact force values.

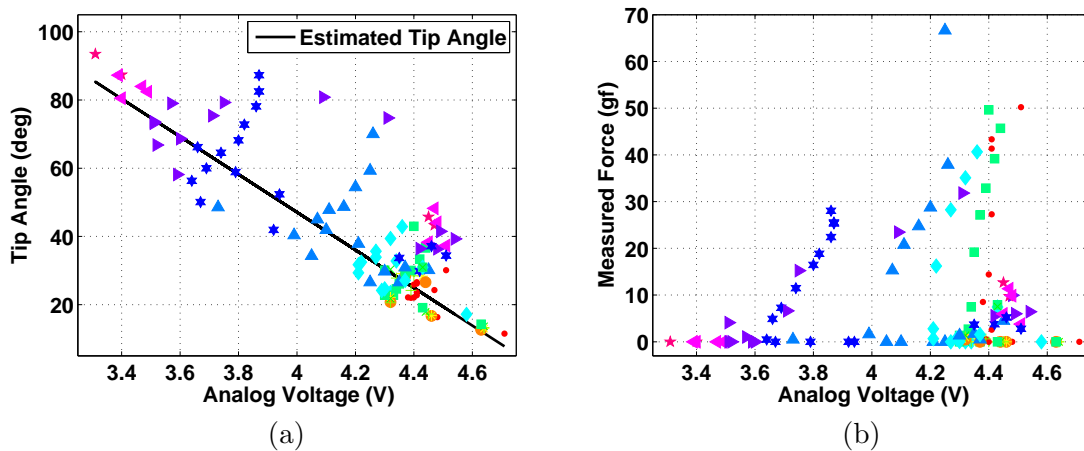


Figure 4.17: Catheter tip angle estimated from sensor output for different contact forces. The handle displacement for a similar marker symbol is the same. Marker symbols represent actual measured values.

sensor output as well as the actual tip angle for each output voltage measured from the captured images. Figure 4.17b shows the corresponding contact force for each voltage value. It is observed that for each handle displacement, different contact forces result in different tip angles, but this change in the tip angle remains hidden from the sensor. This is explained by observing that the shape of the flexed tip depends greatly on the magnitude and direction of the force that it is applying: although the angle at the

ablation tip increases to apply greater force, the base of the bending section where the optical strain sensor is mounted, becomes more straight. This results in an error in estimating the tip angle and hence deteriorating the control system performance. This problem will be addressed in future designs of the strain sensor. The results with the visual feedback suggest that the tip angle can be a good indicator of the applied forces and that observing the catheter shape may suggest an alternative for placing force sensors at the tip of ablation catheters. The system proposed here is presented as a proof of concept that designing a model-based force controller for the *conventional steerable catheters* is feasible.

4.7 Conclusions

In this chapter, different features of a steerable ablation catheter were studied with the purpose of developing a model-based force control system. To the best of our knowledge, this is the first attempt to perform model-based force control of the tip of a conventional steerable ablation catheter *without directly measuring the force applied at the catheter tip*. The custom designed strain sensor is a prototype that can be used with conventional steerable catheters and is capable of detecting the changes in the catheter tip angle to some extent. The proposed mappings together with the data from the strain sensor provide the information required for a control system which yields a desired contact force at the catheter tip. The performance of the proposed system was evaluated empirically and the results suggest that model-based force control of the catheter tip is feasible. Moreover, this approach allows for estimating the applied force from the catheter tip angle, without using a force sensor. This is a great advantage, since placing a force sensor at the tip of an ablation catheter is a challenge because of tip electrodes.

This work studied the problem of modeling and controlling a steerable ablation catheter under the assumption that the force applied on the catheter tip does not change very rapidly and that the force acts in the plane of the bent catheter. Developing a general model that is also capable of estimating the out-of-plane deflections of the catheter tip and evaluating the model and the control system in an experimental

environment with mimicking heart motion will lead to designing a control system that can potentially be used in robot-assisted catheter control.

References

- [1] M. Khoshnam, A. Yurkewich, and R.V. Patel, “Model-based force control of a steerable ablation catheter with a custom-designed strain sensor,” in *IEEE International Conference on Robotics and Automation (ICRA)*, 2013, pp. 4464–4469.
- [2] G. Ndrepepa and H. Estner, “Ablation of cardiac arrhythmias energy sources and mechanisms of lesion formation,” in *Catheter Ablation of Cardiac Arrhythmias*. Steinkopff, 2006, pp. 35–53.
- [3] F. Perna *et al.*, “Assessment of catheter tip contact force resulting in cardiac perforation in swine atria using force sensing technology / clinical perspective,” *Circulation: Arrhythmia and Electrophysiology*, vol. 4, no. 2, pp. 218–224, Apr 2011.
- [4] L. Di Biase *et al.*, “Relationship between catheter forces, lesion characteristics, popping, and char formation: experience with robotic navigation system.” *Journal of Cardiovascular Electrophysiology*, vol. 20, no. 4, pp. 436–40, Apr 2009.
- [5] K. Yokoyama *et al.*, “Novel contact force sensor incorporated in irrigated radiofrequency ablation catheter predicts lesion size and incidence of steam pop and thrombus,” *Circulation: Arrhythmia and Electrophysiology*, vol. 1, no. 5, pp. 354–362, Dec 2008.
- [6] “TactiCath Catheter.” [Online]. Available: www.endosense.com
- [7] “THERMOCOOL SMARTTOUCH Catheter.” [Online]. Available: www.biosensewebster.com

-
- [8] “Hansen Medical Sensei X Robotic Catheter System.” [Online]. Available: www.hansenmedical.com/sensei
- [9] W. Saliba *et al.*, “Novel robotic catheter remote control system: feasibility and safety of transseptal puncture and endocardial catheter navigation.” *Journal of Cardiovascular Electrophysiology*, vol. 17, no. 10, pp. 1102–5, Oct 2006.
- [10] “Stereotaxis NIOBE Magnetic Navigation.” [Online]. Available: www.stereotaxis.com
- [11] C. Pappone *et al.*, “Robotic magnetic navigation for atrial fibrillation ablation.” *Journal of the American College of Cardiology*, vol. 47, no. 7, pp. 1390–400, Apr 2006.
- [12] “Catheter Robotics Amigo RCS.” [Online]. Available: catheterrobotics.com/rcs-main.htm
- [13] J.W. Park *et al.*, “Development of a force-reflecting robotic platform for cardiac catheter navigation,” *Artificial Organs*, vol. 34, no. 11, pp. 1034–1039, Nov 2010.
- [14] Y. Fu, A. Gao, H. Liu, and S. Guo, “The master-slave catheterisation system for positioning the steerable catheter,” *International Journal of Mechatronics and Automation*, vol. 1, no. 3/4, pp. 143–152, Nov 2011.
- [15] Y. Fu, A. Gao, H. Liu, K. Li, and Z. Liang “Development of a novel robotic catheter system for endovascular minimally invasive surgery,” in *IEEE/ICME International Conference on Complex Medical Engineering (CME)*, 2011, pp. 400–405.
- [16] S.B. Kesner and R.D. Howe, “Force control of flexible catheter robots for beating heart surgery,” in *IEEE International Conference on Robotics and Automation (ICRA)*, 2011, pp. 1589–1594.
- [17] S.B. Kesner and R.D. Howe, “Position control of motion compensation cardiac catheters,” *IEEE Transactions on Robotics*, vol. 27, no. 6, pp. 1045–1055, Dec. 2011.

-
- [18] D.B. Camarillo, C.F. Milne, C.R. Carlson, M.R. Zinn, and J.K. Salisbury, “Mechanics modeling of tendon-driven continuum manipulators,” *IEEE Transactions on Robotics*, vol. 24, no. 6, pp. 1262–1273, Dec 2008.
- [19] P. Dupont, J. Lock, B. Itkowitz, and E. Butler, “Design and control of concentric-tube robots,” *IEEE Transactions on Robotics*, vol. 26, no. 2, pp. 209–225, Apr 2010.
- [20] K. Xu and N. Simaan, “Intrinsic wrench estimation and its performance index for multisegment continuum robots,” *IEEE Transactions on Robotics*, vol. 26, no. 3, pp. 555–561, Jun 2010.
- [21] K. Xu and N. Simaan, “Analytic formulation for kinematics, statics and shape restoration of multi-backbone continuum robots via elliptic integrals,” *Journal of Mechanisms and Robotics*, vol. 2, no. 1, pp. 011 006–1,011 006–13, Feb 2010.
- [22] M. Khoshnam, M. Azizian, and R.V. Patel, “Modeling of a steerable catheter based on beam theory,” in *IEEE International Conference on Robotics and Automation (ICRA)*, May 2012, pp. 4681–4686.
- [23] “Luna Fiber Optic Shape Sensing.” [Online]. Available: www.lunainc.com/growth-area/fiber-optic-shape-sensing
- [24] “Technobis Fibre Technologies.” [Online]. Available: www.technobis-fibre-technologies.nl
- [25] L. Howell, *Compliant Mechanisms*, ser. A Wiley-Interscience publication. Wiley, 2001, pp. 45–55.

Chapter 5

Analysis of the Tip Shape in Free Space and in Contact with the Environment

5.1 Introduction

Arrhythmia or the abnormal heart rhythm is the result of a problem within the heart's electrical system. When medications prove insufficient in restoring the normal heart rhythm, the next widely accepted remedy is a minimally invasive procedure, namely cardiac ablation, which is realized using long flexible catheters. During the ablation procedure, a steerable ablation catheter is steered through blood vessels into the heart chambers and then the catheter tip is used to deliver some type of energy (most commonly radio-frequency (RF)) to the heart tissue and ablate those parts that are considered to be the source of arrhythmia. During this procedure, the vasculature and the catheter are usually visualized via X-ray fluoroscopy, but a good visualization of the heart is not available due to low visibility of soft tissue in X-ray images. The efficacy of ablation treatment clearly depends on successfully detecting and ablating the parts of cardiac tissue that interfere with normal heart electrical signal activity. The other important factor is the quality of contact between the catheter tip and tissue, *i.e.*, the force that the catheter tip applies on the tissue [1–3]. Recently, RF ablation catheters with force sensors integrated within their tip have been introduced. The THERMOCOOL[®] SMARTTOUCH[™] Catheter (Biosense Webster, Diamond Bar, CA) [4] and the TactiCath[®] irrigated ablation catheter (Endosense[™], Switzerland) [5] report and visualize the magnitude and direction of the tip/tissue contact force [1, 3]. The axial force at the tip of Artisan[®] Extend Control Catheter (Hansen Medical, Mountain View, CA) [6] is measured by a sensor placed in its steerable sheath and is reported to the surgeon by visual as well as haptic feedback. Although,

these catheters use different methods to measure and report the contact force, they have one common feature: In order to operate, these catheters must be integrated with their custom navigation systems and interfaces, which are not widely available.

In order to propose an implementable technique for estimating the contact force at the tip of *conventional steerable catheters*, in this chapter, we investigate how the shape of the deflectable tip changes as the tip exerts a force on the environment and we show that the flexibility of the tip provides a means to estimating the contact force. The basic idea is close to the idea of “intrinsic force sensing” in the context of continuum robots [7–9], where a measure of contact force is provided using a kinematic model of the robot and information on actuation force at its joint. Rucker and Webster [10] used uncertain pose measurements in a probabilistic approach based on the Extended Kalman Filter to estimate the external loads applied on a tendon-driven continuum robot.

Several research groups have studied the kinematic modeling of steerable ablation catheters. A kinematic model was proposed for a tendon-driven catheter by Camarillo *et al.* [11]. The parameters of this model were determined using either the information from the actuation system or a vision-based shape sensing technique and the model predicted how tendon actuation would affect the catheter shape [11,12]. In another approach, the kinematic model developed primarily for continuum robots [13] was applied to model a commercially available pull-wire ablation catheter [14]. However, the basic assumption in developing these models is that the catheter bends with constant curvature along its length when the driving tendons/pull wires are actuated. This assumption was shown to be invalid when the effect of nonlinear internal friction is considered [15]. Moreover, these models deal with the problem of modeling the catheter tip in free space, *i.e.*, how the catheter tip deflects in response to actuating the driving tendons/pull-wires when the tip is not in contact with the environment. Thus, the effect of contact force on the tip shape has not been addressed.

Kesner and Howe [16–18] presented a robotic catheter system that can compensate for heart motion and provide force control at the catheter tip during mitral valve annuloplasty. In order to measure the contact force, they designed and placed a 3D force sensor [19] at the tip of the catheter. However, their method is not well

suiting for the case of ablation catheters, where the catheter tip is reserved for ablation electrodes.

Steerable catheters have been considered as continuum manipulators due to the fact that they do not have distinct rigid joints and links and that they bend continuously along their length [20]. However, most of the methods proposed for “intrinsic force sensing” in the context of continuum robots (*e.g.*, [7–10]) are built on information about the manipulator actuation mechanism and/or the kinematic model of the robot. This information is not available for *conventional steerable catheters* and thus many of the existing methods cannot be readily applied to the case of conventional steerable ablation catheters. Moreover, mounting sensors on the flexing tip changes the bending characteristics of the tip and introduces new difficulties with placing the corresponding wires inside the catheter body. It is expected that a thorough understanding of the behavior of conventional catheters would be very helpful in designing strategies to manipulate the catheter inside the complex anatomy, while guaranteeing a safe contact force at the catheter tip. During the ablation procedure, a medical imaging modality provides visual feedback from the surgical site. It would be very desirable if the data from this imaging modality can be used in determining the contact force as well. The work presented in this chapter provides the basis for two potential applications: (1) It shows that estimating contact forces from imaging data is feasible. The shape of the catheter can be analyzed to provide an estimate of the range of contact forces; and (2) this work determines what sections of the catheter tip should be monitored for determining changes in the contact force, and if an application requires mounting sensors on the catheter tip, what would be the best location for mounting such sensors.

In our previous work, we showed that it is possible to control the contact force at the catheter tip without mounting force sensors on the catheter [21]. This result was achieved through using the tip shape data from a custom-designed optical strain sensor and a previously developed model of the catheter tip that translates the tip angle into its corresponding contact force value [22, 23]. However, the designed optical strain sensor worked for a limited range of external loads, suggesting that either the sensor should be relocated on the tip or multiple sensors should be used. In

this chapter, understanding the necessity of studying the catheter behavior and estimating the contact force with minimal alterations to the structure of a conventional catheter, we use imaging data to study the effect of the actuation force as well as the in-plane external force on the catheter shape. Based on this study, a kinematic model for catheter deflection in free space is proposed and compared with existing models in the literature. Analyzing the catheter shape in contact with the environment, we define a force index to identify the range of forces exerted by the catheter tip. Studying the force data reported during ablation procedures [3], we determine the range of tip/tissue contact forces that are required for an effective ablation treatment. Experimental results on two different catheters prove that the defined force index can correctly detect the range of applied external forces in a majority of cases. Moreover, this study suggests a framework for evaluating the performance of sensors mounted on the tip, which can be used to determine the optimal number of sensors and their locations for different applications. This study is performed under the assumption that the applied forces act in the plane of the bent catheter. This is a valid assumption considering how the catheter tip is positioned with respect to the heart tissue for ablating a target point. To the best of our knowledge, the results presented in this chapter are the first to demonstrate the feasibility of determining catheter tip/environment contact force by analyzing the changes in the shape of the catheter tip.

The organization of the rest of this chapter is as follows: The experimental setup used for data collection and evaluation is described in Section 5.2. In Section 5.3, the catheter behavior in free space is analyzed and a kinematic model is proposed and evaluated. The effect of contact force on the catheter shape is analyzed and a force index is defined in Section 5.4. Experimental results for evaluating the proposed technique are presented in Section 5.5. Section 5.6 concludes the chapter with suggestions for future work.

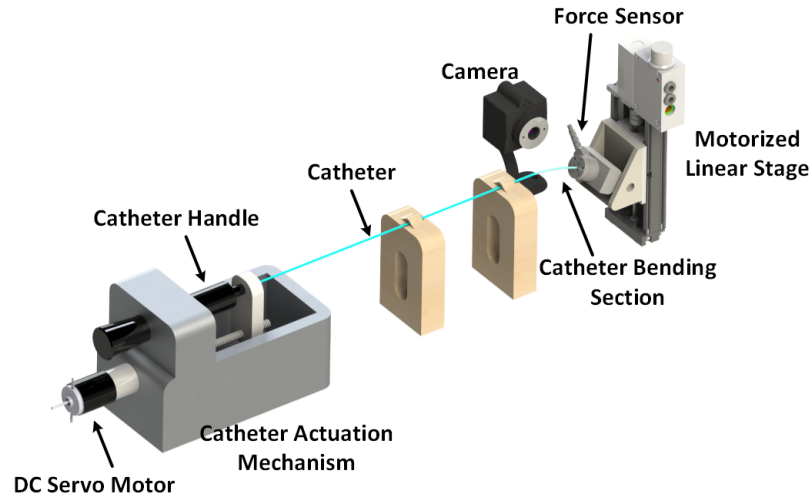


Figure 5.1: Schematic of the experimental setup.

5.2 Methodology

In this chapter, rather than making assumptions on the behavior of the catheter under applied loads (*e.g.*, bending with constant curvature in free space), we start with a careful observation and analysis of the changes in the catheter shape under different loading scenarios. In this section, the experimental setup used for collecting shape and force information and our method for extracting the catheter shape from the acquired images are explained.

5.2.1 Experimental Setup

The experimental setup used for data collection is shown schematically in Figure 5.1. The catheter is a 7-Fr unidirectional steerable ablation catheter (Biosense Webster, Diamond Bar, CA) that is actuated manually using the prismatic knob on its proximal handle (Figure 5.3). The prismatic knob can move from 0 mm to 15 mm: for a displacement of 0 mm, the catheter tip is completely straight and for a displacement of 15 mm, the catheter tip reaches its ultimate bent configuration.

To manipulate this catheter without any modifications to its structure, a 1-DOF actuation mechanism is designed which holds the catheter handle and actuates the manual knob using a DC servo motor (Maxon Precision Motors, Inc., Fall River,

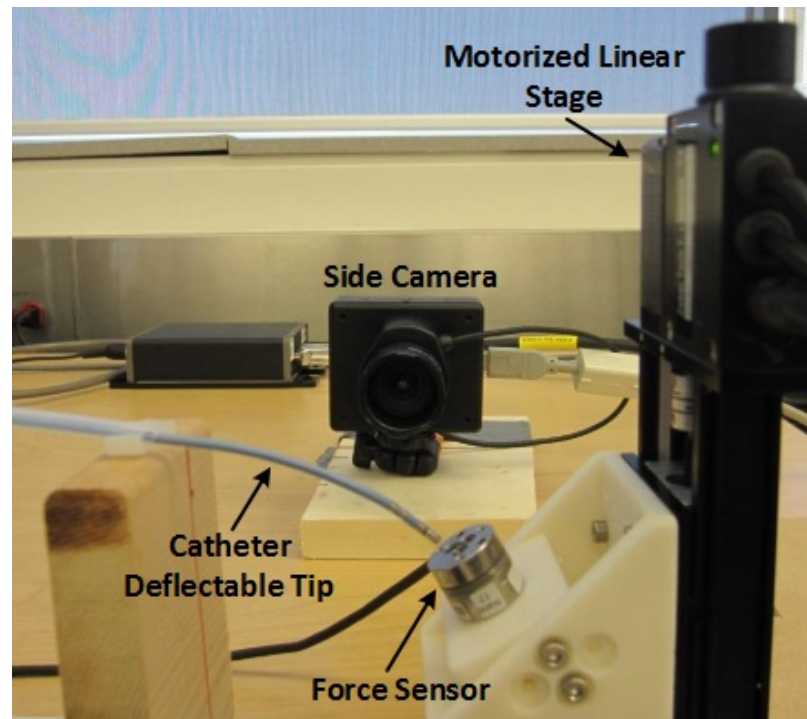


Figure 5.2: A view of the catheter tip, camera and force sensor in the experimental setup.

MA, US) and a small adapter. The catheter is passed through a standard sheath and is free to slide back and forth in it, but the sheath is fixed in two places along its length. The distal 8 cm of the catheter is the bending section, from which 1.5 cm is reserved for the ablation tip and electrodes, leaving 6.5 cm that flexes when the proximal handle is actuated (Figure 5.3). In this chapter, catheter tip refers to this bending section unless otherwise stated and “base point” refers to the starting point of the bending section (Figure 5.3). To ensure that the results are not affected by the non-flexible ablation tip, we focus on 5.5 cm of the bending section measured from the base point.

It should be noted that this study is aimed at understanding how the shape of the catheter tip changes if the proximal handle is actuated or if the catheter comes in contact with the environment. To ensure that the configuration of the catheter sheath does not affect the result of this study, the sheath was arranged in different configurations: completely straight, twisted midway first in the form of a half circular

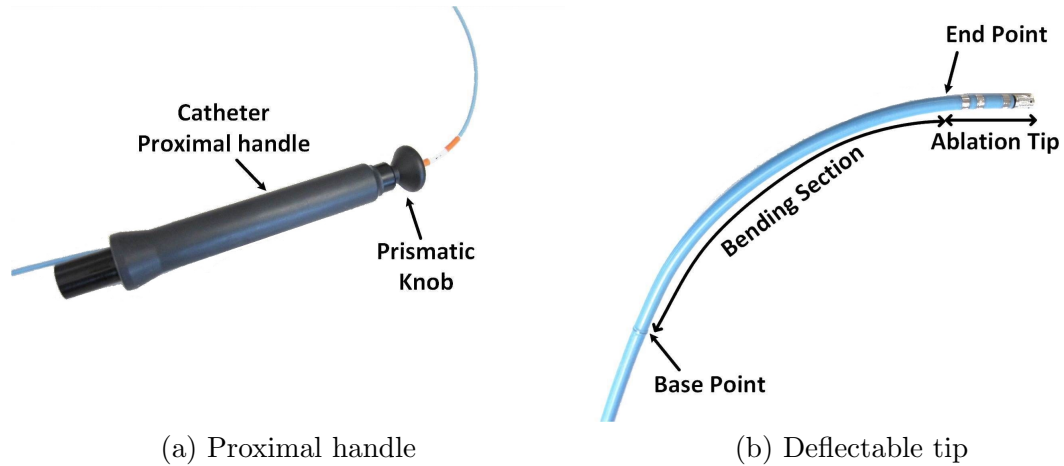


Figure 5.3: A close view of the proximal handle and the bending tip of a steerable ablation catheter

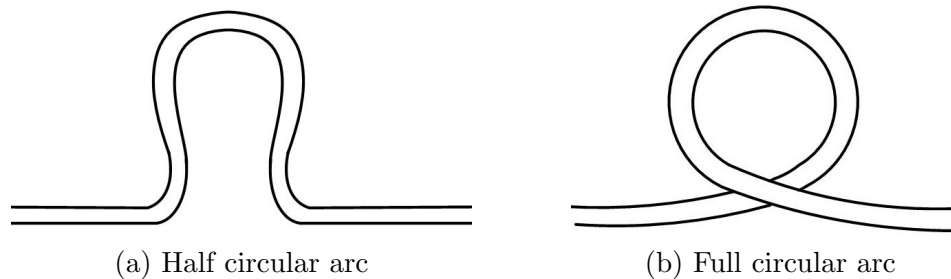


Figure 5.4: Different configurations of the catheter sheath to determine its effect on the results of the study.

arc and then in the shape of a full circular arc (Figure 5.4). A quick study reveals that different configurations of the sheath affect the dynamic relationship between the handle actuation and the tip shape, *e.g.*, actuation delay and backlash, as Kesner and Howe have indicated previously [17]; but have no effect on the static shape of the tip, which is the focus of this study.

A force sensor (Nano17, ATI Industrial Automation, Apex, NC, USA) is used as the environment with which the catheter interacts and thus a measure of contact forces acting on the ablation tip is provided. To apply forces with different magnitudes and directions, the force sensor is attached to a small adapter mounted on a motorized linear stage (Zaber Technologies Inc., Vancouver, BC, Canada). A cam-

era (Dragonfly[®], Point Grey Research Inc., Richmond, BC, Canada) is positioned to show a planar view of the catheter tip and provides images with a resolution of 640×480 pixels.

To investigate the catheter behavior with minimal modifications to the conventional practical method of performing the ablation procedures, this study starts with an observation on how the catheter tip shape changes when forces are applied to it. Using the force sensor as the environment, the contact forces are measured and recorded without mounting additional sensors on the catheter tip. The camera provides a means to monitor the catheter shape without affecting its bending characteristics. For each data sample, the shape and force values are recorded before proceeding to the next sample, so the time interval between each two consecutive data samples is about 1-2 seconds. All data points are saved to be processed later.

5.2.2 Extracting the Tip Shape from Images

In this section, the algorithm for extracting the shape of the tip from captured images and obtaining the curvature is explained.

An image captured by the camera is shown in Figure 5.5a. Hannan and Walker proposed a method for estimating the shape of continuum robots using images [24]. Since they had assumed constant curvature for each section of the manipulator, identifying three points of each section was sufficient to determine the curvature. Herein, in order to analyze the actual behavior of the catheter, we do not make any pre-assumptions on the catheter characteristics, including its bending curvature and we use a custom algorithm to find the curve representing the catheter shape. In this regard, masking the unwanted objects and thresholding the image to obtain the catheter pixels are the first steps in the image processing. The result is the black and white image shown in Figure 5.5b. In the next step, a vertical mask of 5-pixel width is defined. This mask is moved along the catheter and the centroid point of the masked image is determined (Figure 5.5c). If the catheter tip is flexed to reach a tip angle of about 90° or more, the vertical mask fails to find the centroid points accurately. Hence, it is replaced by a horizontal mask and the process of finding the centroid

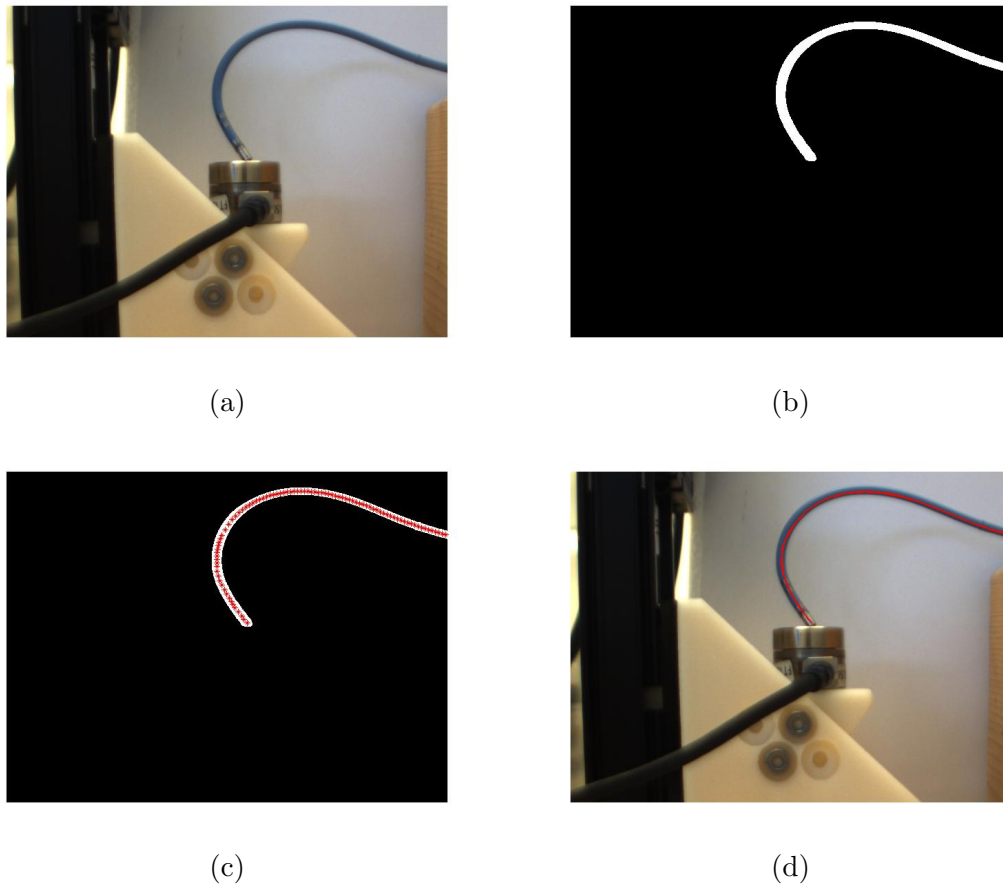


Figure 5.5: Catheter shape estimation. Step-by-step. Catheter shape estimation. Step-by-step - (a) Sample original image. (b) Masked black and white image. (c) Centroid points. (d) Comparing the calculated curve to the catheter shape.

points is continued until the tip end is reached. The centroid data points are then smoothed using a moving average, and a spline curve, f_{curve} , is fitted on data points to give the final line representing the shape. More details on this algorithm are given in Algorithm 1.

To ensure that the developed algorithm faithfully preserves the changes in the tip shape, the extracted line is overlaid with each captured image (Figure 5.5d). This final manual check demonstrates the performance of the implemented algorithm.

Using the information of the pixel size in the captured images, the calculated curve (f_{curve}) can be expressed in millimeters. Choosing a point P on the tip that

is located at a certain distance from the base point is then straight forward:

$$L = 0.1 \int_{BP}^P \sqrt{1 + \left(\frac{d f_{curve_{mm}}(x)}{dx} \right)^2} dx \quad (5.1)$$

where BP is the base point, P is the desired point, $f_{curve_{mm}}$ is the calculated curve expressed in millimeters, and L is the distance of P from BP in centimeters. As an example, the points that are located between 3.5 cm and 5 cm from the base point are marked in red in Figure 5.14.

This technique was tested by marking several points along the catheter tip. The error in finding the distance between the marked points and the defined base point never exceeded 2%, which provides an acceptable accuracy for the aim of this study.

5.3 Analysis of the Tip Curvature in Free Space

Observing the image data acquired with the technique explained in Section 5.2 suggests that the loads applied at the tip cause a change in its curvature. In this section, the effect of actuating the proximal handle on the tip curvature is studied, a kinematic model for the flexing tip is proposed and the reachable workspace and singular configurations are briefly discussed.

The curvature of a smooth curve is defined as:

$$\kappa = \frac{d\phi}{ds} \quad (5.2)$$

where ϕ is the tangential angle and s is the arc length. To obtain the curvature value along the catheter tip, the tangential angle is calculated at equispaced points located at 0.5 mm from one another and then Equation (5.2) is applied. Possible inflection points are those at which the obtained curvature changes sign.

The catheter's distal shaft bends in response to the proximal handle actuation. Although the prismatic knob on this handle has a range between 0 and 15 mm, noticeable changes in the tip angle occur for displacements of more than 7 mm [21]. Steering the knob from 7 mm to 15 mm, the resulting curvature is demonstrated in

Algorithm 1 Extract the curve representing the shape of the catheter tip in the image.

Require: Images of the catheter tip captured by the camera

```

1: for i=1:number of images do
2:    $I \leftarrow image(i)$ 
3:   if base point is marked with color then
4:      $filteredI \leftarrow color\ filter(I)$ 
5:      $BP \leftarrow centroid(filteredI)$ 
6:   else
7:     Prompt user to click on the base point
8:      $BP \leftarrow$  Point of click
9:   end if
10:   $ROI \leftarrow mask(I)$  // Removing unwanted objects
11:   $BWROI \leftarrow binary(ROI)$ 
12:   $vMask \leftarrow$  Define a 5-pixel width vertical mask
13:   $cPts(1) \leftarrow BP$ 
14:   $cntr \leftarrow 1$ 
15:   $Flag \leftarrow vertical$ 
16:  while  $cPts(cntr)$  exists do
17:    if  $Flag = vertical$  then
18:       $MROI \leftarrow overlay(BWROI, vMask)$ 
19:       $cPts(cntr + 1) \leftarrow centroid(MROI)$ 
20:       $vMask \leftarrow$  Shift  $vMask$  horizontally by 5-pixels
21:    end if
22:    if  $distance(cPts(cntr+1), cPts(cntr)) > 10$  pixels ||  $Flag = horizontal$  then
23:       $hMask \leftarrow$  Replace the vertical mask with a 5-pixel width horizontal mask
24:       $MROI \leftarrow overlay(BWROI, hMask)$ 
25:       $cPts(cntr + 1) \leftarrow centroid(MROI)$ 
26:       $hMask \leftarrow$  Shift  $hMask$  vertically by 5-pixels
27:       $Flag \leftarrow horizontal$ 
28:    end if
29:     $cntr ++$ 
30:  end while
31:   $fPoints \leftarrow smooth(cPts)$ 
32:   $fcurve(i) \leftarrow curvefit(fPoints)$ 
33: end for
34: return  $fcurve$ 

```

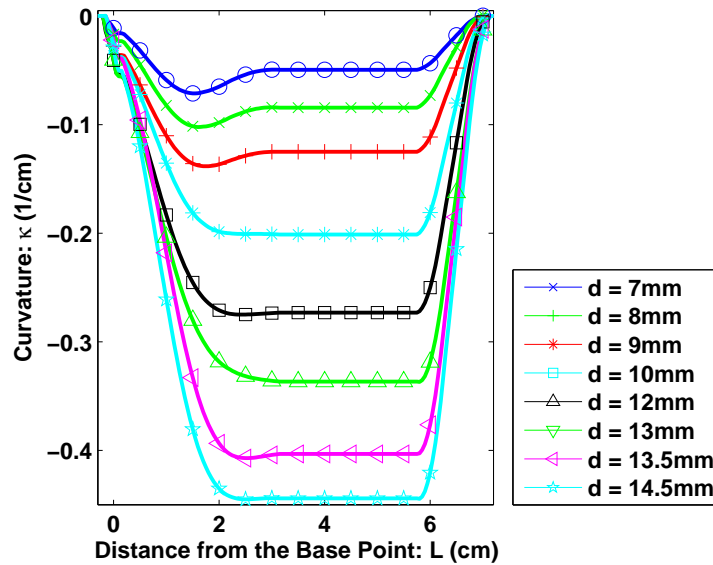


Figure 5.6: Tip curvature when the proximal handle is actuated (d = handle displacement).

Figure 5.6 for a number of handle displacements. It is observed that the curvature is almost zero before the base point, but then increases linearly with the distance from the base point, until it becomes almost constant in the section located between 2 cm from the base point to 6 cm from it. The curvature then decreases linearly and again becomes almost zero at the section containing the ablation tip and electrodes. The question then arises is if a certain displacement always results in the same tip profile. To investigate this, the proximal handle is moved by 10 mm (handle displacement = 10 mm), the tip shape is recorded, the handle is moved back to its initial position (handle displacement = 0 mm). This process is repeated 5 times, allowing the tip to completely restore its straight shape between two consecutive repetitions. The result is shown in Figure 5.7. It is concluded that although there is a small difference in the values of the obtained curvature for each run, the resulting behavior is the same: the curvature is almost zero at the base point and the ablation tip and has a constant value in the mid-section of the tip.

This observation suggests that assuming a constant curvature for the unloaded catheter tip is not very accurate. A possible justification for this behavior is that

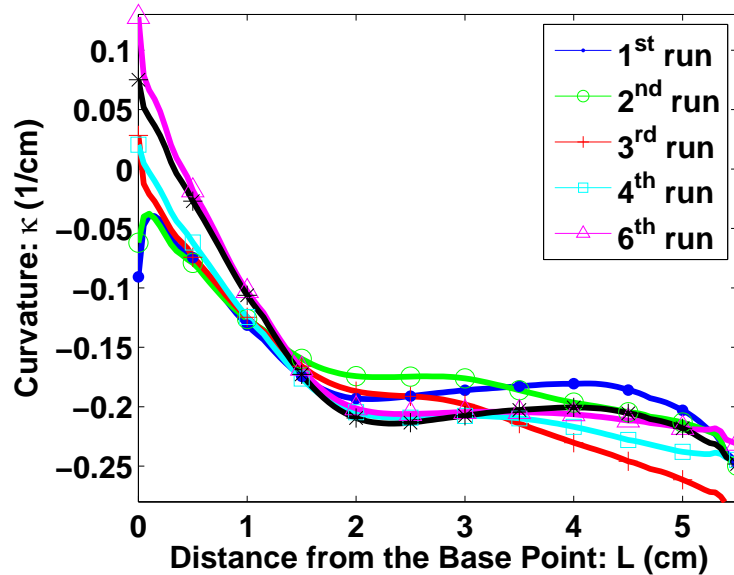


Figure 5.7: Tip curvature when handle displacement is 10 mm.

the internal structure of the catheter tip is designed such that when the handle is actuated, the mid-section of the tip is subjected to a series of loads with the resultant effect that is the same as that of a dominant pure moment load, hence resulting in a constant curvature for this section. However, from the base point upto this section, the acting loads have the effect of a dominant shear force. A detailed discussion on the arrangement of internal forces of the catheter is possible by examining the internal structure of the tip more closely, but this is beyond the scope of this chapter.

5.3.1 Kinematic Model

Figure 5.6 shows that only the mid-section of the flexing tip bends with constant curvature. Based on this observation, additional joints and links are added to the kinematic model for a continuum robot [13] to develop a kinematic model for the catheter tip. In deriving this model, it is assumed that the catheter bends with zero torsion. This assumption was validated experimentally: the deflected catheter lies in a plane.

The proposed kinematic model is demonstrated in Figure 5.8. This model is characterized by three sections ($P_i = (x_i, y_i)$, $i = 1, \dots, 7$ is the origin of the coordinate

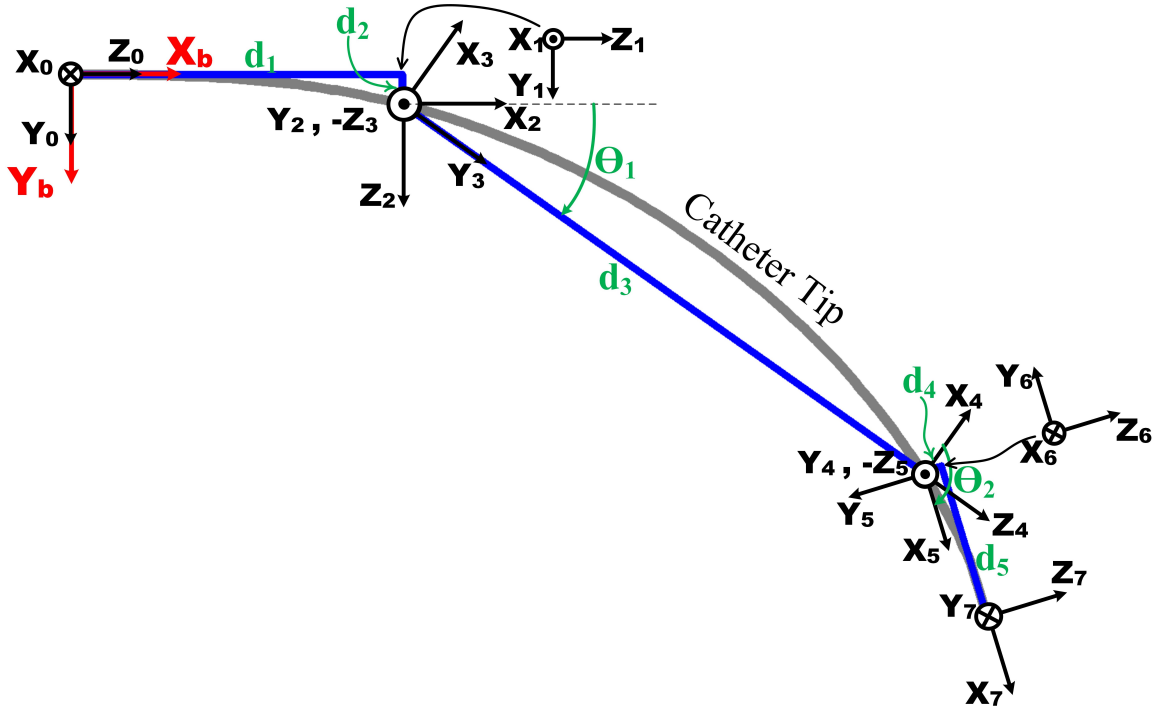


Figure 5.8: Kinematic model for the catheter tip and the assigned D-H coordinate frames.

frames i):

- $P_0P_1P_2$: the section with the constant curvature does not start immediately from the base point, P_0 . Section $P_0P_1P_2$ represents this variable offset by two perpendicular prismatic joints d_1 and d_2 . The reason for choosing P_0 as the base point (Figures 5.3b and 5.8) becomes clear: The curvature before this point is zero and the flexing tip is aligned with the catheter body at the base point. P_0 can act as the virtual basis of the tip in this model.
- P_3P_4 : this section consists of one rotation θ_1 , one translation d_3 and another rotation θ_2 to model the planar constant-curvature arc in accordance with [13].
- $P_5P_6P_7$: in this section, two perpendicular prismatic joints, d_4 and d_5 replace the variable offset between the last point on the constant-curvature arc and the last point of the flexing tip, *i.e.* end point (Figure 5.3b). The ablation tip is then reached by a linear extension from this point and is not shown in the figure.

Table 5.1: Link parameters of the proposed kinematic model for the catheter tip.

i	α_{i-1}	a_{i-1}	d_i	θ_i	Joint Variable Limits
1	0	0	d_1	0	$19.3 \text{ mm} < d_1 < 20 \text{ mm}$
2	$-\pi/2$	0	d_2	$-\pi/2$	$0 \text{ mm} < d_2 < 4 \text{ mm}$
3	$\pi/2$	0	0	$-(\pi/2 - \theta_1)$	$0 < \theta_1 < \pi/2.15$
4	$-\pi/2$	0	d_3	0	$33.2 \text{ mm} < d_3 < 40 \text{ mm}$
5	$\pi/2$	0	0	θ_2	$\pi/2 < \theta_2 < \pi/1.03$
6	$\pi/2$	0	d_4	$\pi/2$	$0 \text{ mm} < d_4 < 2.04 \text{ mm}$
7	$\pi/2$	0	d_5	0	$9.64 \text{ mm} < d_5 < 10 \text{ mm}$

The assigned Denavit-Hartenberg (D-H) frames are also shown in Figure 5.8 and D-H parameters are given in Table 5.1. It should be noted that although the proposed model is planar, to comply with D-H convention [25], all three axes are considered. The coordinate frame $\{0\}$ is the virtual base for the model and a rotation about Y_0 axis relates this frame to the base frame $\{b\}$. The limits of joint variables are obtained experimentally. It should also be noted that the flexing of the tip is a result of actuating the catheter handle, so the joint variables change according to the handle displacement and cannot take independent values in their corresponding range.

The homogeneous transformation matrix that relates frame $\{7\}$ to frame $\{0\}$ is obtained as in Equation (5.3).

$${}^0_7T = \begin{bmatrix} -1 & 0 & 0 & 0 \\ 0 & -s\theta_1\theta_2 & -c\theta_1\theta_2 & d_2 + d_3s\theta_1 - d_4s\theta_1\theta_2 - d_5c\theta_1\theta_2 \\ 0 & -c\theta_1\theta_2 & s\theta_1\theta_2 & d_1 + d_3c\theta_1 - d_4c\theta_1\theta_2 + d_5s\theta_1\theta_2 \\ 0 & 0 & 0 & 1 \end{bmatrix} \quad (5.3)$$

The workspace of the catheter tip is realized by varying joint variables in their corresponding range. The model is also rotated about axis Y_0 by angle $\theta_r \in [0, 2\pi]$ to yield the 3D workspace shown in Figure 5.9. For the sake of clarity, the catheter tip is also shown for a number of cases. The workspace can be translated in space by inserting/retracting the catheter from the proximal end.

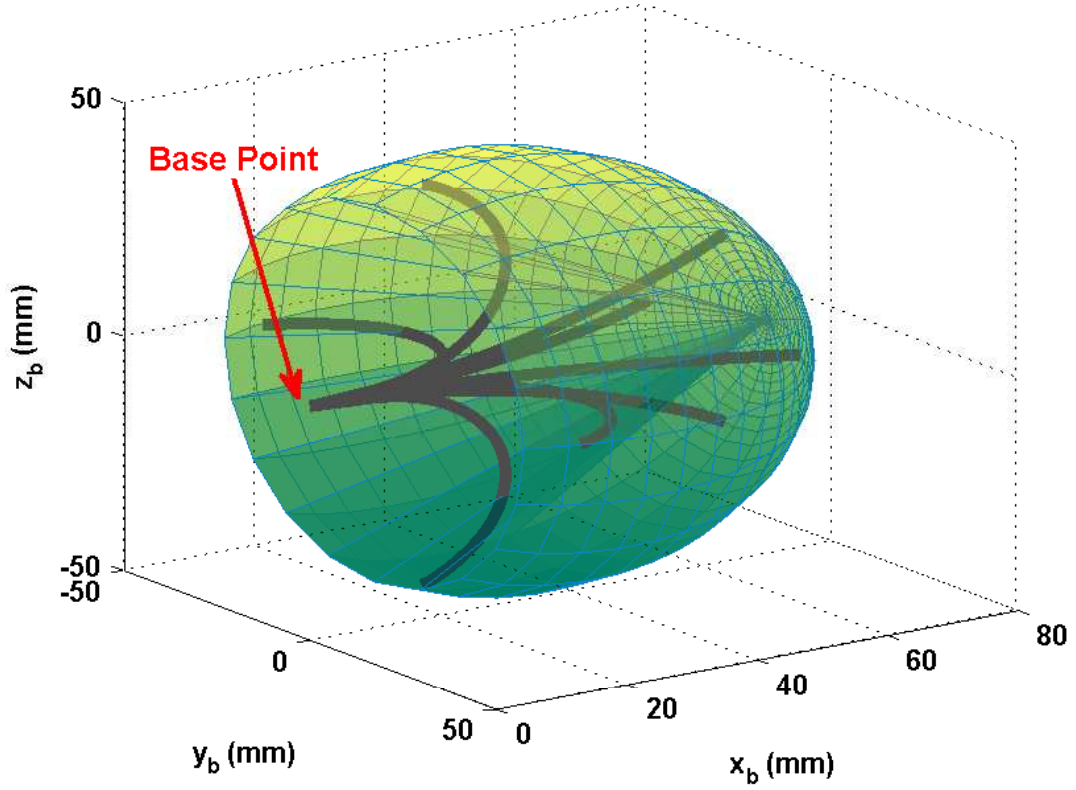


Figure 5.9: Catheter tip workspace in 3D with respect to frame $\{b\}$. The joint variables are changing in their experimentally obtained range and θ_r is varied between 0 and 2π . The thick gray lines represent the tip shape.

The Jacobian matrix (Equation (5.4)) is a 2×7 matrix with respect to the base frame $\{b\}$.

$${}^b J_v = \begin{bmatrix} 1 & 0 & d_5 c \theta_1 \theta_2 + d_4 s \theta_1 \theta_2 - d_3 s \theta_1 & c \theta_1 & d_5 c \theta_1 \theta_2 + d_4 s \theta_1 \theta_2 & -c \theta_1 \theta_2 & s \theta_1 \theta_2 \\ 0 & 1 & d_5 s \theta_1 \theta_2 - d_4 c \theta_1 \theta_2 + d_3 c \theta_1 & s \theta_1 & d_5 s \theta_1 \theta_2 - d_4 c \theta_1 \theta_2 & -s \theta_1 \theta_2 & -c \theta_1 \theta_2 \end{bmatrix} \quad (5.4)$$

The determinant of ${}^b J_v {}^b J_v^T$ never becomes zero, showing that there are no singularities in the workspace of the developed model. Considering the structure of a catheter, the tip is bent when the proximal handle is actuated and in the base frame $\{b\}$, x_7 , y_7 and Φ cannot be defined independently. This means that each point in

the workspace can be reached only from one orientation and that the catheter tip has one degree of freedom. This degree of freedom is never lost in the physical workspace, matching with the result obtained from the model that the determinant of ${}^b J_v {}^b J_v^T$ never becomes zero.

Recalling that the section located between 2 cm and 6 cm from the base point is a circular arc, *i.e.*, its curvature is constant, the relationship between the model parameters and the tip shape is derived:

- d_1 and d_2 are the horizontal and vertical distances from the starting point of the curvature, P_2 , to the base point, P_0 , respectively.
- θ_1 is the slope of the line connecting P_3 to P_4 .
- θ_2 , d_4 and d_5 are obtained taking into account that the position and orientation of the manipulator end-effector should be the same as those of the catheter tip. Figure 5.10 shows how the model links are arranged with respect to the catheter tip. From this figure, it can be seen that the following equations hold:

$$\theta_2 = \frac{\pi}{2} + \Phi - \theta_1 \quad (5.5)$$

$$d_4 = \frac{|mx_5 - y_5 - mx_7 + y_7|}{\sqrt{1 + m^2}}, m = \tan \Phi \quad (5.6)$$

$$d_5 = ||P_6 - P_7|| \quad (5.7)$$

where x_i and y_i correspond to the coordinates of point P_i , $i = 1, \dots, 7$ (Figure 5.8).

If the catheter tip shape is completely known, the model variables are known and the modeling error will be zero as expected. However, in real applications, detailed information about the tip shape is not available. To propose a practical method for obtaining the model parameters, for each handle displacement, the model parameters are derived from experimental data and then for each parameter of the model, a mapping is found to relate it to the handle displacement. Using these mappings, the model performance in estimating the tip shape is evaluated. Table 5.2 provides statistical measures that show the model performance, where MAE and RMSE denote the mean absolute error and the root mean squared error, respectively. The results

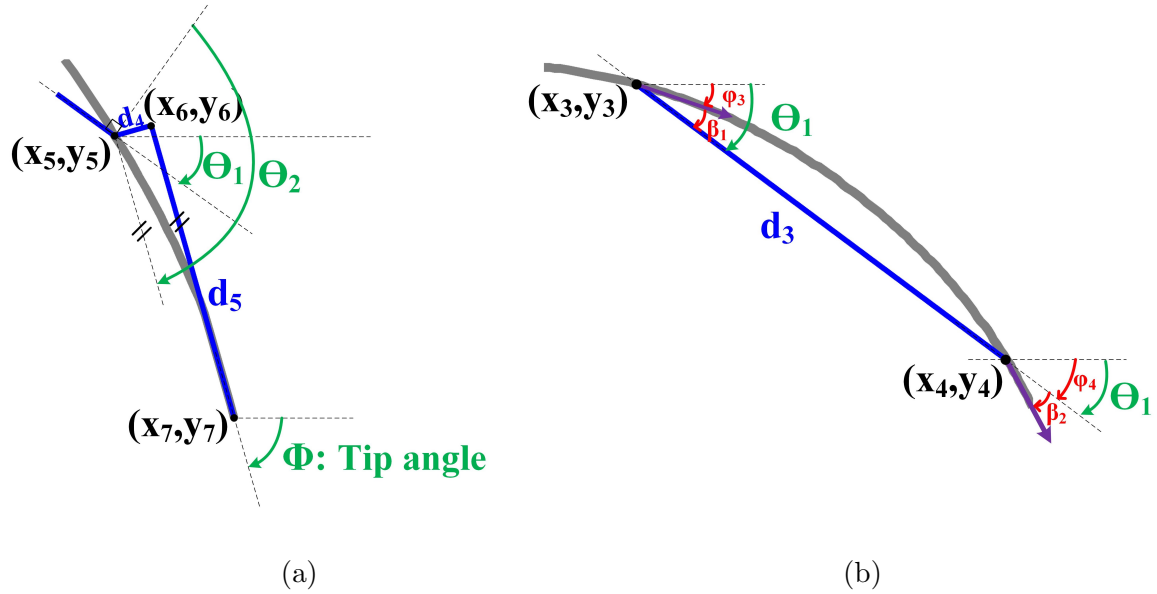


Figure 5.10: (a) Model end-effector and the catheter tip. (b) Section of the tip with constant curvature.

Table 5.2: Statistical measures showing the performance of the proposed kinematic model, the kinematic model obtained assuming constant curvature for the flexing tip and the pseudo-rigid-body (PRB) 3R model, when the proximal handle is moved from 7 mm to 15 mm. \hat{x} , \hat{y} , $\hat{\Phi}$ are the estimated values for x_7 , y_7 , Φ using each model.

	$MAE(\hat{x})$	$RMSE(\hat{x})$	$MAE(\hat{y})$	$RMSE(\hat{y})$	$MAE(\hat{\Phi})$	$RMSE(\hat{\Phi})$
Proposed kinematic model (θ_1 obtained from mapping)	1.88 mm	2.38 mm	1.92 mm	2.98 mm	4.57°	5.77°
Proposed kinematic model (θ_1 obtained from curvature values)	0.41 mm	0.45 mm	0.61 mm	0.72 mm	1.91°	2.49°
Constant-curvature kinematic model	1.68 mm	2.21 mm	2.05 mm	3.35 mm	11°	12.67°
PRB 3R model	0.42 mm	0.59 mm	0.79 mm	1.02 mm	2.21°	2.39°

show an error in estimating the position of the end-effector. A closer look reveals that the accuracy of the model is highly dependent on the value of θ_1 and thus having a good estimate of θ_1 is necessary. There are a few methods to obtain this angle:

1. θ_1 is the angle of the line connecting P_3 to P_4 . If the position of these two

points is known, *e.g.*, by using electromagnetic sensors, obtaining θ_1 is straight forward.

2. The constancy of the tip curvature between P_3 and P_4 means that $\beta_1 = \beta_2$ in Figure 5.10. Consequently:

$$\theta_1 = \frac{\phi_3 + \phi_4}{2} \quad (5.8)$$

where ϕ_3 and ϕ_4 are tangential angles at P_3 and P_4 , respectively.

3. A mapping can be defined to express θ_1 in terms of the curvature values at P_3 and P_4 .

θ_1 may be estimated with either of these methods. The results presented in Table 5.2 are obtained using the third method and show a clear improvement over the last case where θ_1 was directly mapped to the handle displacement.

5.3.2 Model Performance

The performance of the proposed kinematic model in estimating the tip shape in free space is now compared to that of two other models, namely, the kinematic model that is derived based on the assumption of curvature constancy for the catheter tip [13, 14] and the pseudo-rigid-body (PRB) 3R model proposed in [23].

Assuming a constant curvature for the catheter tip implies modeling the tip with a circular arc that passes through the base point with a slope equal to zero. A circular arc which satisfies these rules is fitted to the tip shape and the results are given in Table 5.2.

The optimal link parameters and spring stiffness values for the PRB 3R model are obtained by recording the displacements that different values of contact force impose on the end point and using the same algorithm proposed in [23]:

$$\gamma_0 = 0.2, \quad \gamma_1 = 0.4, \quad \gamma_2 = 0.25, \quad \gamma_3 = 0.15 \quad (5.9)$$

$$k_{\theta_1} = 2.8, \quad k_{\theta_2} = 5, \quad k_{\theta_3} = 2.1$$

where $\gamma_i, i = 0, 1, 2, 3$ are the normalized link lengths and $k_{\theta_i}, i = 1, 2, 3$ are the nor-

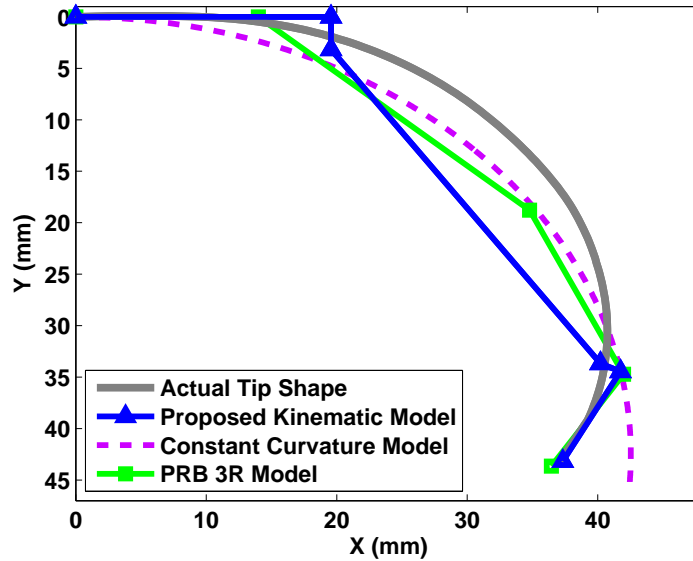


Figure 5.11: Configuration of links in the proposed kinematic model, the kinematic model obtained assuming constant curvature for the flexing tip and the pseudo-rigid-body PRB 3R model versus the actual tip shape.

malized spring stiffness values. The results of estimating the position and orientation of the tip point with this model are also given in Table 5.2.

Figure 5.11 shows how the model links are arranged with respect to the actual catheter shape when the proximal handle is moved by 13 mm. Observing this figure and the statistical results presented in Table 5.2, the kinematic model presented in this chapter is more accurate in estimating the position of the end point and the tip angle. Assuming constant curvature for the tip produces a noticeable estimation error. When there is a contact force between the tip and the environment, both of these models become invalid, while the PRB 3R model can still predict the tip angle under applied loads. If reconstructing the catheter shape in free space is desired, the proposed kinematic model can achieve this goal when θ_1 is known, however, the two other models do not give a hint about the catheter's actual shape in free space. It is possible to use the proposed kinematic model for describing the catheter in free space and use the PRB 3R model to estimate the tip angle when there is a contact between the catheter tip and the environment. Experimental results show that when there is a force at the catheter tip, the error in estimating the position of y_4 is greater than

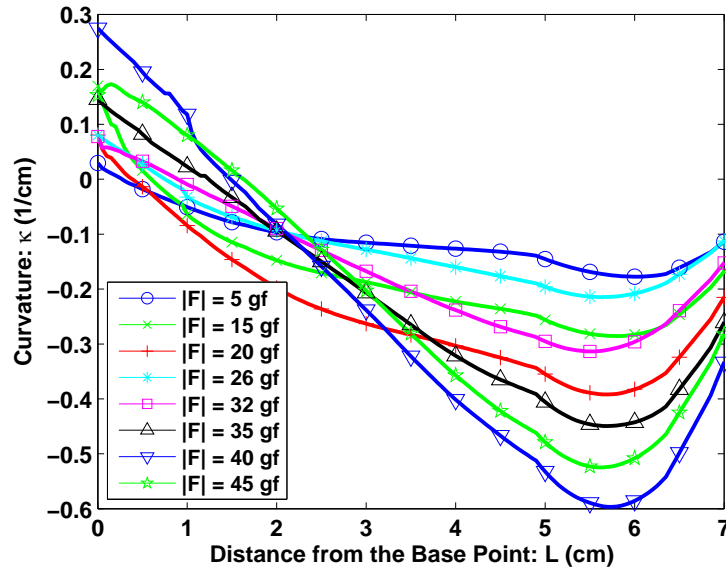


Figure 5.12: Tip curvature when forces are applied at the tip.

3 mm. The force index defined in the next section is another way to decide when to switch between the two models.

5.4 Effect of Contact Force on the Tip Shape

To study how the tip shape changes when the catheter comes in contact with the environment, using the experimental setup described in Section 5.2, the catheter tip is pushed against the force sensor in different in-plane directions. Figure 5.12 shows the tip curvature obtained from the acquired images for a number of force magnitudes and handle displacements. As expected, there are considerable variations in the curvature values along the tip length and a section with constant curvature is not observed anymore. In fact, this figure does not immediately suggest a relationship between the contact force and the tip shape, and a more in-depth study is required. In this regard, twelve equispaced points are chosen along the tip, the first of which is located at the base point. Figure 5.13 shows the extent of curvature variations caused by the contact force at each selected point for several handle displacements. The impact of the contact force on the tip curvature is best seen at the points closer

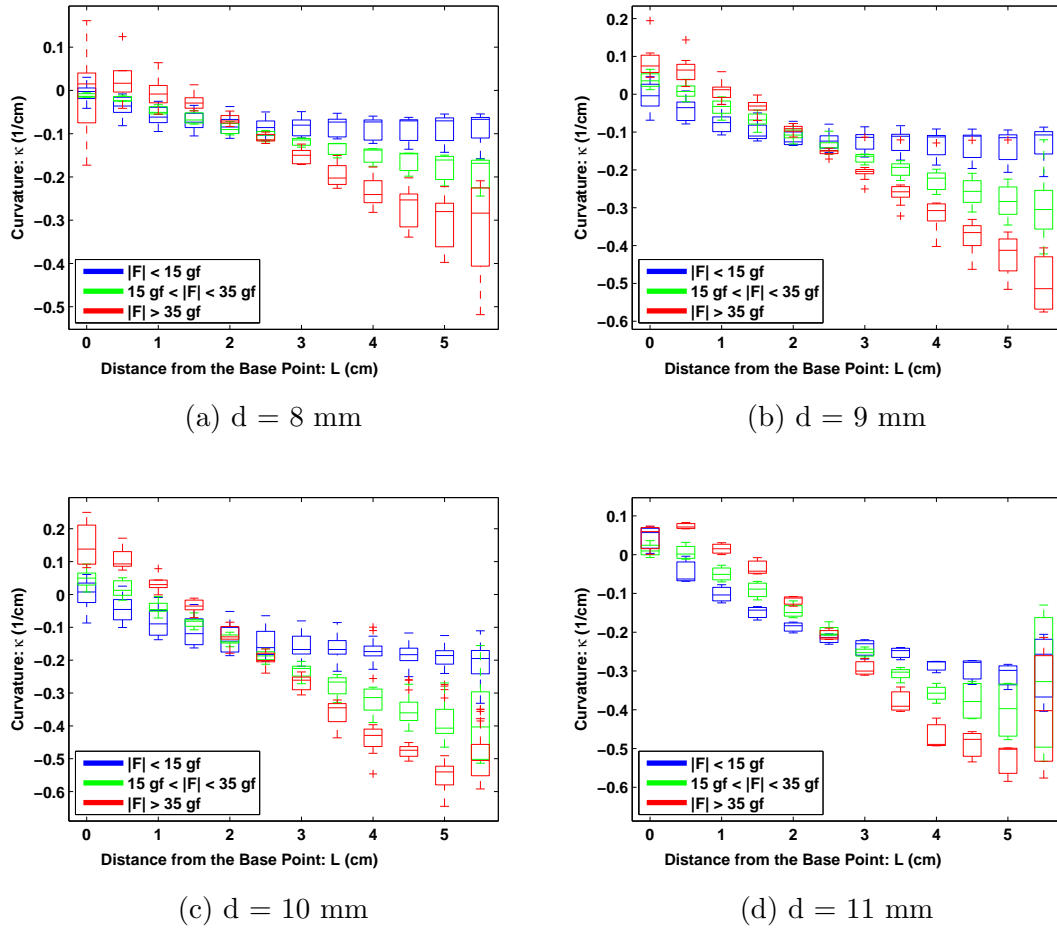


Figure 5.13: Tip curvature versus force magnitude for different handle displacements at a number of points along the catheter (d : handle displacement).

to the end point. Moreover, at each handle displacement, if the magnitude of the contact force is in a certain range, the resulting curvature at points between 3.5 cm and 5 cm will be in a certain range as well. This observation suggests that the effect of contact forces can be best seen in the section of the tip located between 3.5 cm and 5 cm measured from the base point. This section is marked in red color on the catheter shown in Figure 5.14.

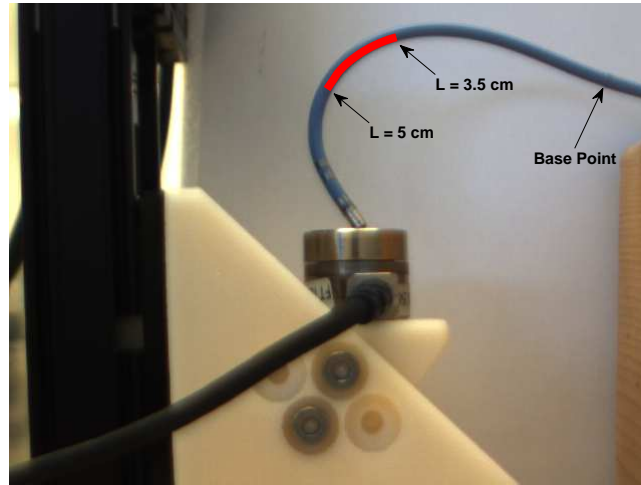


Figure 5.14: The effect of contact forces can be best seen by studying the section marked in red color on the catheter.

5.4.1 Force Index

Di Biase *et al.* [3] reported that lesion formation inside the heart depends on both the ablation power and the tip/tissue contact force. We define three ranges for the contact force based on their findings presented in [3]:

- *Safe contact* is when the contact force is between 15 *gf* and 35 *gf*.
- *Excessive force* is when contact force has a magnitude greater than 35 *gf*. Cardiac perforation is one of the risks of applying excessive force on heart tissue.
- *Insufficient force* is contact force with a magnitude less than 15 *gf*. Incomplete ablation is the result of insufficient contact between the catheter tip and heart tissue.

These regions are denoted by \mathcal{S} , \mathcal{E} and \mathcal{I} , respectively.

We define the dimensionless force index, λ_F , by observing the relation between the contact force and changes in the tip curvature:

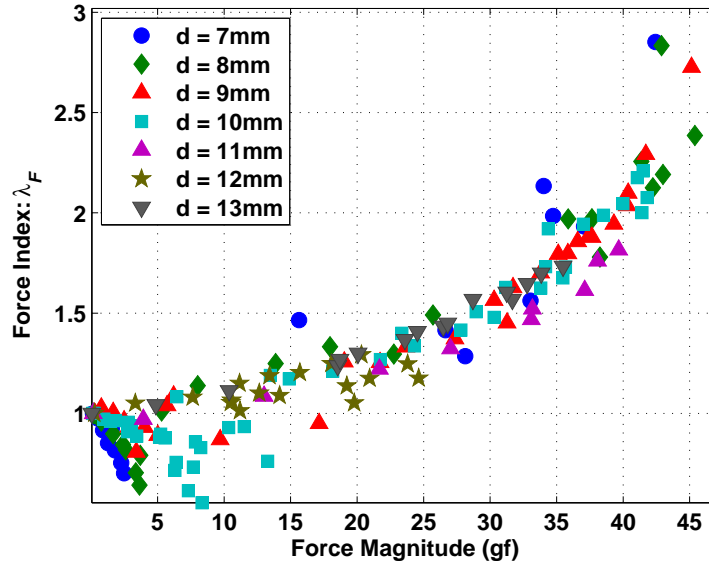


Figure 5.15: Defined force index for different contact force values.

$$\lambda_F = \frac{E \{ \kappa_c(L, d) \} |_{L=3.5-5}}{E \{ \kappa_{fs}(L, d) \} |_{L=3.5-5}} = \frac{\sum_{L=3.5}^5 \kappa_c(L, d)}{\sum_{L=3.5}^5 \kappa_{fs}(L, d)} \quad (5.10)$$

where $E\{.\}$ represents the averaging operator, κ_c is the curvature obtained for each sample, κ_{fs} is the curvature in free space, L is the distance from the base point in cm (Equation (5.1), Figure 5.14) and d is the handle displacement in mm. The defined load index quantifies the effect of contact force on the curvature, *i.e.*, λ_F gives a measure of how the curvature is different when the catheter is in contact with the environment from when the catheter moves in free space. Figure 5.15 shows that the proposed load index can detect the range of contact forces, although it cannot give the precise value of the applied forces.

In the next step, each force range is modeled with Gaussian distribution, and a Gaussian Mixture Model (GMM) with three components is used to cluster the obtained force index. The cumulative distribution function (CDF) of the fitted distributions is shown in Figure 5.16. Having three different distributions for the collected data, we employ a three-component Gaussian-Mixture Model (GMM) to cluster the

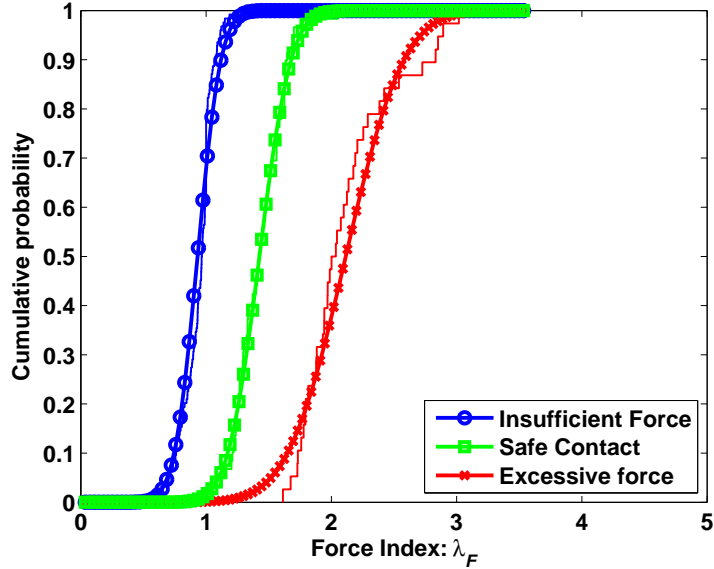


Figure 5.16: CDF of fitted Gaussian distribution to the force index corresponding to each force range.

obtained force index. The probability of associating each sample to any of the three force regions is estimated using the GMM and the region with the highest probability is selected as the estimated force region.

The probability distribution function (PDF) of a GMM is a weighted sum of several Normal PDF:

$$p_x(x) = \sum_{k=1}^N \frac{\omega_k}{\sigma_k \sqrt{2\pi}} \exp\left(-\frac{(x - \mu_k)^2}{2\sigma_k^2}\right), \quad \sum_k \omega_k = 1 \quad (5.11)$$

where μ_k and σ_k are the mean and variance of each Gaussian component and ω_k is their weighting factor. Without any prior information about the force range, the *a priori* probabilities of being in each force range are equal, *i.e.*, $P_I = P_S = P_E$. Therefore, $\omega_k = \frac{1}{3}$, $k = 1, 2, 3$. More details on GMM clustering methods can be found in [26].

Table 5.3: Conditional probability of estimating force ranges for test data with the first catheter.

$k \rightarrow$	\mathcal{I}	\mathcal{S}	\mathcal{E}
$P_{\hat{\mathcal{I}} k}$	0.96	0.04	0
$P_{\hat{\mathcal{S}} k}$	0.11	0.89	0
$P_{\hat{\mathcal{E}} k}$	0	0.13	0.87

5.5 Experimental Validation

To evaluate the performance of the proposed technique, two series of experiments were carried out. The first set of data was collected with the same ablation catheter used for studying and modeling the relation between shape and applied force. The experiments were then repeated with a different steerable ablation catheter to provide a basis for comparing the results.

5.5.1 Experiments Using the Same Catheter

A series of force loads with the aforementioned conditions was applied to the catheter tip and the tip shape was recorded for each load. The applied force region was estimated using the proposed technique. Table 5.3 lists the probabilities of estimating each force range given the measured loading state. In this table, $P_{\hat{k}|k}$, $k = \mathcal{I}, \mathcal{S}, \mathcal{E}$ represents the probability of correctly estimating the insufficient, safe and excessive force, respectively. Similarly, $P_{\hat{k}|l}$, $k \neq l$ represents erroneous detection. From this table, the force range is correctly decided in more than 87% of the samples. While safe contact was detected as insufficient force in 11% and excessive load was declared safe contact in 13%, there is no incidence of reporting insufficient load as too much force or vice versa. Moreover, further analysis reveals that in almost all of the latter cases, the force magnitude is very close to the defined threshold for the excessive force.

The average curvature versus force magnitude is shown in Figure 5.17 for each range. It is observed that while $E\{\kappa_c\}$ does not reveal any information about the

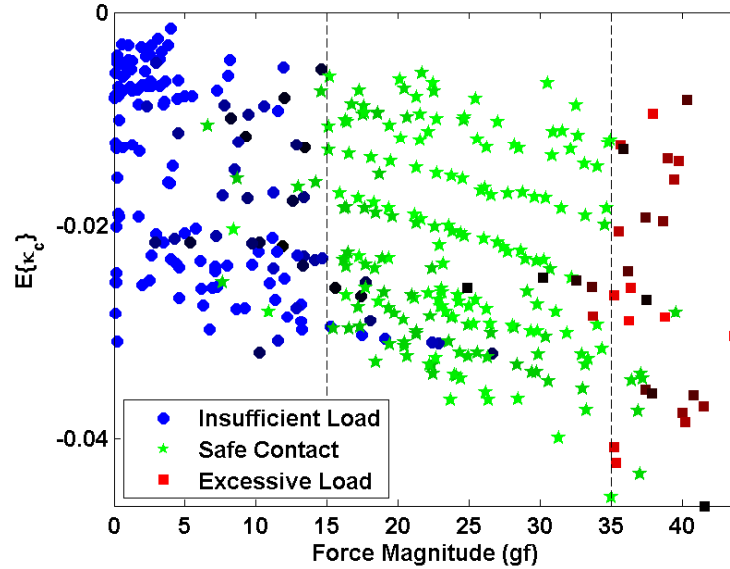


Figure 5.17: Mean curvature vs. force magnitude for different force range estimations.

contact force, the proposed technique can effectively distinguish between different force ranges. The misdetected points are recognized when the symbols representing each force range appear in their non-corresponding regions, *e.g.*, the star symbols to the left of line $|F| = 15$ gf are the points classified as safe contact. The color intensities at each point represent the clustering score.

5.5.2 Experiments Using a Different Catheter

The catheter used for this experiment is a 7-Fr unidirectional steerable ablation catheter (Biosense Webster, Diamond Bar, CA). This catheter is a non-irrigated tip catheter, while the catheter used previously was one with an irrigated tip. Both types are commonly used in cardiac ablation procedures. The experimental results reported in Table 5.4 demonstrate the same trend as that of the previous test and highlight the applicability of the proposed technique for different catheters that have a similar structure.

Table 5.4: Conditional probability of estimating force ranges for test data with the second catheter.

$k \rightarrow$	\mathcal{I}	\mathcal{S}	\mathcal{E}
$P_{\hat{\mathcal{I}} k}$	0.94	0.06	0
$P_{\hat{\mathcal{S}} k}$	0.05	0.92	0.03
$P_{\hat{\mathcal{E}} k}$	0	0.19	0.81

5.5.3 Obtaining the Force Index from Sensor Outputs

Experimental results prove the usefulness of the defined force index in estimating the range of contact forces. This force index is defined using the mean curvature value over a section of the catheter tip (Equation (5.10)). In practical situations, an image from the catheter tip may not be available, so it would be desirable to obtain the load index by using one or more shape sensors. Figure 5.13 suggests that the curvature data of one or more points along the deflecting tip may provide the necessary information for defining the load index and estimating the range of the contact force to some extent. In this section, we study if such points in fact exist.

Figure 5.18a shows the probability of correctly estimating the force ranges when one curvature sampling point moves along the catheter between $L = 2.0$ cm and 5.5 cm. The probability of correctly detecting the range of the contact force increases as the sensing point is moved from the base point to the ablation tip. This suggests that when the tip comes in contact with the environment, the changes in its shape occur mostly near the ablation tip. Based on this result, if a sensor (*e.g.*, a strain sensor similar to the one used in [21]) is placed at 4.5 cm from the base point without altering the flexing characteristics of the deflecting tip, it can determine the range of contact forces in more than 80% of the cases.

The proposed technique also provides a framework for evaluating the performance of using multiple sensors. For instance, consider mounting two shape sensors on the catheter tip: one at $L = 3.5$ cm and the other at $L = 5$ cm. The force index is obtained for each of these points and the probability of correct estimation is calculated. To determine range of the contact forces, we should decide how to jointly

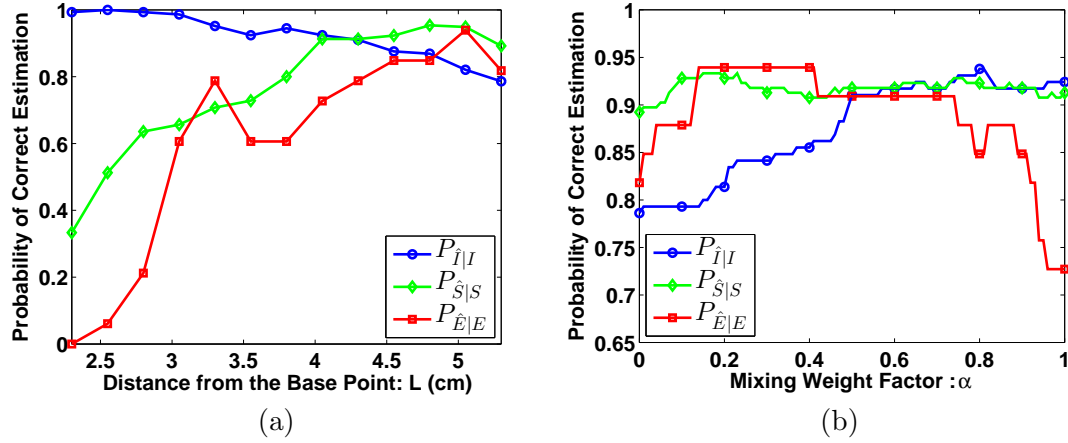


Figure 5.18: Probability of correctly estimating the force ranges: (a) with one sensing point, (b) with two sensing points located at $L = 3.5$ cm and $L = 5$ cm.

apply this information. Let's define:

$$\begin{cases} P_{\hat{I}|I} &= \alpha P_{\hat{I}|I}|_{L=3.5} + (1 - \alpha) P_{\hat{I}|I}|_{L=5} \\ P_{\hat{S}|S} &= \alpha P_{\hat{S}|S}|_{L=3.5} + (1 - \alpha) P_{\hat{S}|S}|_{L=5} \\ P_{\hat{E}|E} &= \alpha P_{\hat{E}|E}|_{L=3.5} + (1 - \alpha) P_{\hat{E}|E}|_{L=5} \end{cases} \quad (5.12)$$

where $\alpha \in [0, 1]$ is the mixing weight factor. Figure 5.18b shows that when $\alpha = 0.57$, the force range is estimated correctly in 92% of the cases. The same analysis can be repeated for different configurations of sensors to find the optimum number of sensors and their locations for a desired performance.

Remark 1: Although this work is focused on unidirectional ablation catheters, the proposed technique can also be applied to other types of ablation catheters, *e.g.*, bidirectional catheters. The curvature of an arbitrary type of ablation catheter can be analyzed using the proposed approach and the section which is most susceptible to contact force can be determined. It is expected that the results would then be valid for catheters with similar design and construction and the same actuation mechanism. Nevertheless, further study is required to compare the results for different types of ablation catheters.

Remark 2: The stiffness of the environment may have an impact on the results.

During data collection, the catheter tip interacted with the rigid surface of the force sensor in the experimental setup. A small piece of artificial tissue was then used to cover the surface of the force sensor and a limited number of data points were collected. Analyzing this data revealed no noticeable difference from the previous result. For a complete understanding of the relationship between tissue stiffness, amount of contact force and the tip shape, a more detailed study is required. Such study should consider the actual stiffness of cardiac tissue as well as how it changes during the ablation procedure, *i.e.*, when the tissue is being ablated.

5.6 Conclusions

In this chapter, we studied the behavior of the tip of an ablation catheter in free space and in contact with the environment. In this regard, instead of making assumptions on the catheter characteristics, we started with a careful observation of how actuating the proximal handle affects the tip shape. The tip curvature was analyzed and a kinematic model was proposed for the catheter tip. The performance of the proposed model was then evaluated experimentally and the model was shown to be more accurate than two previously developed models. Bringing the tip in contact with the environment, the tip curvature was analyzed and a force index was defined. Experiments with two conventional but different ablation catheters show that the defined force index can successfully identify the range of the contact force in more than 80% of the cases. Moreover, it was shown that the proposed technique provides a framework for evaluating the performance of sensors. This framework provides a way of estimating the performance of the sensors before they are physically mounted on the catheter tip.

To the best of our knowledge, this work is the first to investigate the actual behavior of *conventional steerable ablation catheters* under contact forces. The study shows that implementing the “intrinsic force sensing” technique [7–10] is feasible for conventional ablation catheters. Ongoing work is focusing on extending this work to include 3D cases where external forces drive the catheter tip out-of-plane; using a medical imaging modality such as ultrasound (US) to provide shape data; investigat-

ing the effect of distributed loads on the catheter tip and implementing the proposed technique in a fast moving environment with a varying stiffness. The study presented in this chapter is the first step toward these future goals.

References

- [1] K. Yokoyama *et al.*, “Novel contact force sensor incorporated in irrigated radiofrequency ablation catheter predicts lesion size and incidence of steam pop and thrombus,” *Circulation: Arrhythmia and Electrophysiology*, vol. 1, no. 5, pp. 354–362, Dec 2008.
- [2] G. Ndrepepa and H. Estner, “Ablation of cardiac arrhythmias energy sources and mechanisms of lesion formation,” in *Catheter Ablation of Cardiac Arrhythmias*. Steinkopff, 2006, pp. 35–53.
- [3] L. Di Biase *et al.*, “Relationship between catheter forces, lesion characteristics, popping, and char formation: experience with robotic navigation system.” *Journal of Cardiovascular Electrophysiology*, vol. 20, no. 4, pp. 436–40, Apr 2009.
- [4] “THERMOCOOL SMARTTOUCH Catheter.” [Online]. Available: www.biosensewebster.com
- [5] “TactiCath Catheter.” [Online]. Available: www.endosense.com
- [6] “Artisan Extend Control Catheter.” [Online]. Available: www.hansenmedical.com/us/products/ep/artisan-control-catheter.php
- [7] K. Xu and N. Simaan, “An investigation of the intrinsic force sensing capabilities of continuum robots,” *IEEE Transactions on Robotics*, vol. 24, no. 3, pp. 576–587, Jun 2008.
- [8] K. Xu and N. Simaan, “Intrinsic wrench estimation and its performance index for multisegment continuum robots,” *IEEE Transactions on Robotics*, vol. 26, no. 3, pp. 555–561, Jun 2010.

- [9] A. Bajo and N. Simaan, “Finding lost wrenches: Using continuum robots for contact detection and estimation of contact location,” in *IEEE International Conference on Robotics and Automation (ICRA)*, 2010, pp. 3666–3673.
- [10] D. Rucker and R. Webster, “Deflection-based force sensing for continuum robots: A probabilistic approach,” in *IEEE/RSJ International Conference on Intelligent Robots and Systems (IROS)*, 2011, pp. 3764–3769.
- [11] D.B. Camarillo, C.F. Milne, C.R. Carlson, M.R. Zinn, and J.K. Salisbury, “Mechanics modeling of tendon-driven continuum manipulators,” *IEEE Transactions on Robotics*, vol. 24, no. 6, pp. 1262–1273, Dec 2008.
- [12] D.B. Camarillo, K.E. Loewke, C.R. Carlson, and J.K. Salisbury, “Vision based 3-d shape sensing of flexible manipulators,” in *IEEE International Conference on Robotics and Automation (ICRA)*, 2008, pp. 2940–2947.
- [13] B. Jones and I. Walker, “Kinematics for multisection continuum robots,” *IEEE Transactions on Robotics*, vol. 22, no. 1, pp. 43–55, Feb 2006.
- [14] Y. Ganji and F. Janabi-Sharifi, “Catheter kinematics for intracardiac navigation,” *IEEE Transactions on Biomedical Engineering*, vol. 56, no. 3, pp. 621–632, Mar 2009.
- [15] J. Jung, R. S. Penning, N. J. Ferrier, and M. Zinn, “A modeling approach for continuum robotic manipulators: Effects of nonlinear internal device friction,” in *IEEE/RSJ International Conference on Intelligent Robots and Systems (IROS)*, 2011, pp. 5139–5146.
- [16] S. Kesner and R. Howe, “Force control of flexible catheter robots for beating heart surgery,” *IEEE International Conference on Robotics and Automation (ICRA)*, 2011, pp. 1589–1594.
- [17] S.B. Kesner and R.D. Howe, “Position control of motion compensation cardiac catheters,” *IEEE Transactions on Robotics*, vol. 27, no. 6, pp. 1045–1055, Dec. 2011.

- [18] S.B. Kesner and R.D. Howe, “Discriminating tissue stiffness with a haptic catheter: Feeling the inside of the beating heart,” in *IEEE World Haptics Conference (WHC)*, 2011, pp. 13–18.
- [19] S.B. Kesner and R.D. Howe, “Design principles for rapid prototyping forces sensors using 3-D printing,” *IEEE/ASME Transactions on Mechatronics*, vol. 16, no. 5, pp. 866–870, Oct 2011.
- [20] R.J. Webster and B.A. Jones, “Design and kinematic modeling of constant curvature continuum robots: A review,” *The International Journal of Robotics Research*, vol. 29, no. 13, pp. 1661–1683, Nov 2010.
- [21] M. Khoshnam, A. Yurkewich, and R.V. Patel, “Model-based force control of a steerable ablation catheter with a custom-designed strain sensor,” in *IEEE International Conference on Robotics and Automation (ICRA)*, 2013, pp. 4464–4469.
- [22] M. Khoshnam, M. Azizian, and R.V. Patel, “Modeling of a steerable catheter based on beam theory,” in *IEEE International Conference on Robotics and Automation (ICRA)*, 2012, pp. 4681–4686.
- [23] M. Khoshnam and R.V. Patel, “A pseudo-rigid-body 3R model for a steerable ablation catheter,” in *IEEE International Conference on Robotics and Automation (ICRA)*, 2013, pp. 4412–4417.
- [24] M.W. Hannan and I.D. Walker, “Vision based shape estimation for continuum robots,” in *IEEE International Conference on Robotics and Automation (ICRA)*, vol. 3, 2003, pp. 3449–3454.
- [25] J. Craig, *Introduction to Robotics: Mechanics and Control*, ser. Addison-Wesley series in electrical and computer engineering: control engineering. Pearson Education, Incorporated, 2005.
- [26] C. Bishop, *Pattern Recognition and Machine Learning*. Springer, 2006.

Chapter 6

Robotics-Assisted Catheter Manipulation

6.1 Introduction

During cardiac arrhythmia, the normal heart rhythm is affected by false electric signals originating from the myocardium. Minimally invasive treatment of arrhythmia is realized using steerable ablation catheters. The flexibility, length and small diameter of the catheter allow it to be steered to the appropriate heart chamber through the vasculature. The catheter tip is positioned on the cardiac tissue to ablate the source of false signals by delivering some type of energy (most commonly radiofrequency (RF)) to the tissue. The ablation procedure is usually performed under X-ray fluoroscopy guidance, which does not provide a good visualization of the cardiac tissue, but displays the position of catheters and guidewires.

The recent development of force sensing catheters has facilitated research on defining the relationship between the amount of contact force and the outcome of the ablation procedure [1–5]. Considering that insufficient force results in incomplete tissue ablation and possible recurrence of arrhythmia and excessive force increases the risk of perforation, it is important to keep the contact force within a certain range at all times during the ablation procedure. Moreover, a recent study suggests that the quality of contact plays an important role in the efficacy of the procedure [6]. Using a bench model that simulates the beating heart, Shah *et al.* [6] define three contact patterns: 1) constant contact, 2) variable contact ($F_{min} = 10\text{ gf}$ and $F_{max} = 20\text{ gf}$) and 3) intermittent contact ($F_{min} = 0\text{ gf}$ and $F_{max} = 20\text{ gf}$) with loss of contact [6]. Establishing a constant contact between the catheter tip and the tissue results in complete ablation and reduces the maximum applied force [7]. However, due to heartbeat and respiration, there is an intermittent contact between

the catheter tip and cardiac tissue [8]. If the procedure is performed under apnea, where the respiratory movements are minimal, a variable contact can be achieved and the contact quality is improved considerably [8]. Providing a constant contact force further improves the quality of contact. It is expected that a constant force can be attained if the catheter tip moves synchronously with the cardiac tissue and compensates for cardiac and respiratory motions.

Motion compensation of beating heart in robotics-assisted minimally invasive cardiac interventions is usually realized through tracking visual clues on the heart surface and/or using a motion compensation robotic tool [9–14]. However, these techniques are mainly developed for surgeries performed on the external surface of the heart using rigid tools. Yuen *et al.* designed a rigid motion compensation device for performing intracardiac procedures under ultrasound guidance [15–17]. Kesner and Howe [18–21] then adapted a similar approach to design a flexible robotic motion compensation catheter for intracardiac surgeries, namely the mitral valve annuloplasty procedure. The designed catheter is translated in and out of the sheath to compensate for the beating heart motion. The contact force is measured by a prototype force sensor that is integrated within the catheter tip [22].

In our previous work, we studied the static behavior of the catheter tip under applied forces [23, 24]. We also showed that controlling the contact force at the tip of an ablation catheter can be achieved through adjusting the position of the prismatic knob on the catheter’s proximal handle [25]. In this chapter, we propose a technique for compensating for heart motion to reduce the variations in the contact force between the tip of a *conventional unidirectional steerable ablation catheter* and the environment (cardiac tissue). A thorough study is carried out to determine the characteristics of a conventional ablation catheter when the catheter handle is actuated in different frequencies. The results of this study are then used in designing a control system that estimates the frequency of the environmental motion, calculates the actuation delay and generates the proper control signal. The experimental results show that the proposed technique is capable of reducing the variations in the contact force caused by the moving tissue and noticeably improves the performance of the uncompensated system.

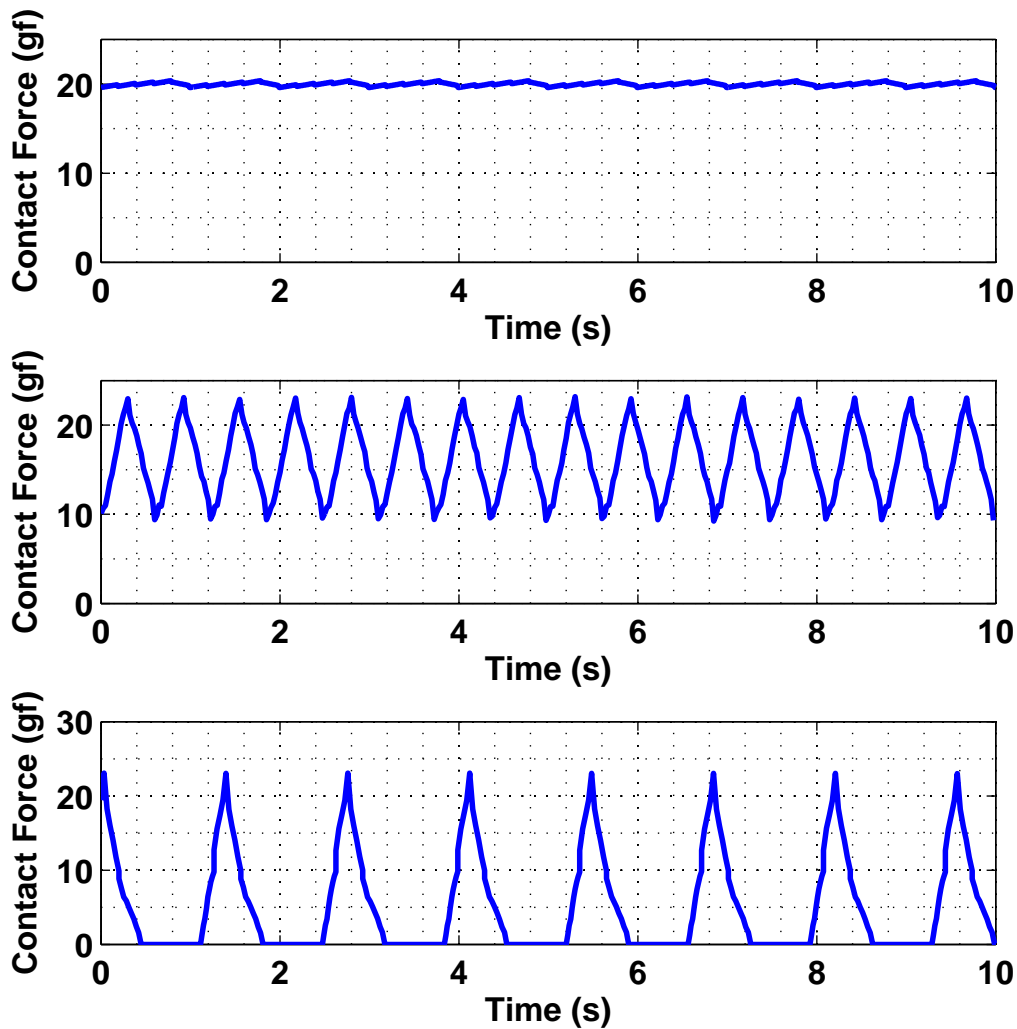


Figure 6.1: Different patterns of the contact force between the catheter tip and cardiac tissue as defined in [6]: (top) constant contact, (middle) variable contact, (bottom) intermittent contact (Figure obtained from [6]).

The organization of the rest of the chapter is as follows: Section 6.2 describes the experimental setup. The characteristics of the catheter are studied in Section 6.3. The proposed scheme for compensating for cardiac motion and reducing variations in the contact force is discussed and experimental results are presented in Section 6.4. Section 6.5 discusses the limitations of the system as well as the clinical applicability of the proposed approach. Section 6.6 concludes the chapter with suggestions for

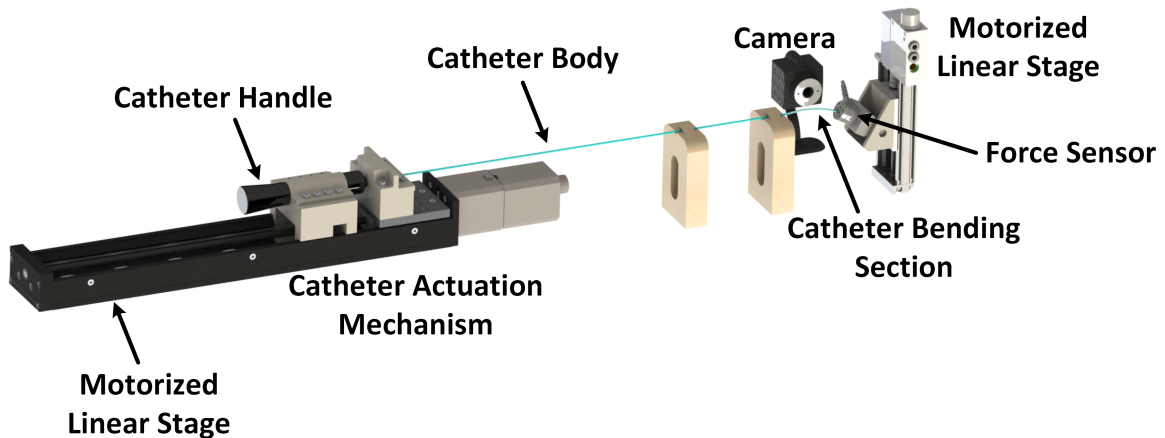


Figure 6.2: Schematic of the experimental setup.

future research.

6.2 Experimental Setup

The setup is shown schematically in Figure 6.2. The proximal catheter handle is fixed to the base of a motorized linear stage (T-LSR300B, Zaber Technologies Inc., Vancouver, BC, Canada) by an adapter piece. The prismatic knob on the catheter handle is attached to the sliding platform on the linear stage and the catheter actuation is realized by moving the sliding platform back and forth. In this setup, the catheter proximal handle can be actuated with a maximum speed of 20 mm/s. A conventional unidirectional 7-Fr RF ablation catheter (Biosense Webster, Diamond Bar, CA) is passed through a standard catheter sheath which is fixed in place along its length. With this configuration, the catheter can translate in and out of the sheath.

The distal section of the catheter is the deflectable shaft that can be actuated by moving the proximal prismatic knob. The prismatic knob on the adapted catheter can move from 0 to about 21 mm (Figure 6.3). When the knob is at its initial position (handle displacement = 0), the catheter tip is completely straight. For a displacement of about 21 mm, the catheter tip bends to over 90°, which is its ultimate bending configuration (Figure 6.3).

To measure the contact force without altering the structure of the catheter, a

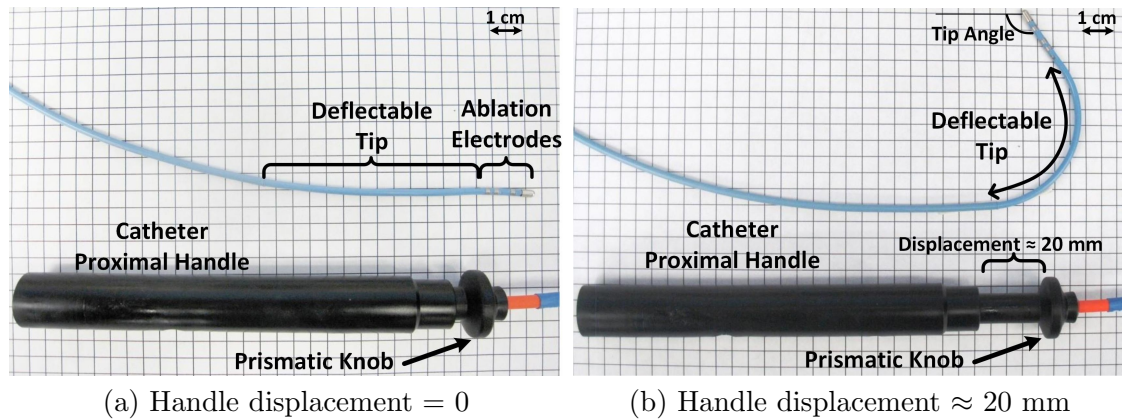


Figure 6.3: A close view of the proximal handle and the bending tip of a steerable ablation catheter.

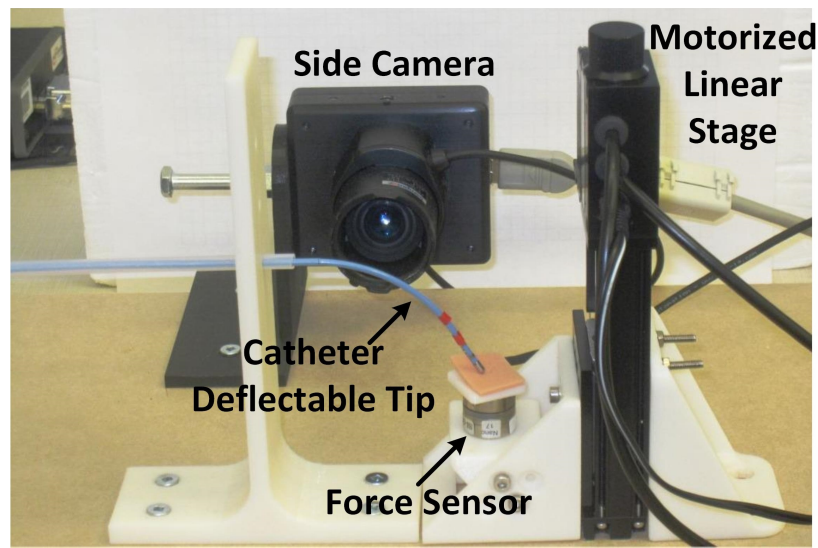


Figure 6.4: A view of the catheter tip, camera and force sensor in the experimental setup.

force sensor (Nano17, ATI Industrial Automation, Apex, NC, USA) is used as the environment with which the catheter interacts (Figure 6.4). A small piece of artificial tissue is fixed to the top plate of the sensor. The force sensor provides a measure of the actual contact force between the artificial tissue and the catheter tip. To adjust the angle between the catheter tip and the force sensor, the sensor is mounted on a small adapter piece. A motorized linear stage (T-LSM050A, Zaber Technologies Inc., Vancouver, BC, Canada) follows the commands to move the force sensor up and

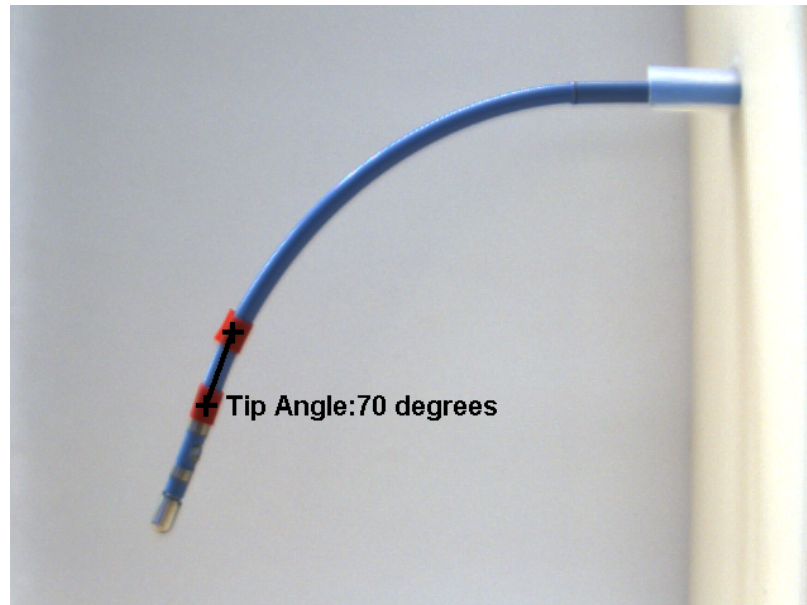


Figure 6.5: A sample frame. The tip angle is calculated using the centroid points of the red markers.

down and thus provides a moving target for the experiments. This linear stage can provide a maximum speed of 7 mm/s. A camera (Dragonfly[®], Point Grey Research Inc., Richmond, BC, Canada) is positioned to show a planar view of the catheter tip and provides images with a resolution of 640×480 pixels from the deflectable tip. The images are streamed at 30 frames per second (fps). A customized library is designed using the C++ language in the MATLAB[®] environment to utilize the setup in real-time.

In order to have real-time feedback from the position and orientation of the catheter tip, two small red markers are fixed on the tip and are tracked in the streamed video. The markers are positioned at the end of the deflectable section behind the rigid part reserved for ablation electrodes. For each captured frame, the red component of the image is extracted and the resulting grayscale image is converted into a binary image. The position of the catheter tip is then given by the centroids of the detected regions. Calculating the tip orientation is then straight forward (Figure 6.5).

In this study, the largest motion frequency in the experiments is lower than the frequency of cardiac motion (≈ 1 Hz). The reason for this is explained in detail

in Section 6.5. It is reported in [26] that the motion of the aortic root has a mean amplitude of 11.6 mm and that of the atrial wall is about 8.5 mm [27].

6.3 System Characteristics

Catheters have applications in a variety of vascular and cardiac interventions, *e.g.*, cardiac ablation, coronary angioplasty and mitral valve annuloplasty. These catheters are designed to satisfy the requirements of their intended application and as a result, the characteristics of the catheters are very different from one application to another.

Cardiac ablation is usually performed using 5-Fr or 7-Fr catheters and can be either unidirectional or bidirectional. It is shown that even forces as low as 77 gf (≈ 0.75 N) can result in cardiac perforation [28] and force levels for achieving efficient ablation are generally lower than 35 gf (≈ 0.34 N) [5]. Cardiac ablation catheters are designed to apply forces in the required range. Howe *et al.* [15–21] introduced motion compensation for surgical tools for repairing mitral valves. In such an application, the force required to manipulate the tissue is at least 1.5 N (≈ 153 gf) [29, 30]. Hence, the catheters used in annuloplasty are usually of larger diameter so to be able to apply greater forces (for an example of such catheters see [31]). Moreover, adjusting the catheter orientation is achieved by bending the sheath [18–21], and is different from the case of ablation catheters, where the catheter tip is flexed by actuating the proximal handle regardless of the sheath configuration. Kesner and Howe [18–21] studied the problem of motion compensation and force control in the mitral annuloplasty procedure. Recognizing the differences between the types of catheters used in such surgeries and the types of catheters used in cardiac ablation procedures, we study the problem of improving the quality of catheter/tissue contact during the ablation procedures performed using conventional unidirectional steerable catheters.

In this section, we study how the catheter tip responds to actuating the proximal handle at different frequencies. Hereinafter, the tip position refers to the position of the red marker closest to the ablation tip (Figure 6.5) and the tip angle is defined as shown in Figure 6.3b.

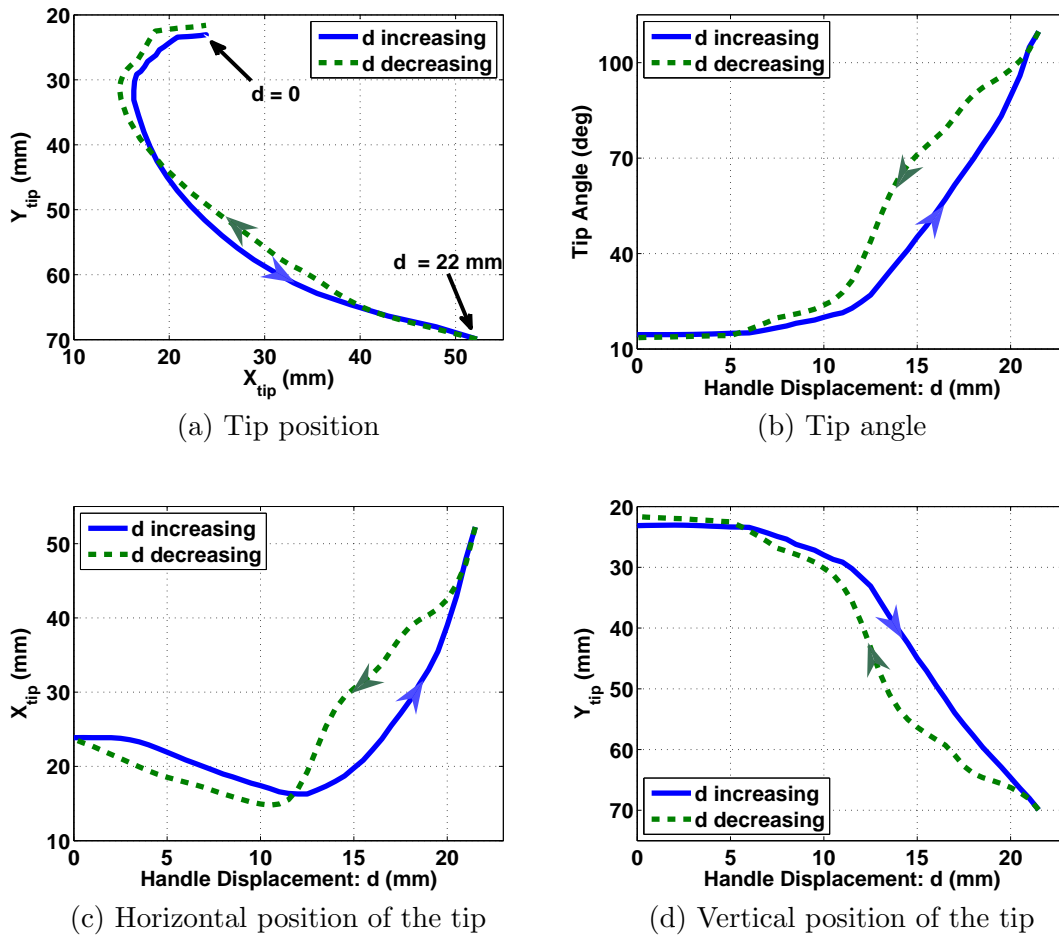


Figure 6.6: Static relationship between the handle displacement (d) and deflection of the tip.

6.3.1 Static Response in Free Space

In order to study the static relationship between the displacement of the proximal handle and the resulting tip deflection, the handle is moved very slowly from 0 to 22 mm, allowing the tip to reach its final configuration in each displacement. The result is shown in Figure 6.6. It is observed that the catheter tip follows almost the same path with pushing/pulling the proximal prismatic knob (Figure 6.6a). However, for the same handle displacement, the position and orientation of the tip depends on whether the knob is being pushed or pulled (Figure 6.6b-d). This observation suggests the hysteresis behavior for the catheter. Another point worth mentioning is that the

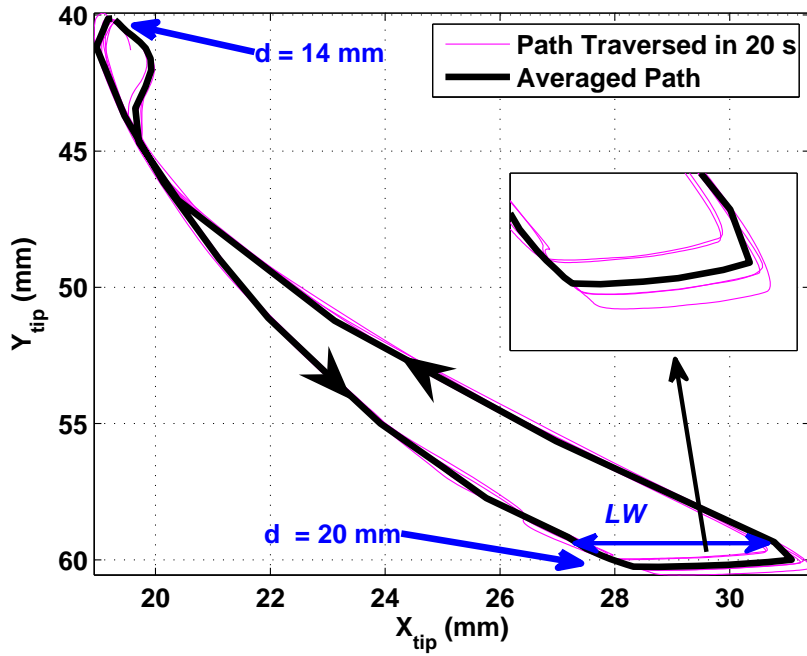


Figure 6.7: The path that the tip follows when the proximal handle is actuated at $F_a = 0.27$ Hz.

linear displacement of the handle knob results in the planar motion of the tip, *i.e.*, the knob moves in the X direction, but the position of the tip changes in both the X and Y directions. This is yet another difference between this study and the case presented in [18–21] where the linear motion of the catheter base results in linear motion of the catheter tip in the direction dictated by the configuration of the sheath.

6.3.2 Frequency Response in Free Space

From the results presented in [25], the contact force can be controlled through adjusting the position of the handle knob. Since the target environment, *i.e.*, the heart tissue, is moving very fast, it is expected that for maintaining a constant contact, the catheter handle should be actuated with a high frequency (≈ 1 Hz) as well. In this section, we study how the catheter tip responds to actuation at the proximal knob. The catheter handle is actuated with a 6 mm sinusoidal command centered at $d = 14$ mm, taking into account that for $d < 9$ mm, the deflection of the catheter tip

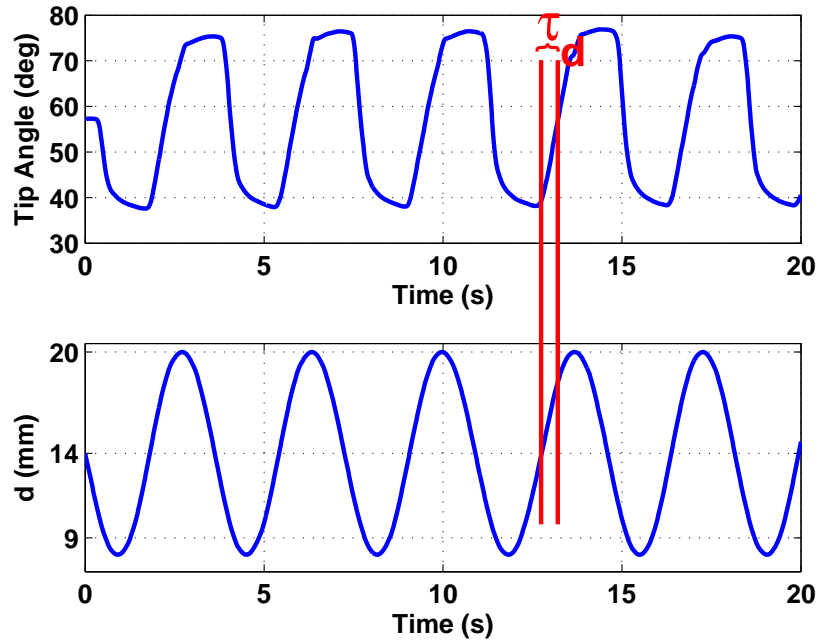


Figure 6.8: Variations in the tip angle when the proximal handle is actuated at $F_a = 0.27$ Hz: (top) tip angle, (bottom) handle displacement

is insignificant (Figure 6.6). The handle is actuated at 20 different frequencies, ranging from 0.02 Hz to 0.65 Hz for 20 s. At each actuation frequency, F_a , the experiment is repeated 3 times. The corresponding signals are recorded and for each repetition, the following features are extracted (Figures 6.7 and 6.8):

- F_a (Hz) is the frequency of actuating the proximal handle.
- F_t (Hz) is the frequency at which the tip moves.
- LW (mm) is the maximum width of the hysteresis loop corresponding to the tip position.
- PL (mm) is the average length of the path that the catheter tip traverses when the knob is actuated from $d = 0$ to $d = 22$ mm and back to $d = 0$.
- Φ_{min} (deg) is the minimum angle that the catheter tip returns to when $d = 0$.
- Φ_{max} (deg) is the maximum angle that the catheter tip reaches for $d = 22$ mm.
- τ_d (s) is the time delay, *i.e.*, the time elapsed between when $d = 14$ mm and the time at which the tip angle reaches its mean value.

Table 6.1: Effect of actuation frequency F_a on different features of the response.

F_a (Hz)	F_t (Hz)	LW (mm)	PL (mm)	Φ_{min} (deg)	Φ_{max} (deg)	τ_d (s)
0.02	0.02	3.69	119.61	40.37	126.7	3.05
0.05	0.05	4.78	91.1	37.88	115.89	1.42
0.13	0.14	4.14	55.91	39.57	82.55	0.71
0.25	0.25	3.64	48.66	42.86	80.39	0.48
0.36	0.36	3.78	47.12	35.71	70.69	0.39
0.46	0.46	3.93	39.27	35.57	63.15	0.39
0.52	0.52	4.34	37.14	34.76	60.28	0.41
0.63	0.63	3.58	36.2	28.12	49.5	0.45

During the actuation period of 20 s, the handle is displaced between $d = 0$ and $d = 22$ mm repeatedly and each cycle takes $1/F_a$ seconds. As a result, the catheter tip traverses the same path recurrently. The defined parameters are derived for each actuation cycle and the final value for each parameter would then be the average of the corresponding value in all cycles. The values obtained for different repetitions of the same actuation frequency are found to be very close. The values presented in Table 6.1 are the mean values of all three repetitions for the selected F_a . Samples of the obtained results are shown in Figures 6.7 and 6.8. These figures show how the tip position and orientation respond to an actuation frequency of $F_a = 0.27$ Hz.

The experimental results suggest that the frequency of the tip motion is the same as the actuation frequency as expected, *i.e.*, $F_t \approx F_a$, and the maximum width of the position hysteresis loop, LW , does not depend on F_a . However, increasing the actuation frequency causes:

- the catheter tip to traverse a shorter path. The catheter tip returns to almost the same position for $d = 0$, but as F_A is increased, the catheter tip does not reach its maximum bending configuration and the furthest point that it can reach gets closer to its starting point.
- the range of Φ decreases, *i.e.*, $\Phi_{max} - \Phi_{min}$ has a smaller value for higher F_a .

Considering the handle displacement as the system input and the tip angle as the system output, the frequency response of the system is shown in Figure 6.9. The

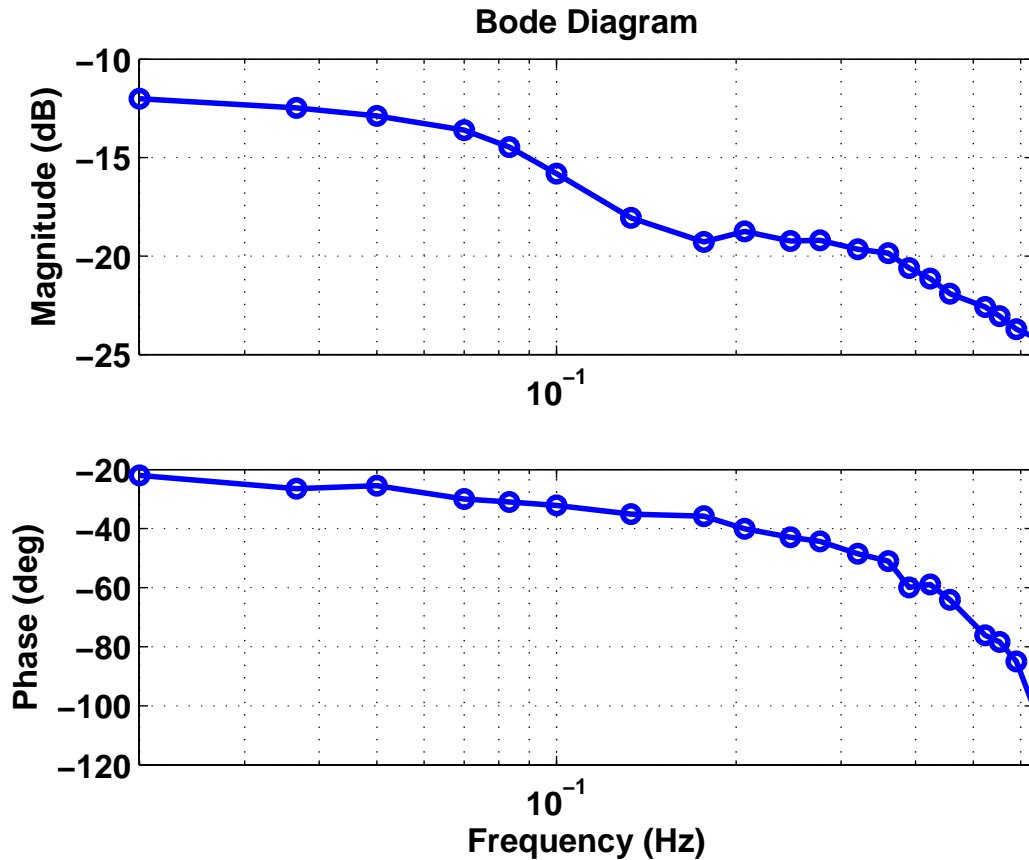


Figure 6.9: Bode diagram for the catheter in free space.

Bode plot clearly shows the existence of a time delay in the system.

6.3.3 Achieving a Desired Tip Angle

Having studied the effect of actuation frequency on the flexing of the tip, we now investigate the problem of controlling the catheter tip in free space. A basic control system (Figure 6.10) is used to flex the catheter to reach a desired angle.

Figure 6.11a shows the regulation performance of the control system. The controller parameters were adjusted experimentally and the best result (Figure 6.11a) was achieved with $P = 0.03$, $I = D = 0$ with a settling time of about 3 s.

The same control system is then commanded to follow a time-varying tip angle in the shape of a sinusoidal signal centered at 42° with an amplitude of 10° . The experiments show that the system output is in the shape of a sinusoidal. However,

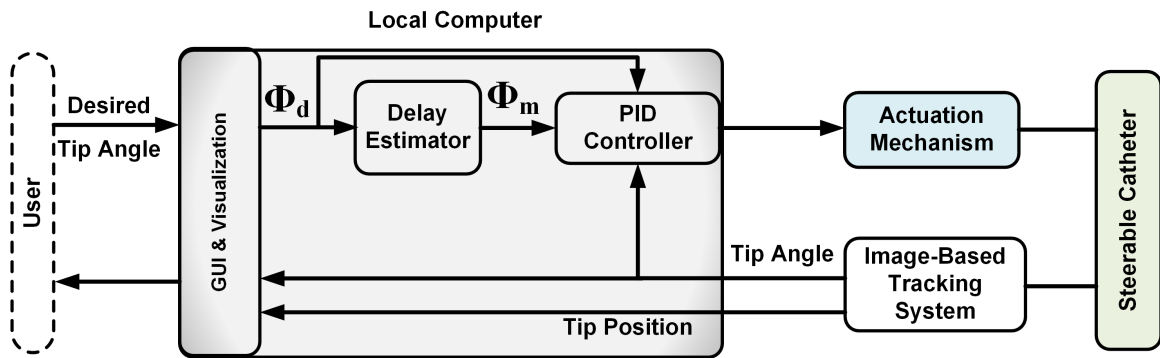


Figure 6.10: The control system for achieving a desired angle at the catheter tip.

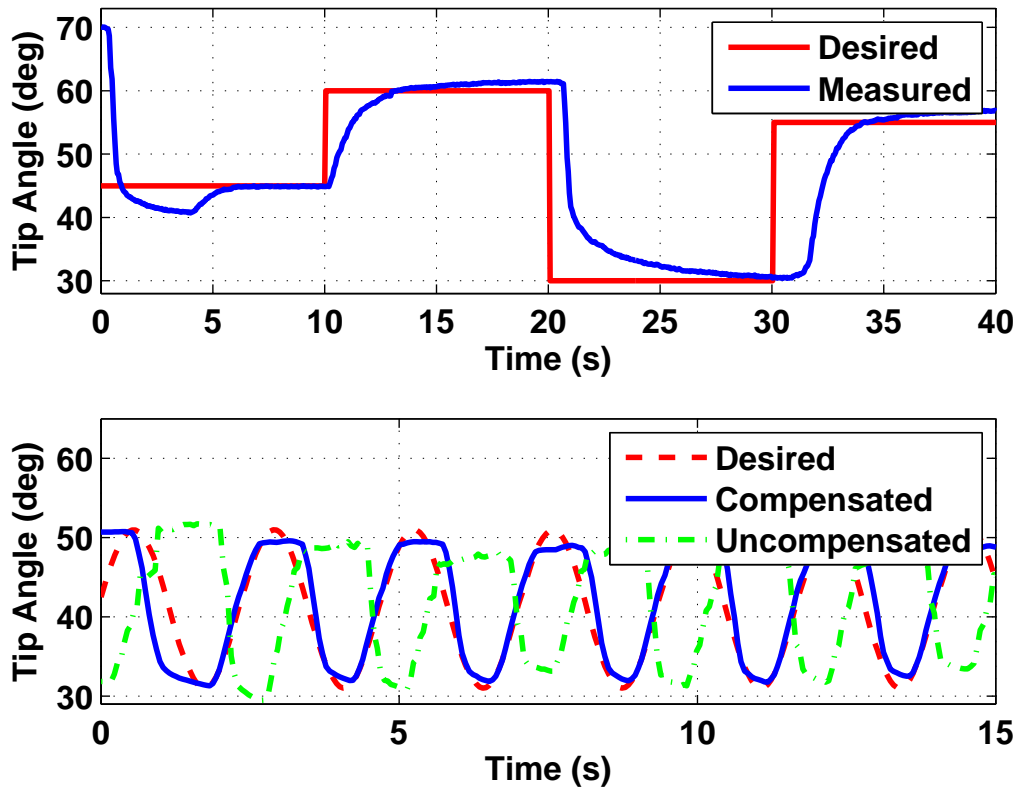


Figure 6.11: Performance of the control system in following a desired tip angle.

the observed time delay has an undesirable but noticeable effect on the response (Figure 6.11b). Using the results presented in the previous section, the commanded

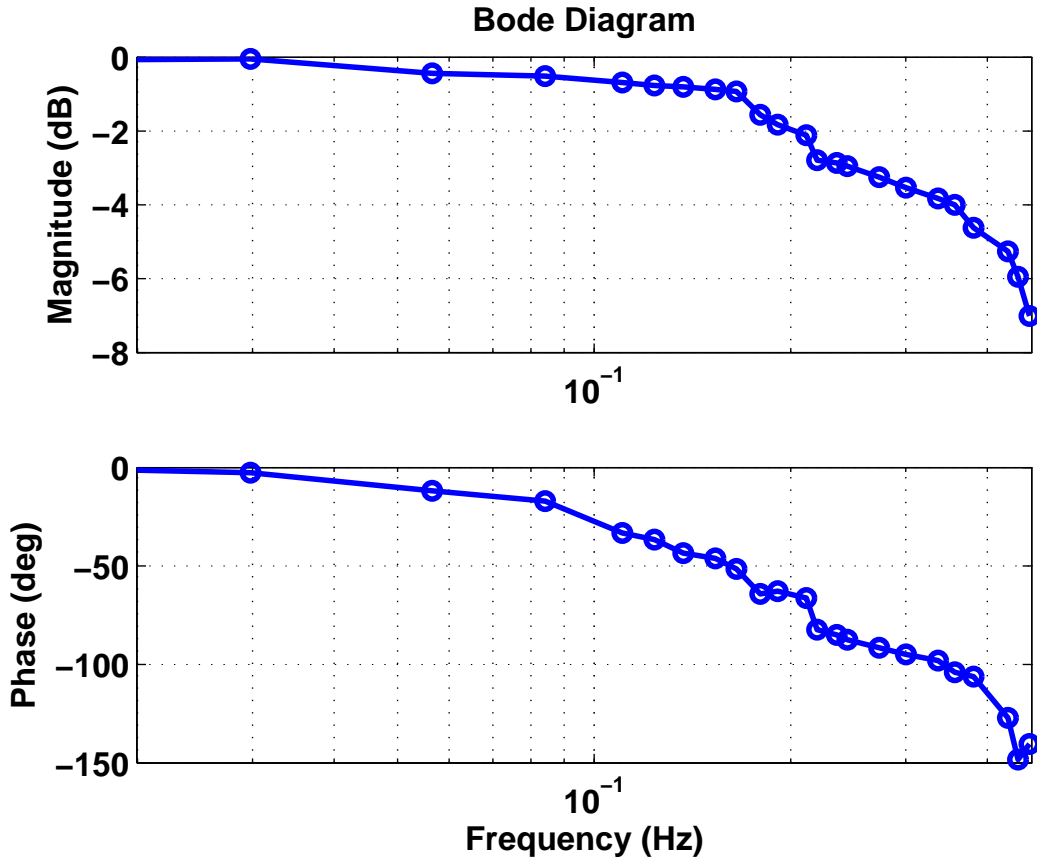


Figure 6.12: Bode diagram for the system with the desired tip angle as input and the actual tip angle as output.

trajectory is modified to compensate for the delay:

$$\Phi_m(t) = \Phi_{des}(t + \tau_d) \quad (6.1)$$

where Φ_{des} is the desired trajectory. τ_d is the time delay between actuating the handle and the change in the tip angle and can be obtained from Figure 6.12. Φ_m is the modified trajectory that is fed into the control system. Since the main source of error in tracking the desired tip angle is the time delay, the modified trajectory is the desired trajectory with a phase shift. Figure 6.11b shows that reshaping the desired trajectory and compensating for the time delay improves the tracking performance noticeably, reducing the root mean square of tracking error from 12.71° to 2.83° .

It should be noted that in this step the goal of the control is to synchronize

the input and output of the system. The maximum range in which the tip angle changes at each actuation frequency is a physical property of the system (Table 6.1) and cannot be extended. The control system ensures that the output follows the trajectory dictated from the input.

6.4 Tip/Tissue Motion Synchronization

In the previous section, we studied how the catheter tip responds to actuating the proximal handle in free space and identified the delay inherent in the system. In this section, we study the catheter behavior in contact with static as well as moving environments.

6.4.1 Static Environment

During the ablation procedure, the catheter tip is in contact with a relatively fast-moving environment, *i.e.*, cardiac tissue. It is evident that as the tissue moves further from the tip, its contact with the catheter tip might be lost. The question that arises is if it is possible to maintain the contact by controlling the flexing of the tip. To investigate the answer, we first study if flexing the tip will change the force applied on a static environment.

In the experimental setup, the force sensor is placed such that when the tip flexes, it comes in contact with the artificial tissue. The proximal knob is then commanded with a sinusoidal signal at different frequencies. The results are given in Figure 6.13 and show how the contact force changes when the handle is actuated: when the handle is displaced between 5 mm and 20 mm, the variations in the contact force are about 15 gf.

These results confirm that the catheter tip/tissue contact force changes when the catheter proximal handle is actuated.

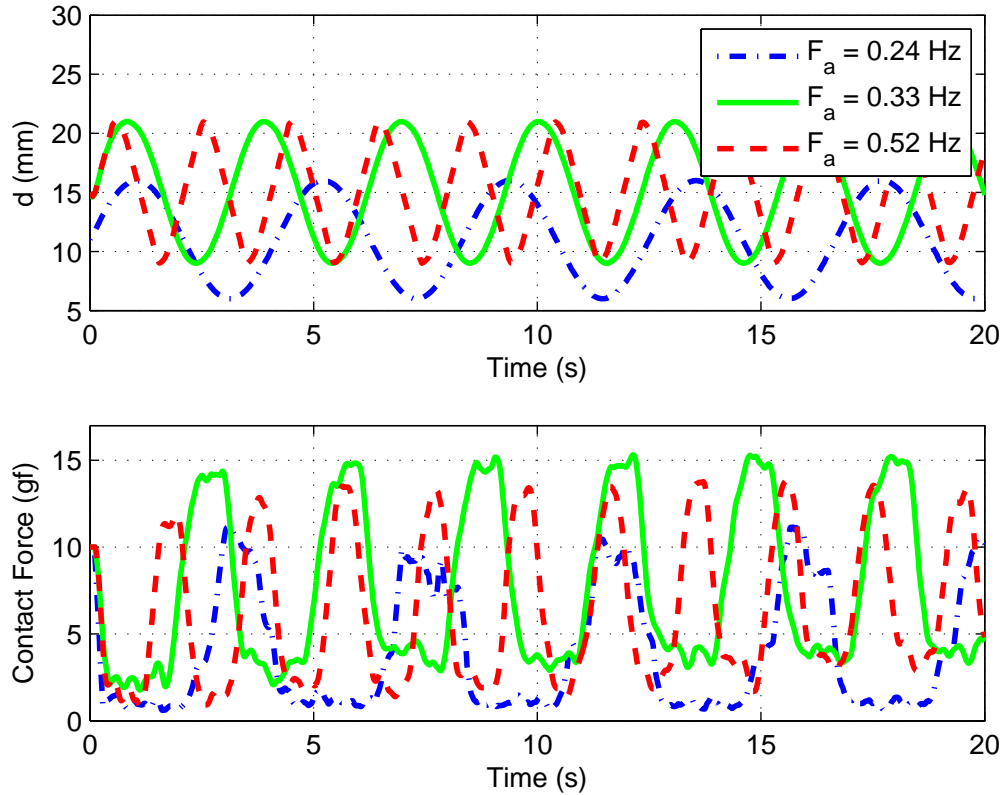


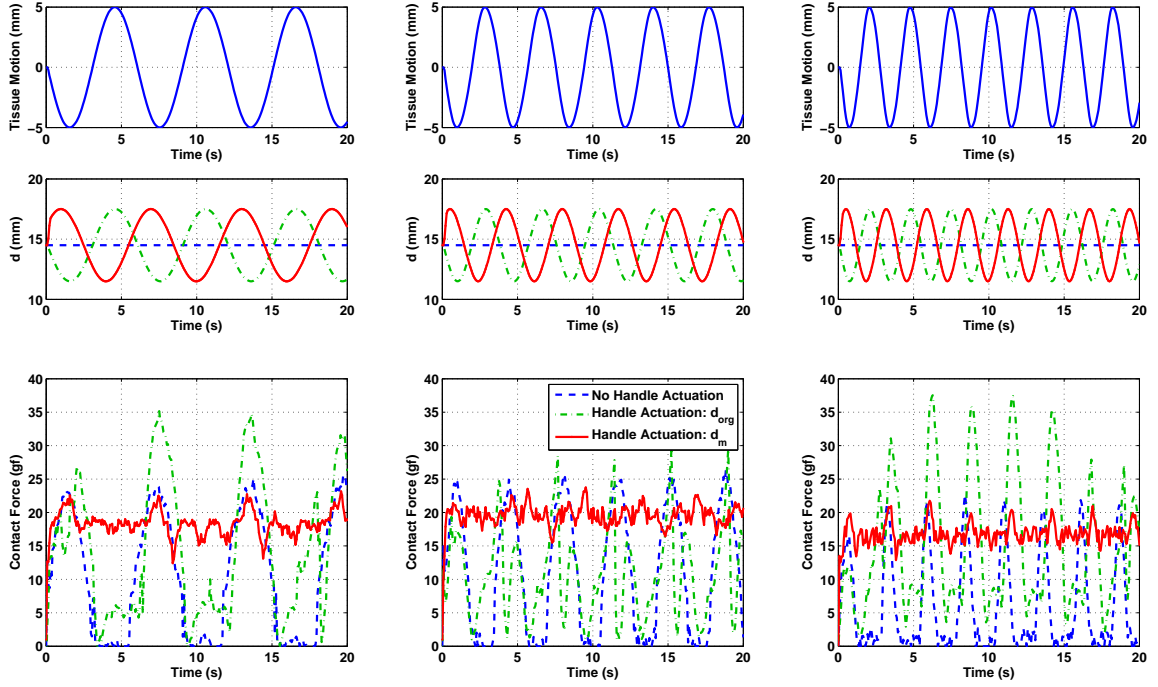
Figure 6.13: Catheter interacting with a static environment: (top) commanded handle displacement, (bottom) resulting tip/tissue contact force.

6.4.2 Moving Environment

In this section, we investigate if we can maintain a constant contact force with a moving environment using the results from the previous sections.

In the experimental setup, the force sensor is commanded to follow a 5 mm sinusoidal signal as a simplified version of the motion of the atrial wall. The proximal handle is also commanded to follow a sinusoidal signal to provide the necessary motion of the catheter tip. It is intuitive that in order to synchronize the motion of the tip with that of the environment, the frequency of handle actuation and the frequency of motion should be the same.

Based on the results presented in Section 6.3, the input command to the proximal knob is reshaped to compensate for the time delay between the handle displace-



(a) Frequency of motion = 0.17 Hz

(b) Frequency of motion = 0.27 Hz

(c) Frequency of motion = 0.37 Hz

Figure 6.14: Catheter tip/tissue contact force when the tissue has a sinusoidal motion: (top) motion of the tissue. (middle) different scenarios for actuating the proximal handle, (bottom) contact force.

ment and the resulting change in the shape of the tip:

$$d_m(t) = d_{org}(t + \tau_d) \quad (6.2)$$

where d_{org} is the sinusoidal signal with the same phase as that of the motion signal. In Equation (6.2), τ_d is the time delay between actuating the handle and the change in the tip shape, obtained from the Bode plot shown in Figure 6.12; and d_m is the modified command to the proximal handle which compensates for the time delay.

Figure 6.14 shows the tissue motion, the handle displacement and the measured contact force at three different frequencies. The force sensor is placed such that the pattern of the contact force matches the intermittent contact as defined in [6]. It is observed that actuating the catheter handle without compensating for the system

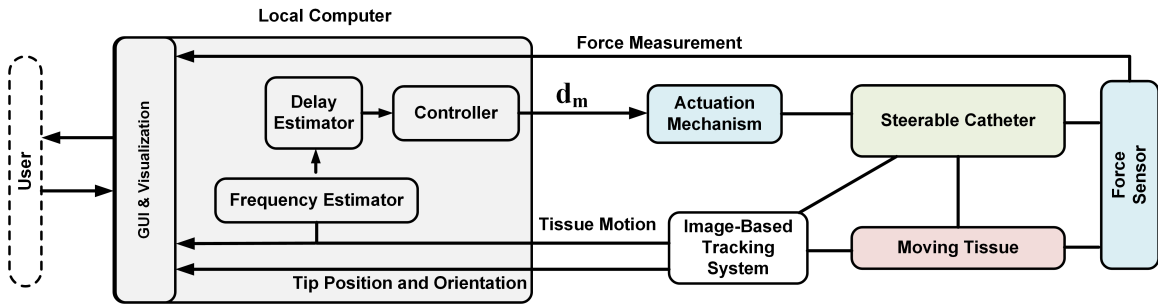


Figure 6.15: Schematic of the control system with online frequency estimation.

delay causes larger variations in the contact force. However, obtaining the frequency response of the system allows the time delay to be estimated at each frequency and to modify the command to the proximal handle accordingly. Figure 6.14 shows that synchronizing the motion of the catheter tip with that of the tissue results in a noticeable improvement in the quality of contact.

6.4.3 Online Estimation of Motion Frequency

In the previous section, it was assumed that the frequency of tissue motion is known. The input signal d_m was then designed to compensate for the system delay. Knowing that in order to have effective tip/tissue motion synchronization, the proximal knob should move with the same frequency as that of the tissue, it is necessary that the frequency of tissue motion can be estimated in real-time.

Figure 6.15 shows the scheme used for online estimation of the motion frequency: The catheter is brought in contact with the tissue and the handle actuation starts at a pre-defined initial frequency. The position of the tissue is tracked in real-time, a window of position samples is monitored and the instant when the direction of motion changes is detected and recorded. The frequency of motion is calculated for each motion cycle and the actuation frequency is regulated accordingly. Since the frequency of the control loop is much higher than the frequency of motion, the actuation frequency adjusts to the calculated motion frequency quite rapidly. With this scheme, the changes in the frequency of motion are detected and compensated for in one or two cycles.

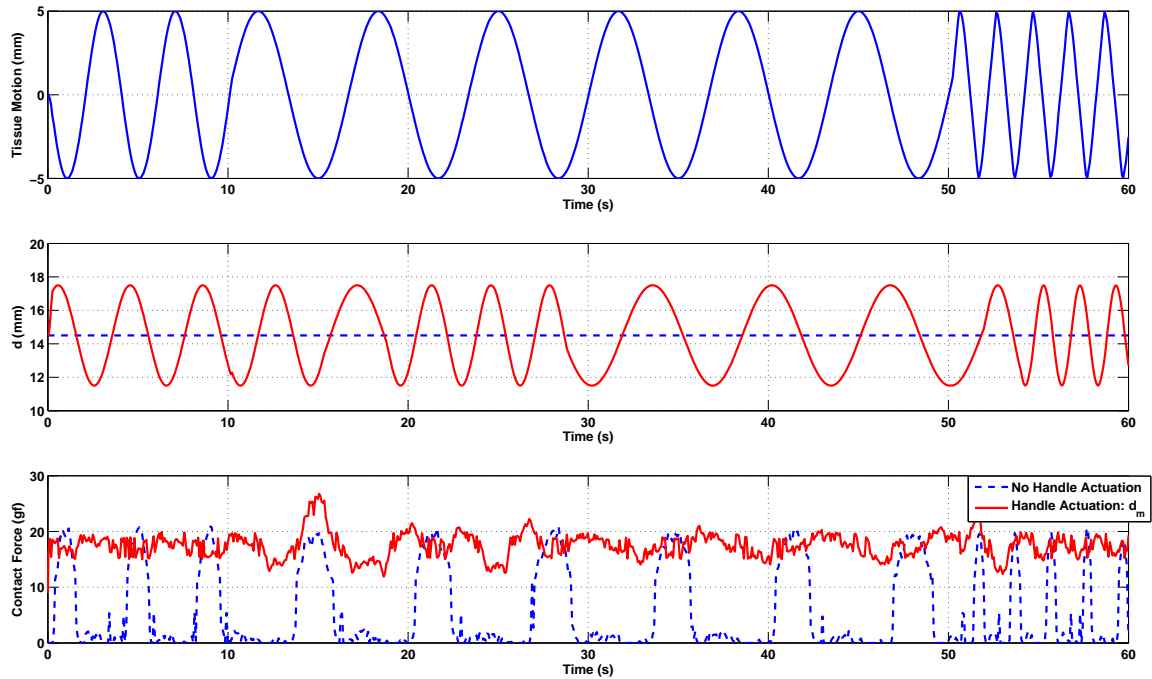


Figure 6.16: Catheter tip/tissue contact force when the frequency of the tissue motion changes: (top) motion of the tissue. (middle) different scenarios for actuating the proximal handle, (bottom) contact force.

Figure 6.16 shows the performance of the system with online estimation of the motion frequency. It is observed that the synchronization between actuation and motion is lost for the first cycles after the change in the frequency occurs, but after that the frequency change is detected, the corresponding time delay is calculated and the tip/tissue motion synchronization is restored.

6.4.4 Evaluating Force-Time Integral

Shah *et al.* [6] showed that force-time integral (FTI) can predict the size of lesion formed during tissue ablation. Therefore, the FTI can be used as a measure to quantify the quality of contact between the catheter tip and the tissue. To study how synchronizing the motion of the catheter tip and that of the tissue affects the quality of tip/tissue contact in the experimental setting, the FTI, *i.e.*, the area under the contact force curve, is calculated for the cases shown in Figures 6.14 and 6.16. Table 6.2 summarizes the results. For the first three entries, the FTI is calculated

Table 6.2: FTI calculated for the cases shown in Figures 6.14 and 6.16.

Case	FTI (gf.s) with $d = 0$	FTI (gf.s) with $d = d_m$	improvement%
Figure 6.14a	212.77	367.25	173%
Figure 6.14b	227.8247	391.5554	172%
Figure 6.14c	122.8314	337.8225	275%
Figure 6.16	341.24	1050	307%

over 20 s and the last entry is calculated over 60 s. It is observed that the proposed technique significantly improves the quality of contact.

6.4.5 Evaluating the Static Force-Deflection Model

In Chapter 3, the distal shaft of the catheter was described with a PRB 3R model. The proposed model was used to estimate contact forces from the shape of the catheter tip in the static case, *i.e.*, for collecting each data sample, a constant force was applied to the tip and the catheter tip was allowed enough time to find its final configuration. In this section, the performance of the proposed PRB 3R model is evaluated for the case where the catheter is in contact with a moving environment.

The optimal link parameters and spring stiffness values for the PRB 3R model are obtained using the algorithm described in Chapter 3:

$$\begin{aligned} \gamma_0 = 0.05, \quad \gamma_1 = 0.4, \quad \gamma_2 = 0.5, \quad \gamma_3 = 0.05 \\ k_{\theta_1} = 3.3, \quad k_{\theta_2} = 2.05, \quad k_{\theta_3} = 4.51 \end{aligned} \tag{6.3}$$

where $\gamma_i, i = 0, 1, 2, 3$ are the normalized link lengths and $k_{\theta_i}, i = 1, 2, 3$ are the normalized spring stiffness values.

The obtained PRB 3R model is used to estimate the contact force from the position and orientation of the catheter tip in two different scenarios: (1) the tissue is moving with a constant frequency of about 0.37 Hz, (2) the frequency of tissue motion changes during data collection. In both cases, before the data collection is started,

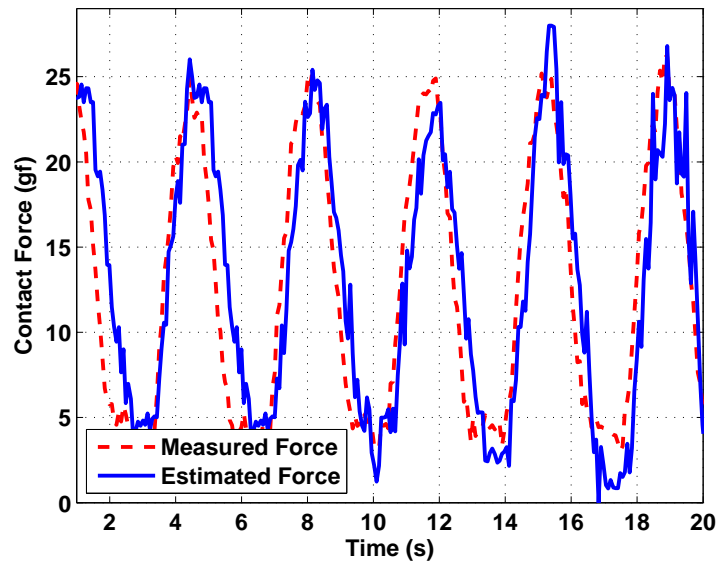


Figure 6.17: Performance of the PRB 3R model in estimating the contact force when the frequency of tissue motion is 0.37 Hz.

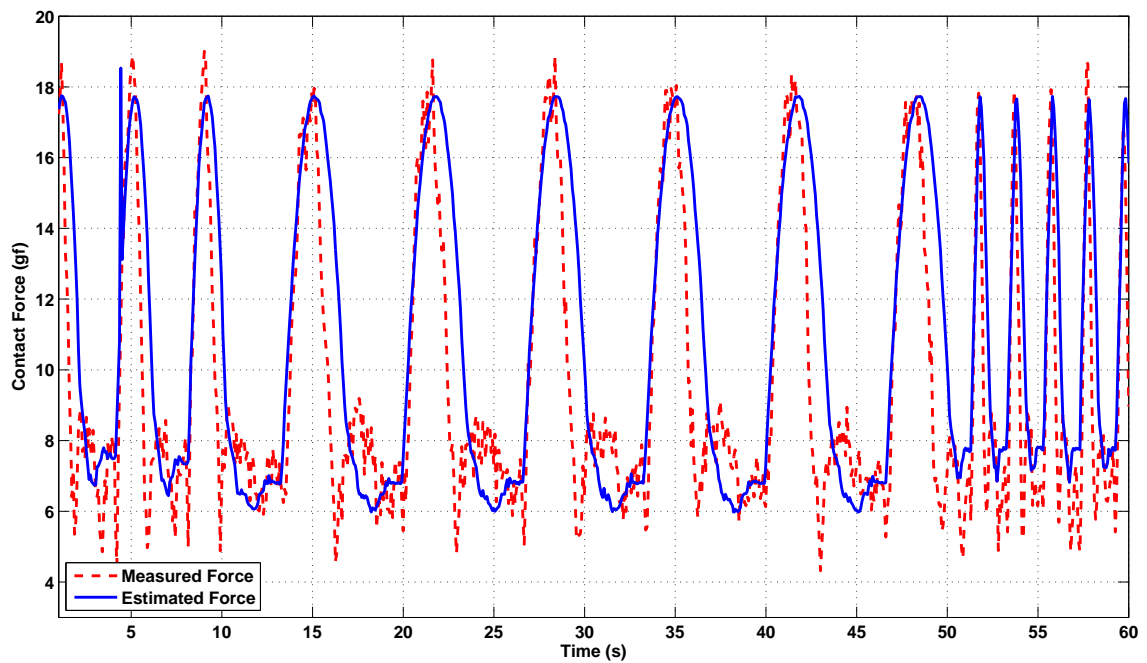


Figure 6.18: Performance of the PRB 3R model in estimating the contact force when the frequency of tissue motion is changing.

the proximal handle is adjusted such that the tip angle in free space is about 90° . The proximal handle is then held at the same position during the course of data collection. The results of force estimation are given in Figures 6.17 and 6.18. The estimation error in both cases is less than 4 gf, implying that the frequency of motion does not affect the model performance and the static model has an acceptable performance even when the catheter is in contact with a moving environment. However, due to the noticeable delay that exists in the system, in order to use this model for online estimation of contact force, a motion predictor should be added to the control system.

6.5 Discussion

6.5.1 Performance Limitations

The experiments carried out during this study indicated certain limitations in integrating current ablation catheters within motion compensated robotic catheter manipulation. The observed limitations are listed below:

- The actuation mechanism of the catheter breaks when it is actuated in frequencies above 0.65 Hz. The pull-wires that connect the prismatic knob to the flexing tip could not stand the 60 s of actuation which was required for doing this study. At frequencies of about 0.65 Hz, the tendon connections inside the proximal handle snapped and the catheter needed to be replaced.
- Performance of the catheters deteriorates significantly with continuous actuation of the handle. Figure 6.19 shows an example of how the catheter behavior changes as a result of continuous actuation. In this experiment, the catheter handle is actuated with a sinusoidal signal, while the environment is static (see Section 6.4-A). The experiment is done first with a less used catheter and then with a catheter worn out during the experiments. The handle actuation is similar in both cases, nevertheless, the measured contact force is very different. The reason is that the actuation mechanism of the catheter loses its functionality over time, especially with repeated actuation. Initially, the catheter tip bends more than 90° , but after repeated usage, the maximum bending angle reduces

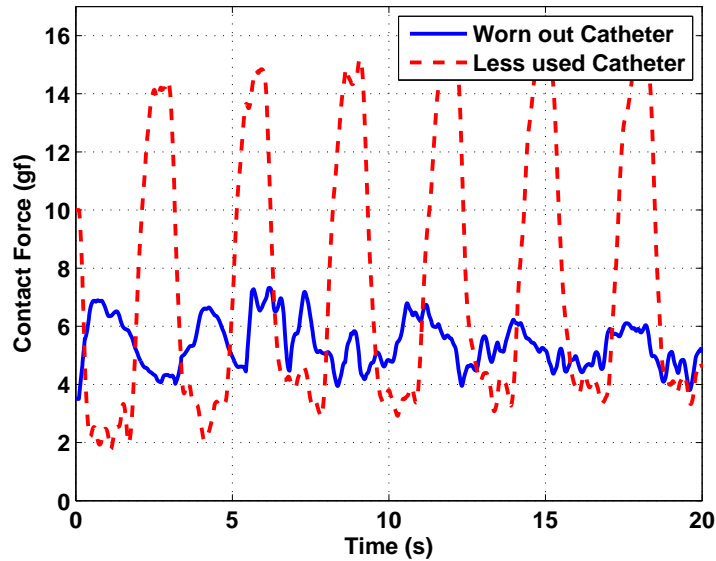


Figure 6.19: The effect of wear of the catheter on the experimental results.

to less than 60° .

- The orientation of the catheter tip with respect to the myocardium affects the lesion formation (*e.g.*, [32, 33]). During the experiments, the angle of the catheter tip related to the artificial tissue is between 70° and 90° . It was found out that if the catheter is flexed to a smaller angle, the performance of the catheter decreases rapidly mainly due to the effect of hysteresis, and has a negative impact on the repeatability of the results.

Due to these limitations, the catheter had to be replaced several times during the experiments and data collection. The catheters used were of the same type; nevertheless, discrepancies existed in some of their features, such as the maximum displacement of the proximal knob and the maximum angle that the tip can reach in its ultimate bending configuration.

The observations on the limitations of the actuation mechanism suggest that this mechanism should be redesigned for using the ablation catheters with robotic manipulators.

Remark 1: In the experimental setting, the catheter is free to move back and forth in the sheath. However, the catheter does not actually slide in the sheath. For

this study, the position of the base of the proximal handle is fixed, *i.e.*, the catheter body is not inserted/retracted. The actuation is applied on the prismatic knob of the handle, which flexes the catheter tip.

The average contact force that the catheter tip can apply on the tissue depends on the relative position between the catheter tip and the tissue. If higher contact forces are desired, the catheter body should be inserted further into the sheath to bring the tip closer to the tissue. Arrangements for inserting/retracting the catheter in/from the sheath is not included in the preliminary experimental setting used for this study, but will be considered in future work. In such a setting, the effects of backlash and friction on motion compensation should be considered as well [18–20, 34].

Remark 2: The simulated motion for the atrial wall is very simplified. To better evaluate the performance of the proposed technique, a thorough study should be carried out on how different points inside the atria move during each heartbeat and the pattern as well as the amplitude of wall motion should be determined. The motion compensation system can then benefit from motion estimators to predict the wall motion and adjust the handle actuation accordingly to maintain constant contact with the tissue. In such a case, a more robust method for estimating the frequency of motion should be implemented.

6.5.2 Relevance to Clinical Application

The proposed system improves the quality of catheter tip/tissue contact by synchronizing the motion of the catheter tip with that of the cardiac tissue. To use this system in a clinical setting, the electrophysiologist manually guides the catheter through the vasculature and places the distal end of the catheter inside the atrium. After the target points for ablation are identified, the catheter tip is manually placed in proximity of the myocardium. The robotic catheter manipulator is then initialized to flex the catheter tip in accordance with the heart tissue to maintain the tip/tissue contact. Depending on the medical imaging modality used for visualizing the procedure, appropriate techniques should be implemented for estimating the frequency of motion and determining the position of the catheter in 3D. It is expected that the proposed

robotics-assisted catheter manipulation approach will decrease procedure times by improving the quality of contact between the catheter tip and cardiac tissue.

6.6 Conclusions

In this chapter, the initial steps towards designing a motion compensated robotics-assisted catheter manipulation system were presented. In this regard, the static behavior of *conventional steerable ablation catheters* was examined. Then the behavior of these catheters in free space when their proximal handles are actuated at different frequencies was investigated. The frequency analysis revealed that the main factor that must be considered in designing robotics-assisted catheter control systems is the time delay that exists between the handle actuation and the flexing of the catheter tip. By actuating the catheter handle at the same frequency as that of the moving target and reshaping the input handle displacement to compensate for the time delay, the motion of the catheter tip was synchronized with the target motion. Evaluating the force-time integral shows that the proposed technique improves the quality of tip/tissue contact noticeably. The experiments also pointed out the limitations in the design of actuation mechanisms for current steerable ablation catheters. This issue would need to be addressed in order to actuate the catheters at frequencies close to those of cardiac motion.

The study presented in this chapter is a fundamental step in identifying the behavior of conventional steerable ablation catheters. To achieve the ultimate goal of developing a robotics-assisted catheter manipulation system that compensates for the cardiac motion, the motion of the atrial wall during the ablation procedure should be characterized; the actuation mechanism of current ablation catheters should be improved; a robust estimator for extracting the features of tissue motion, such as frequency and amplitude, should be designed and the problem of tip/tissue motion synchronization in 3D should be studied.

References

- [1] “Endosense TactiCath.” [Online]. Available: www.endosense.com
- [2] “Biosense Webster THERMOCOOL SMARTTOUCH.” [Online]. Available: www.biosensewebster.com
- [3] K. Yokoyama *et al.*, “Novel contact force sensor incorporated in irrigated radiofrequency ablation catheter predicts lesion size and incidence of steam pop and thrombus,” *Circulation: Arrhythmia and Electrophysiology*, vol. 1, no. 5, pp. 354–362, Dec 2008.
- [4] G. Ndrepepa and H. Estner, “Ablation of cardiac arrhythmias energy sources and mechanisms of lesion formation,” in *Catheter Ablation of Cardiac Arrhythmias*. Steinkopff, 2006, pp. 35–53.
- [5] L. Di Biase *et al.*, “Relationship between catheter forces, lesion characteristics, popping, and char formation: experience with robotic navigation system.” *Journal of Cardiovascular Electrophysiology*, vol. 20, no. 4, pp. 436–40, Apr 2009.
- [6] D.C. Shah *et al.*, “Area under the real-time contact force curve (force–time integral) predicts radiofrequency lesion size in an in vitro contractile model,” *Journal of Cardiovascular Electrophysiology*, vol. 21, no. 9, pp. 1038–1043, Sept 2010.
- [7] P.A. Friedman, “Hitting a moving target: Catheter ablation and respiration,” *Heart Rhythm*, vol. 9, no. 7, pp. 1048–1049, Jul 2012.
- [8] S. Kumar *et al.*, “Effect of respiration on catheter-tissue contact force during ablation of atrial arrhythmias,” *Heart Rhythm*, vol. 9, no. 7, pp. 1041–1047.e1, Jul 2012.

-
- [9] Y. Nakamura, K. Kishi, and H. Kawakami, “Heartbeat synchronization for robotic cardiac surgery,” in *IEEE International Conference on Robotics and Automation (ICRA)*, vol. 2, 2001, pp. 2014–2019.
- [10] T. Ortmaier, M. Groger, D.H. Boehm, V. Falk, and G. Hirzinger, “Motion estimation in beating heart surgery,” *IEEE Transactions on Biomedical Engineering*, vol. 52, no. 10, Oct 2005.
- [11] D. Stoyanov and G.-Z. Yang, “Stabilization of image motion for robotic assisted beating heart surgery,” in *Medical Image Computing and Computer-Assisted Intervention (MICCAI)*, 2007, vol. 4791, pp. 417–424.
- [12] R. Richa, P. Poignet, and C. Liu, “Efficient 3D tracking for motion compensation in beating heart surgery,” in *Medical Image Computing and Computer-Assisted Intervention (MICCAI)*, 2008, vol. 5242, pp. 684–691.
- [13] M. Dominici, P. Poignet, R. Cortesao, E. Dombre, and O. Tempier, “Compensation for 3D physiological motion in robotic-assisted surgery using a predictive force controller. experimental results,” in *IEEE/RSJ International Conference on Intelligent Robots and Systems (IROS)*, 2009, pp. 2634–2639.
- [14] J. Florez, D. Bellot, and G. Morel, “LWPR-model based predictive force control for serial comanipulation in beating heart surgery,” in *IEEE/ASME International Conference on Advanced Intelligent Mechatronics (AIM)*, 2011, pp. 320–326.
- [15] S.G. Yuen, S.B. Kesner, N.V. Vasilyev, P.J. del Nido, and R.D. Howe, “3D ultrasound-guided motion compensation system for beating heart mitral valve repair,” in *Medical Image Computing and Computer-Assisted Intervention (MICCAI)*, 2008, vol. 5241, pp. 711–719.
- [16] S.G. Yuen *et al.*, “Robotic force stabilization for beating heart intracardiac surgery,” in *Medical Image Computing and Computer-Assisted Intervention (MICCAI)*, 2009, vol. 5761, pp. 26–33.

-
- [17] S.G. Yuen, D.T. Kettler, P.M. Novotny, R.D. Plowes, and R.D. Howe, “Robotic motion compensation for beating heart intracardiac surgery,” *The International Journal of Robotics Research*, vol. 28, no. 10, pp. 1355–1372, Oct 2009.
- [18] S.B. Kesner and R.D. Howe, “Design and control of motion compensation cardiac catheters,” in *IEEE International Conference on Robotics and Automation (ICRA)*, 2010, pp. 1059–1065.
- [19] S.B. Kesner and R.D. Howe, “Force control of flexible catheter robots for beating heart surgery,” in *IEEE International Conference on Robotics and Automation (ICRA)*, 2011, pp. 1589–1594.
- [20] S.B. Kesner and R.D. Howe, “Position control of motion compensation cardiac catheters,” *IEEE Transactions on Robotics*, vol. 27, no. 6, pp. 1045–1055, 2011.
- [21] S.B. Kesner and R.D. Howe, “Discriminating tissue stiffness with a haptic catheter: Feeling the inside of the beating heart,” in *IEEE World Haptics Conference (WHC)*, 2011, pp. 13–18.
- [22] S.B. Kesner and R.D. Howe, “Design principles for rapid prototyping forces sensors using 3-D printing,” *IEEE/ASME Transactions on Mechatronics*, vol. 16, no. 5, pp. 866–870, Jul 2011.
- [23] M. Khoshnam, M. Azizian, and R.V. Patel, “Modeling of a steerable catheter based on beam theory,” in *IEEE International Conference on Robotics and Automation (ICRA)*, 2012, pp. 4681–4686.
- [24] M. Khoshnam and R.V. Patel, “A pseudo-rigid-body 3R model for a steerable ablation catheter,” in *IEEE International Conference on Robotics and Automation (ICRA)*, 2013, pp. 4412–4417.
- [25] M. Khoshnam, A. Yurkewich, and R.V. Patel, “Model-based force control of a steerable ablation catheter with a custom-designed strain sensor,” in *IEEE International Conference on Robotics and Automation (ICRA)*, 2013, pp. 4464–4469.

- [26] G. Akgün and C. Layton, “Aortic root and left atrial wall motion. an echocardiographic study.” *British Heart Journal*, vol. 39, no. 10, pp. 1082–1087, Oct 1977.
- [27] J. Kubica *et al.*, “Left atrial size and wall motion in patients with permanent ventricular and atrial pacing,” *Pacing and Clinical Electrophysiology*, vol. 13, no. 12, pp. 1737–1741, Dec 1990.
- [28] F. Perna *et al.*, “Assessment of catheter tip contact force resulting in cardiac perforation in swine atria using force sensing technology,” *Circulation: Arrhythmia and Electrophysiology*, vol. 4, no. 2, pp. 218–224, Apr 2011.
- [29] C.R. Wagner, D.P. Perrin, R.D. Howe, N.Vasilyev, and P.J. del Nido, “Force feedback in a three-dimensional ultrasound-guided surgical task,” in *Symposium on Haptic Interfaces for Virtual Environment and Teleoperator Systems*, 2006, pp. 43–48.
- [30] D.T. Kettler *et al.*, “An active motion compensation instrument for beating heart mitral valve surgery,” in *IEEE/RSJ International Conference on Intelligent Robots and Systems (IROS)*, 2007, pp. 1290–1295.
- [31] “MitraClip Percutaneous Mitral Valve Repair System.” [Online]. Available: www.abbottvascular.com/int/mitraclip.html
- [32] Z. Issa, J.M. Miller, and D.P. Zipes, *Clinical arrhythmology and electrophysiology: a companion to Braunwald’s heart disease*. Elsevier Health Sciences, 2012, ch. 7.
- [33] T. Jest, T. Haber, J. Härtig, J. Melichercik, and B. Ismer, “Simulation of cardiac radiofrequency catheter ablation—the importance of working angle,” *Biomedical Engineering/Biomedizinische Technik*, Sept 2013.
- [34] M. Nordin and P.-O. Gutman, “Controlling mechanical systems with backlash - a survey,” *Automatica*, vol. 38, no. 10, pp. 1633 – 1649, Oct 2002.

Chapter 7

Concluding Remarks and Future Work

This chapter provides overall concluding remarks on the presented work and suggests several directions and guidelines for future work in designing robotics-assisted catheter manipulation systems.

7.1 Concluding Remarks

The work presented in this thesis established a fundamental step in developing a robotics-assisted catheter manipulation system with the capability to provide force control at the tip of *conventional steerable ablation catheters*. In this work, different ideas were developed and several techniques were implemented, but the main concern throughout the course of this research project was that the final robotic system should be compatible with all types of existing ablation catheters and so the suggested methods should be applicable to different catheters with simple calibration steps. Therefore, the proposed approaches are based on observing and analyzing catheter behavior in different experimental settings, and they do not rely on information about the mechanical design of catheters nor the arrangement of tension and/or fictional forces inside the catheter. Moreover, the commonly used ablation catheters do not have the necessary means to measure or estimate contact forces between the tip and cardiac tissue. Thus, one of the main objectives was to investigate methods for estimating the contact force without installing pressure or strain sensors on the catheter tip. Force control at the distal tip would then be realized by using such a method to estimate the force that the catheter tip exerts on tissue.

The objective of our first study was to investigate how contact forces affect the position and orientation of the catheter tip. To achieve this goal, the static behavior

of the distal shaft was studied in a series of experiments. The experimental setup was designed based on the configuration of the catheter during the ablation procedure: the catheter passes through a narrow sheath to enter the open space of the atria. We assumed that in this configuration, the contact force affects the deflectable shaft more than it affects the body of the catheter. Hence, in the first experimental setting, the movement of the distal shaft of the catheter was constrained at one end. A series of forces with different in-plane directions was applied to the catheter tip and the catheter shape was recorded. The tip rigidity was calculated and the initial bending of the catheter was modeled. A large deflection beam model based on Euler-Bernoulli beam theory was then used to describe the force-deflection relation of the catheter tip. It was shown that the model has good performance: the error in estimating the tip angle is less than 2° and the tip position is estimated with an error less than 0.7 mm.

The experimental results suggested that the static behavior of the catheter tip can be described with a large deflection beam model. However, this model has several features that increase the computational cost and hinder its use for developing real-time control systems. PRB 3R model is an approximation of the large deflection beam model with good accuracy, but less computational cost. It was demonstrated that the performance of this model in describing the force-deflection relationship for the catheter tip is the same as that of the large deflection beam model. The algorithm for obtaining the parameters of the model was then customized to describe the behavior of the catheter tip under applied loads. It was shown that if the parameters of the model are obtained with the proposed algorithm, the error in estimating the tip position is reduced from 3.34 mm to 0.85 mm. In the next step, the experimental setup was redesigned to become more realistic: the catheter was passed through a standard sheath. In this configuration the catheter is free to slide in and out of the sheath. The performance of the PRB 3R model and the large deflection beam model was further evaluated with this setup. It was shown that the beam model fails to describe the effect of contact force on the catheter tip position (RMSE = 7.42 mm) and orientation (RMSE = 4.9°). However, the PRB 3R model demonstrates acceptable accuracy in estimating the tip position (RMSE = 2 mm) and orientation (RMSE

= 1.42°). The reason is that the large deflection beam model is developed for a cantilever beam, where one end of the beam is clamped and cannot move or rotate. This assumption does not hold with the second experimental setup and leads to the poor performance of the beam model. On the other hand, the parameters of the PRB 3R model are optimized with the proposed algorithm to describe the static behavior of the catheter in this experimental setting and thus this model demonstrates good performance in this setup as well. The PRB 3R model is described with simple well-established equations and its inverse model can be calculated without increasing the computational cost. Thus, PRB 3R model is well-suited for estimating contact force from the tip position and orientation in real-time.

The static force-deflection model of the distal shaft allows for estimating the contact force from the shape of the catheter. In the next step, a control system for controlling the contact force between the catheter tip and a static environment was designed. To realize force control, the controller moved the proximal handle to achieve more or less bending at the catheter tip and thus changed the amount of force that the tip was applying on the environment. The parameters of the controller were first tuned using force readings from a force sensor. The force feedback to the controller was then provided using the PRB 3R model to estimate the contact force from the tip position and orientation. While in the previous experiments, the shape data was collected using a camera, in-house development of a strain sensor provided an alternative method to estimate the bending of the distal shaft. It was observed that the system can correctly detect when the catheter comes in contact with the environment. It also demonstrated good performance in achieving and attaining low levels of contact force (< 10 gf), but its performance deteriorated at higher levels of contact force (> 10 gf). Analysis of the results revealed that the strain sensor could successfully detect the tip angles within a limited range but outside of which, the changes in the tip angle remained hidden from the strain sensor. The other limitation faced during the experiments was that the design of the setup did not allow for applying higher forces (> 20 gf) at the catheter tip.

These limitations resulted in a revision of the setup and an analysis of the catheter shape to understand how the curvature of the distal shaft changes when

forces are applied. Since the results of this step were highly dependent on accurate extraction of the catheter shape from acquired images, a custom image processing algorithm was developed. Analysis of the tip curvature showed that the distal tip of unidirectional ablation catheters does not bend with constant curvature. This observation led to developing a kinematic model for the distal tip in free space. The model was proposed as a modification to a well-known kinematic model in the field of continuum robots which assumes that a continuum manipulator bends with a constant curvature. Further analysis on how the contact forces affect the tip curvature led to defining a force index that can identify the range of contact forces using a Gaussian-Mixture model. As a result of this study, a framework for estimating the force index from one or more points along the catheter tip was suggested.

Consistent contact between the catheter tip and cardiac tissue is achieved if the catheter tip moves with the target. To this end, the frequency response of the catheter was analyzed and the effect of actuation frequency on different bending characteristics of the distal tip was studied. One of the main features of the system was found to be the delay between the handle actuation and the bending of the tip. Based on the frequency response analysis, a system for tracking a desired trajectory in free space was proposed. The control system was then used to estimate the frequency of the target motion online and to adjust the handle position to compensate for the motion of the environment. Implementing motion compensation at the catheter tip resulted in less variations in the contact force and improved the quality of contact noticeably. The performance of the static PRB 3R model was tested in a case where the catheter tip was in contact with a moving target. The results showed that the proposed PRB 3R model can estimate the contact force from the tip position and orientation in this case as well, but the delay, which is inherent in the system, is a major obstacle in using this model for real-time force estimation.

Although the experiments are done in the laboratory environment, there is no unnecessary or unrealistic assumption that limits the fundamental theory. One of the main assumptions in this work is that the catheter bends with zero torsion in free space, *i.e.*, the deflected tip lies in a plane. This assumption was validated through the experiments. The other assumption is that the camera provides a direct planar

view of the catheter. In a clinical setting, proper techniques for extracting the shape of the catheter from available medical imaging modalities should be developed. It was also assumed that the contact forces act at the catheter tip and in the plane of the deflected catheter. Considering the angle between the catheter and the myocardium, this is a valid assumption. The effect of other forces, such as blood flow inside the atria, is not considered. These forces can be modeled as distributed loads along the catheter tip and considered to enhance the static model to 3D. However, the most significant force applied to the catheter tip during the ablation procedure is the contact force between the tip and cardiac tissue.

It is worthwhile noting that if inserting in/withdrawing and rotating the proximal handle is not considered, the catheter tip has 1-DOF. This means that the catheter can compensate for the target motion only if the motion is in the correct direction. Thus, the correct positioning of the catheter with respect to the tissue is critical for motion compensation.

The objective of this work is to define a model that can be easily tuned for each type of catheter. This was the main notion in developing the models and designing the control system. An opportunity to test this presented during the course of experiments, as the catheters had to be replaced frequently. Due to the fact that the catheters are for single use and they are disposed after each ablation procedure, their actuation mechanism is not very durable and breaks with repeated or prolonged use. However, it was observed that switching catheters does not affect the main features of the system, such as the parameters of the PRB 3R model or the delay in the system. This implies that such parameters depend on the mechanical design of the catheter and are the same for catheters of the same make. Since the fabrication process for catheters made by different companies could vary, further investigation is required to determine how much variability (if any) exists between different makes of catheters.

7.2 Future Research

The results presented in this thesis provide a framework for modeling and control of ablation catheters. The research can be continued in several directions including, but

not limited to the following.

- The static model was developed in 2D, assuming contact forces as in-plane end loads. Identifying and studying other forces affecting the shape of the catheter inside the atria and extending the model to 3D can be the next step. In this regard, the effect of atrial blood flow on the catheter tip before and after establishing contact with the myocardium should be further investigated by studies such as [1].

To ensure motion synchronization between the catheter tip and cardiac tissue, the catheter should be positioned in the correct direction with respect to the tissue. A thorough analysis of the pattern of motion at different points of the atria during each heartbeat would be of great help. The results of such study can be used in developing control systems with motion predictors and robust algorithms for real-time estimation of motion frequency. Moreover, to ensure that the catheter can be placed at the target point with the desired orientation, studies such as [2] are relevant. Manipulation of the catheter distal shaft can also be enhanced by using active catheters, *e.g.*, [3], that provide more degrees of freedom at the distal tip.

- Estimating the contact forces from the tip shape requires detailed information on the curvature of the tip and/or tip position and orientation. Developing robust and reliable imaging techniques that can extract such information in real-time from images provided by a medical imaging modality should be considered. As an example, the model of the distal shaft proposed in this work can be used together with the technique proposed in [4] for intra-operative 3D visualization of the catheter within the beating heart using ultrasound images. Detecting the shape can also be enhanced by fusion of information from multiple sources such as image and magnetic tracking systems [5].
- During the experiments, it was revealed that the actuation mechanism of the commonly used catheters has two limiting features: (1) the pull-wire mechanism cannot endure the rapid and continuous actuation enforced by robotic manipulators and (2) its performance degrades noticeably at frequencies close to that of the cardiac motion. Improving the pull-wire actuation mechanism is

required in order to use these catheters in motion compensated robotics-assisted manipulation systems.

- In this study, it was assumed that the catheter tip is manually guided through the vasculature and positioned inside the atria. Electrophysiologists steer the catheters by inserting/withdrawing, rotating and flexing the tip. This procedure can be facilitated using robotic catheter manipulators that are capable of mimicking the motions of electrophysiologists' hands. To develop a control system for guiding the catheter inside the vasculature, nonlinearities, such as deadband and friction between the catheter body and the environment should be considered. If visual servoing techniques are integrated with such robotic systems, then navigating the catheter in the vasculature can be performed autonomously [6]. The framework proposed herein can be used together with such robotic systems to provide estimation and regulation of contact forces during the ablation procedure. With these robotic systems, it would also be possible to implement teleoperated master-slave control of the steerable catheter with haptic feedback from the catheter tip.
- The results of the research in this thesis were validated via experiments conducted in the laboratory environment. The performance of the proposed techniques should be further evaluated via *in-vivo* experiments.

References

- [1] A. Salimi, J. Mohammadpour, K. Grigoriadis, and N. Tsekos, “Dynamic simulation of blood flow effects on flexible manipulators during intra-cardiac procedures on the beating heart,” in *ASME Dynamic Systems and Control Conference and Bath/ASME Symposium on Fluid Power and Motion Control*. American Society of Mechanical Engineers, 2011, pp. 487–494.
- [2] J. Jayender, R.V. Patel, G.F. Michaud, and N. Hata, “Optimal transseptal puncture location for robot-assisted left atrial catheter ablation,” *The International Journal of Medical Robotics and Computer Assisted Surgery*, vol. 7, no. 2, pp. 193–201, Jun. 2011.
- [3] “Hansen Medical Artisan Extend Control Catheter.” [Online]. Available: www.hansenmedical.com/us/products/ep/artisan-control-catheter.php
- [4] M. Azizian and R.V. Patel, “Intraoperative 3D stereo visualization for image-guided cardiac ablation,” in *Proceedings of SPIE Medical Imaging*, vol. 7964, 2011, pp. 79 640F–79 640F–8.
- [5] M. Azizian and R.V. Patel, “Data fusion for catheter tracking using kalman filtering: applications in robot-assisted catheter insertion,” *Medical Imaging: Visualization, Image-Guided Procedures*, vol. 7964, p. 796413, 2011.
- [6] J. Jayender, M. Azizian, and R.V. Patel, “Autonomous image-guided robot-assisted active catheter insertion,” *IEEE Transactions on Robotics*, vol. 24, no. 4, pp. 858–871, Aug. 2008.

Curriculum Vitae

Mahta Khoshnam Tehrani

Canadian Surgical Technologies & Advanced Robotics (CSTAR)
Electrical and Computer Engineering Department
Western University
London, Ontario, N6A 5B9, Canada.

Education

2009 – present

Doctor of Philosophy

Electrical and Computer Engineering Dept., Western University

2005 – 2008

Master of Science

School of Electrical & Computer Engineering, University of Tehran

2001 - 2005

Bachelor of Science

Electrical Engineering Dept., Amirkabir University of Technology (Tehran Polytechnic)

Related Work & Research Experiences

2009 – present

Research Assistant

Canadian Surgical Technologies and Advanced Robotics (CSTAR)

Electrical and Computer Engineering Dept., Western University

2004 – 2009

Laboratory Instructor

Electrical Engineering Dept., Amirkabir University of Technology (Tehran Polytechnic)

2007 - 2009

Teaching Assistant

Electrical Engineering Dept., Amirkabir University of Technology (Tehran Polytechnic)

2007 – 2008

Teaching Assistant

Amirkabir University of Technology (Tehran Polytechnic) /University of Birmingham

Honors and Awards

- Travel Support Award from International Conference on Robotics and Automation (ICRA), 2013.
- NSERC CREATE Program in Computer-Assisted Medical Interventions (CAMI), Supplementary Funding Institutional, Western University, 2009 - 2011, \$9000 per year.
- Best lab instructor/teaching assistant (as elected by undergraduate students), Amikabir University of Technology, Tehran, Iran, 2006.
- Ranked among top 1% nationwide in university entrance exam for graduate education, Iran, 2005.
- Ranked 3rd among Electrical Engineering-Control undergraduate students, Department of Electrical Engineering, Amirkabir University of Technology, Tehran, Iran, 2005.
- Ranked among top 1% nationwide in university entrance exam, Iran, 2000.

Publications

Refereed Journals

- **M. Khoshnam** and R.V. Patel, “Modeling and estimation of tip contact force for steerable ablation catheters”, submitted to *IEEE Transactions on Biomedical Engineering*, Dec 2013.
- M. Azizian, **M. Khoshnam**, N. Najmaei, and R.V. Patel, “Visual servoing in medical robotics: a survey. Part I: endoscopic and direct vision imaging – techniques and applications,” *International Journal of Medical Robotics and Computer-Assisted Surgery*, published online: Sept 2013.
- M. Azizian, N. Najmaei, **M. Khoshnam**, and R.V. Patel, “Visual Servoing in medical robotics; Part II: tomographic imaging modalities – techniques and applications,” *International Journal of Medical Robotics and Computer-Assisted Surgery*, Accepted Jan 2014.

Refereed Conference Proceedings

- **M. Khoshnam** and R.V. Patel, “Robotics-Assisted Catheter Manipulation for Improving Cardiac Ablation Efficiency,” submitted to *IEEE International Conference on Biomedical Robotics and Biomechanics (BioRob)*, Feb 2014.
- **M. Khoshnam** and R.V. Patel, “Estimating Contact Force for Steerable Ablation Catheters based on Shape Analysis,” submitted to *IEEE/RSJ International Conference on Intelligent Robots and Systems (IROS)*, Feb 2014.
- **M. Khoshnam** and R.V. Patel, “Pseudo-Rigid-Body 3R Model for a Steerable Ablation Catheter,” *IEEE International Conference on Robotics and Automation (ICRA)*, Karlsruhe, Germany, May 2013.
- **M. Khoshnam**, A. Yurkewich, and R.V. Patel, “Model-Based Force Control of a Steerable Ablation Catheter,” *IEEE International Conference on Robotics and Automation (ICRA)*, Karlsruhe, Germany, May 2013.
- **M. Khoshnam**, M. Azizian, and R.V. Patel, “Modeling a steerable catheter based on beam theory,” *IEEE International Conference on Robotics and Automation (ICRA)*, pp.4681-4686, May 2012.
- M. Shahmohammadi, **M. Khoshnam**, and F. Razzazi, “Extracting a model for analyzing Persian poems via speech processing methods,” Electrical Engineering Conference, Student branch, Tehran, Iran, June 2001 (in Persian).

Other

- **M. Khoshnam**, M. Azizian, and R.V. Patel, “Modeling of a Steerable Ablation Catheter”, Poster presented in *3rd North American Robotic Summer School*, Western University, London, Ontario, Canada, Aug 2012.
- “Enlargement of the domain of attraction through nonlinear controllers and its effect on closed-loop system performance,” M.Sc. Thesis, under supervision of Prof. M.J. Yazdanpanah, Feb. 2008.
- “Design and implementation of a wireless sensor network for distributed control,” B.Sc. Thesis, under supervision of Prof. H.A. Talebi and Mr. A. Kashi, Jan. 2005.